UNIVERSITEIT VAN PRETORIA
UNIVERSITY OF PRETORIA
YUNIBESITHI YA PRETORIA

University of Pretoria

Department of Materials Science and Metallurgical Engineering

MSc Dissertation

An assessment of the production of fine material in iron ore sinter

By

T van den Berg

Supervisor: Prof JPR de Villiers
Co-supervisor: Prof AM Garbers-Craig

Submitted in partial fulfillment of the requirements
for the degree MSc (Appl.Sci.): Metallurgy

Department of Materials Science and Metallurgical Engineering
University of Pretoria
Pretoria

02/2008

Abstract

Iron ore sinter is produced from fine-grained ore in order to provide a direct charge to the blast furnace. During the sinter production process fine sinter is produced that is not acceptable as feedstock for the blast furnace. This fine material is screened off and returned to the sinter plant to be recycled. The production of these recirculating fines therefore results in loss of revenue for the sinter producing facility. The aim of this study is to compare the composition and phase chemistry of the fine and normal sinter to determine if chemical or operational changes can be made to reduce the amount of fine sinter formed. This will be achieved through the analyses of real industrial sinter samples, synthetically produced lab-based samples and sinter test pot samples.

Iron ore sinter was collected from the Vanderbijl Park sinter plant in South Africa. The samples were prepared for X-ray diffraction (XRD) and X-ray fluorescence (XRF) analysis to test the reproducibility of the equipment used as well as the reproducibility of the sample preparation method. The results obtained showed that the methods applied produced accurate results and the preparation method was then applied on all samples that were analyzed. The XRD analyses show that the sinter contains spinel (mainly magnetite with variable Mg), hematite, dicalcium silicate (C_2S) and silico ferrite of calcium and aluminum (SFCA) and that there are distinct differences between the fine and normal sinter. Fine sinter contains more hematite and less SFCA than normal sinter. The presence of the SFCA is considered to be essential for the production of strong sinter. The XRF analyses show that there are no distinctive differences in the chemistry of fine and normal sinter. The samples were then analyzed with an electron microprobe. It was found that the compositions of some of the SFCA phases present in the samples do not correspond to those described in the literature.

Optical microscopy combined with point counting was conducted on the fine and normal sinter in order to determine differences and to compare the point counting data to the XRD results. The point counting results showed that the hematite present in the fine sinter is largely relict or unreacted hematite. Sinter pot test samples were analyzed with XRD and XRF. It was found that the pot test samples exhibited similar trends as the samples taken at the sinter plant. This shows that it is not only plant parameters such as sample transport that result in the formation of fines, but that carbon addition, flame temperature and reaction time may also play a role in the formation of fine sinter material.

It has been concluded that the production of fine sinter is a direct function of the amount of hematite present in the sinter. The proposed hypothesis for this phenomenon involves the incomplete reaction of the sinter material during processing. Suggestions to decrease the amount of fine sinter formed include: uniform heat distribution during ignition, pO_2 alteration by reductant addition, lower ignition temperature, regulating the cooling regime and decreasing the grain size of lime.

Keywords

Iron ore sinter, SFCA, hematite, C_2S, magnetite, sol gel

Table of Contents

List of Abbreviations

B	Basicity or $CaO:SiO_2$
C2	$CaO(Al_2O_3,Fe_2O_3)_2$ or $Ca(Al,Fe)_4O_7$ (Patrick & Pownceby 2002:86)
C6	$CaO(Al_2O_3,Fe_2O_3)_6$ or $Ca(Al,Fe)_{12}O_{19}$ (Patrick & Pownceby 2002:86)
CA	$CaO.Al_2O_3$ or $CaAl_2O_4$
CCP	Cubic close packing
CF	$CaO.Fe_2O_3$ or $CaFe_2O_4$
C_2F	$2CaO.Fe_2O_3$ or $Ca_2Fe_2O_5$
CF_2	$CaO.2Fe_2O_3$ or $CaFe_4O_7$
CF_3	$CaO.3Fe_2O_3$ or $CaFe_6O_{10}$
CS	$CaO.SiO_2$ or $CaSiO_3$
C_2S	$2CaO.SiO_2$ or Ca_2SiO_4
C_3S_2	$3CaO.2SiO_2$ or $Ca_3Si_2O_7$
C_4S_3	$4CaO.3SiO_2$ or $Ca_4Si_3O_{10}$
EBI	Electron back scatter image
FFS	Flame front speed
Hem	Hematite (Fe_2O_3)
Liq/L	Quench liquid phase
Mf	Magnesioferrite ($Mg^{2+}Fe^{3+}{}_2O_4$)
Mt	Magnetite (Fe_3O_4)
SEM	Scanning electron microscopy
SFCA	Silico-ferrites of calcium and aluminum
TEOS	Tetraethylorthosilicate
XRD	X-ray diffraction
XRF	X-ray fluorescence

List of Figures

List of Tables

1. Introduction

1.1 The steel industry

The world produced 1.2395 billion metric tons of crude steel in 2006. This indicates an increase of 8.8% on 2005. In 2006 the production was 65.3% above the total production for the world ten years ago. It is also 45.7% above the total five years ago. It should be noted that over the past ten years the most noteworthy growth has been in China and the Asia region (Steel Statistical Yearbook 2006).

According to Figure 1, the trend of iron ore and crude steel production worldwide shows that there is an overall increase since 2001. If China and Asia continue their developments this trend should be maintained for the next few years.

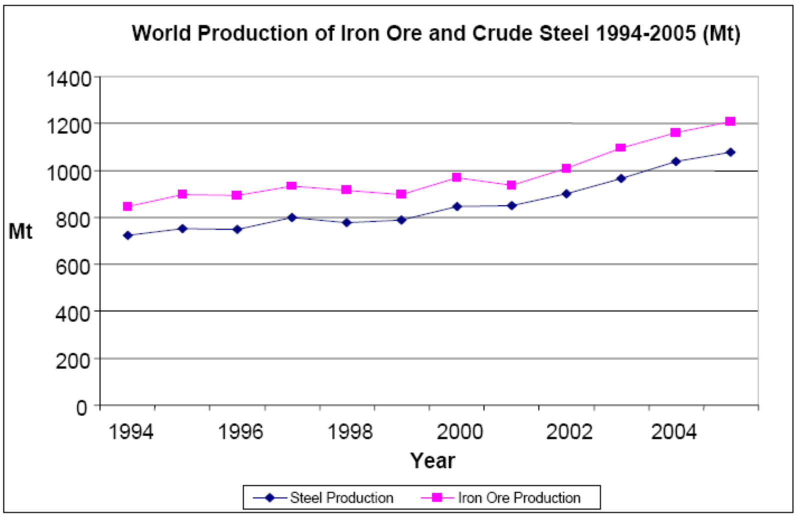

Figure 1: Graph representing world iron ore and crude steel production from 1994-2005 (Baffinland Iron Mines Corporation 2005)

In Table 1 the world steel production in 2006 is depicted. It shows that China, Japan and the USA are the top producers and that South Africa is in 21st place in relation with the other countries.

Table 1: World steel production (in millions of metric tons – mmt) in 2006 (Steel Statistical Yearbook 2006)

Country	**mmt**	**Country**	**mmt**	**Country**	**mmt**	**Country**	**mmt**
China	422.7	Ukraine	40.9	Mexico	16.3	Australia	7.9
Japan	116.2	Italy	31.6	Canada	15.4	Austria	7.1
United States	98.6	Brazil	30.9	United Kingdom	13.9	Czech Republic	6.9
Russia	70.8	Turkey	23.3	Belgium	11.6	Netherlands	6.4
South Korea	48.5	Taiwan, China	20.2	Poland	10.0		
Germany	47.2	France	19.9	Iran	9.8		
India	44.0	Spain	18.4	South Africa	9.7		

Table 2: Production of pig iron (thousands of metric tons) in Africa from 1996-2005 (Steel Statistical Yearbook 2006)

Total Production of Pig Iron in Africa										
	1996	**1997**	**1998**	**1999**	**2000**	**2001**	**2002**	**2003**	**2004**	**2005**
Algeria	850	526	757	807	767	800	960	965	994	952
Egypt	1235	1514	1357	1020	990	1160	1100	1080	1000	1100
South Africa	6014	6192	6893	6005	6292	5820	5823	6234	6011	6130

From the values in Table 2 it is evident that South Africa is the largest producer of pig iron in Africa. It is apparent from the Tables 1 and 2 that South Africa plays an important role in the iron and steel industry not only locally but also internationally. The production of iron and steel thus also proves to be fundamental to our economy. It should be noted that the amount of pig iron does not equate to steel production and is therefore less because scrap iron and direct reduced iron are added to produce steel.

Table 3 relates South Africa's pig iron production with the top producing countries in the world. This shows that South Africa is 14th in world wide production.

Table 3: Top pig iron producing countries in 2006 (in millions of metric tons – mmt) (Steel Statistical Yearbook 2006)

Total Production of Pig Iron			
Country	**mmt**	**Country**	**mmt**
South Africa	6 130	Germany	28 854
Australia	6 203	Ukraine	30 782
Belgium	7 254	Brazil	33 884
Canada	8 274	United States	37 222
United Kingdom	10 189	Russia	48 410
Italy	11 423	Japan	83 058
South Korea	27 309	China	330 405

Some iron ore cannot be used for steel making because it is too fine to be directly used in the blast furnace. The blast furnace accepts iron ore between 8-25mm. Therefore it first needs to be agglomerated into strong, manageable synthetic lumps, and this is accomplished via the process of sintering.

1.2 The sinter process

During the sinter process fine particles are bonded together into lumps (to produce porous material suitable for the blast furnace which will prevent gas flow problems) of sinter by partial melting of the solids, which is followed by re-solidification. When the surface of the particles melts, the liquid phase that is formed on one particle mixes with the liquid formed on adjacent particles to form liquid bridges. When the temperature drops below the melting point of the liquid these bridges solidify, bonding the particles together and forming a highly porous sinter (Woollacott & Eric 1994:252).

The definition of sinter is specified by Bristow and Waters (1991:1) as a heterogeneous material that consists of particles of relict ore surrounded by a bonding matrix. The particles of unassimilated (relict) ore are different from those added initially since the outer portions have reacted with the sintering liquids, forming calcium ferrites and the relict material has undergone thermal treatment. The amount of relict material that remains after sintering will be a function of the following:

1. Resistance to assimilation of the ore.
2. The chemical compositions of the adhering layer of fines.
3. The basicity of the sinter mixture.
4. Sintering conditions.
5. The size of the initial ore particles (the larger the ore particles and the lower their prospect of assimilation, the greater will be the amount of relict material found in the final sinter).

Figure 2 is a general representation of the sinter producing process. Sintering is carried out on a moving grate reactor. The charge consists of agglomerated particles 5-30mm in diameter, which is loaded on a grate. When sintering iron oxides, the reaction is endothermic and additional fuel in the form of coke is added to the charge. Coke is used rather than coal because of the need to control the rate of combustion and the problems created by tars and other volatiles (Hayes 1993:147).

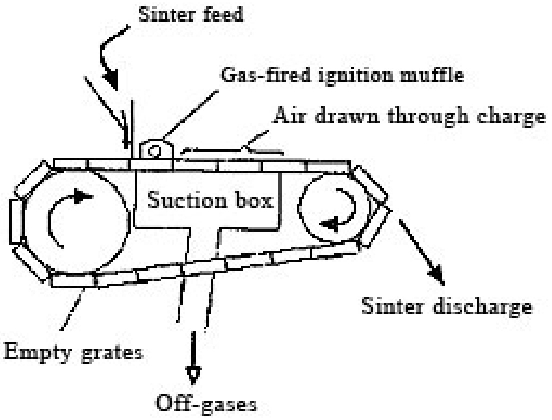

Figure 2: Generalized representation of the sinter process (Woollacott & Eric 1994:255)

It can be seen from Figure 2 that each pallet in turn moves under a charging hopper, from which the sinter mix is loaded. It then passes under a burner, which ignites the surface of the bed. The pallet then moves over a suction system, which draws a continuous stream of air through the burning bed. At the end of the strand, the pallet is carried over the end pulley of the machine, where the now sintered contents of the pallet are discharged. The sinter is then screened and cooled. Undersize material is returned to the sintering process as “recycle” (Woollacott & Eric 1994:255).

The reactions in the sinter bed are initiated by heating the surface of the charge by an external burner. When the charge has attained a temperature sufficient to sustain combustion the grate is passed over a series of wind-boxes, which suck air through the bed and results in the movement of the combustion zone from the top to the bottom of the charge. Grate sintering is thermally very efficient and temperatures up to 1600ºC can be achieved using quite modest amounts of low quality fuels e.g. 5% coke (Hayes 1993:147).

During heating some of the charge can also become molten and on cooling solid state bonds are formed between the particles. Thus, after sintering is complete, the product is physically strong and highly porous. It is then broken down into the required size ranges and fine material recycled (Hayes 1993:148).

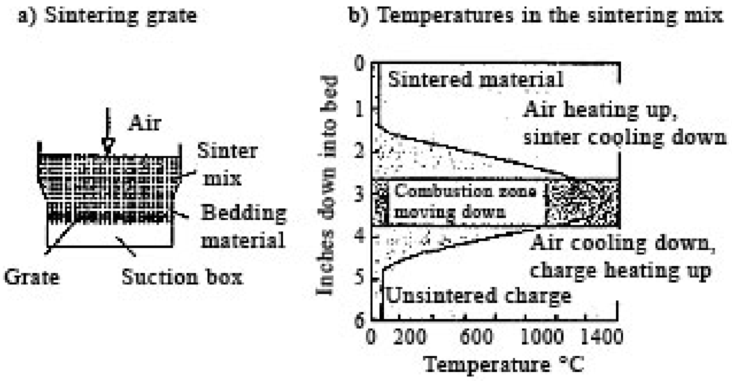

Figure 3: Conditions in a sintering grate and temperatures in the sinter mix (Woollacott & Eric 1994:253)

As shown in Figure 3 the particles become agglomerated in the zone of highest temperature therefore in the region of the combustion zone and the areas immediately adjacent to it. The air that is drawn through the bed cools the material that has already been sintered, and is itself heated in the process. It provides the oxygen needed for combustion and for any oxidation reactions that occur. The hot gases from the combustion zone pass through the unsintered part of the bed, preheating it and driving off the moisture in the mix. As the combustion zone descends, each part of the bed experiences the same sequence of events: rising temperature and evaporation of the water in the mix: very rapid increase in temperature up to the point at which combustion begins: partial liquefaction and subsequent solidification that sinters the particles together; and finally, cooling by the air drawn through the sintered material (Woollacott & Eric 1994:253).

Not only should the heating and cooling schedule be controlled during sintering but to produce components of uniform quality it is important to ensure that the thermal histories of all the components are the same. This involves monitoring the temperatures at different locations in the furnace and also giving attention to the design of components and their arrangement in the furnace. At temperatures below red heat the principal mechanisms of heat transfer are convection and conduction in the gas, and thermal conduction in the solids. At high temperatures heat transfer to the component surface will be primarily through radiation. The stacking or arrangement of components in the furnace should be such that gas can flow readily between them allowing efficient heat transfer and ensuring a uniform oxygen potential in the furnace (Hayes 1993:400).

The water content of the sinter mix affects the porosity of the sinter produced. The water aids the sintering process by bonding particles together prior to sintering. The bonding is not strong because it is the result of moisture bridges between adjacent particles, but in effect it offers to the subsequent sintering process a mass of particles that are already weakly agglomerated. If the water content is too high, the interstices of the particulate mass become flooded, the moisture bridges collapse, and the porosity decreases (Woollacott & Eric 1994:254).

If the coke used is too coarse or un-reactive, it retards combustion and lower temperatures are achieved. If the coke is too reactive the combustion may be too vigorous and the quality of the sinter will suffer. The reason for this is that fusion will be too extensive, resulting in a less porous sinter. In addition certain compounds that are not very reactive (such as FeO.SiO2) may be formed at higher temperatures (Woollacott & Eric 1994:254).

The basic concepts for high quality sinter as described by Ishikawa *et. al.* (1983:17) are reducibility, reduction degradation resistance, cold strength and high-temperature properties.

According to Pownceby and Clout (2003:44) the sinter matrix which includes solid SFCA and pores, directly determines sinter quality parameters:

1. Strength before and after reduction.
2. Sintering fuel rate.
3. Sinter softening and melting behavior in the blast furnace.

The concept of reducibility as explained by Bristow and Waters (1991:8) states that the reducibility of a material is determined by its physical and chemical characteristics. The physical factors are porosity, pore-size distribution and surface area, and the chemical factors are associated with the inherent chemical reducibility of the phases and the effect of impurities within the chemical lattice.

The process of iron ore sintering is complicated by numerous factors. Incomplete reaction in a proportion of the ores and some fluxes cause them to remain in their calcined but unreacted forms. This results in localized solid-melt mixes that are exceptionally heterogeneous and yet moderately mobile and mixing may occur. The nature of the mix may result in dissimilar distances between coke particles and the rest of the material, this will influence the local temperatures in the mix and can result in physical variations in the end product. Granulation behavior is also important in determining the structure and composition of the granules formed and thus influencing the local sintering reactions (Loo 1998:1299).

The origin of sinter porosity can be divided into two sources as explained by Lecomte (1971:25). Most ores have a closed micro-porosity in the unreacted state. When they undergo a weight loss during sintering they also acquire an open micro-porosity, due to the elimination of the carbonates and hydrates. This latter type of porosity obviously characterizes the few "undigested" grains present in the sinter, but most of the pores in sinter are the result of the liberation of gas bubbles in the sintering liquid zone and of the contraction of materials as they solidify during cooling. The pores in the first case are spherical in shape while in the second case they are elongated and irregular in form.

Meunier (1971:16) studied the influence of the Fe content, basicity, alumina content and the degree of burning on a series of sinters produced in an experimental sintering box using hematite ore. Their conclusions can be summarized as follows:

1. An increase in the Fe content (or a reduction in the quantity of gangue) produces a marked reduction in strength in the sinter while increasing its porosity.
2. An increase in the basicity index considerably reduces the coarse fractions of the sinter and markedly increases its reducibility (strength tends to pass through a minimum for a CaO/SiO_2 index of between 1.0 and 1.5).
3. An increase in Al_2O_3 content considerably reduces the strength of the sinter and its coarse fraction.
4. An increase in the fuel content markedly reduces reducibility. Generally strength passes through a maximum or reaches a more or less marked plateau between contents of 6 and 8% fuel, and increases again as fuel content increases. The amount of material in the coarse fractions and porosity decrease.

During the sinter process fines are produced due to several production activities. Sources for this production of fines include the following according to the Hoogovens Technical Services (1997):

1. At the top layer of the strand sinter material is weakened due to the temperature shock it undergoes upon exiting the flame front.
2. Along the side walls of the pallet the sinter material experiences shrinkage due to the consequent inflow of excess air.
3. Edges of the pallet do not receive sufficient heat and therefore results in incomplete sintering.
4. In general fines are also produced due to the action of the crusher and during transport of the material.
5. Fine material can also be produced by the collapse of granules during calcination.
6. Thermal stresses can lead to micro crack formation.

2. Aim of project

The aim of this project is to study the mineralogy of iron ore sinter in order to determine reasons for the production of return fines and means to prevent their formation. One of the leading sinter quality parameters is the particle size. If the sinter is too fine it will result in gas flow problems in the blast furnace. The sinter is therefore screened after production and just before entering the blast furnace. The fine material is then returned to enter the sinter production line again. This recycling process results in the loss of sinter production and therefore also loss of revenue for the sinter producing company.

If this can be accomplished then Mittal Steel South Africa at the Vanderbijl Park sinter plant will be able to increase their revenue, since less money and effort will be spent on the recycling of fines.

The aims of this project will be achieved through the following:

1. Chemical, textural and mineralogical analyses of sinter samples from the Vanderbijl Park sinter plant.
2. Verification of the composition of the SFCA phase from the Vanderbijl Park sinter plant through the synthesis and characterization of synthetic SFCA.
3. A comparison of the mineralogy of sinter from the industrial plant to the mineralogy developed in lab-based sinter test pots that were run under more controlled test conditions. This will permit an assessment of some of the hypotheses regarding fine sinter formation that were developed on the basis of analyses of industrial plant sinter.

3. Literature survey

3.1 Sinter mineralogy (previous work)

The composition of sinter according to Patrick and Lovel (2001:128) includes the following phases: iron oxides (~40-~70 vol.%), ferrites (mostly SFCA ~20-~50 vol.%), glasses (up to ~10 vol.%) and dicalcium silicates (up to ~10 vol.%). Minor phases may include quartz, sulphides, pyroxenes, serpentine and lime can also be present, but the total of these rarely accounts for more than a few percent of the total sinter volume.

A brief discussion of each phase follows.

3.1.1 Hematite

Hematite is one of the most abundant phases in sinters and it can be present as either relict hematite or secondary hematite. The relict hematite is present as a result of the incomplete reaction of the original phase present in the ore and can be recognized by its irregular shape and its reacted or corroded grain boundaries. The secondary hematite forms during the sinter process and it is characterized by its euhedral crystal shapes and smooth grain boundaries.

The hematite phase tends to diminish with increasing temperature thus favouring the formation of the magnetite and calcium ferrite phases. In the case of a relatively low temperature the hematite phase is mostly polycrystalline residual (primary) hematite. Nevertheless at a higher temperature rhombohedral skeletal hematite (secondary hematite) forms (Pimenta & Seshadri 2002:170). Secondary hematite is usually square in form and larger in size than primary hematite (Kama *et. al.* 1984:330).

Figure 4 depicts a grain of relict hematite which is surrounded by the SFCA phase under reflected light. The porous nature of the sinter material is apparent. Hematite is distinguished by its high reflectance (bright white color) and its anisotropic nature. This sample was obtained from the Vanderbijl Park sinter plant.

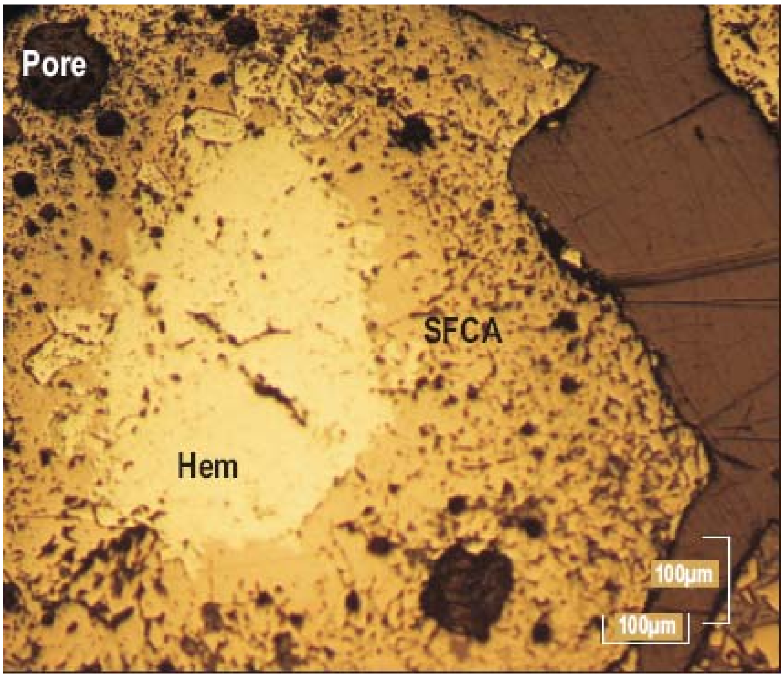

Figure 4: Optical micrograph of relict hematite (Hem) surrounded by the ferrite phase (SFCA). Pores of variable size can also be seen.

Rhombohedral hematite has been ascribed as the phase in which much cracking in sinter is initiated, and petrographic examination of sinters have revealed that C_2S is often closely associated with this phase and tends to crystallize along its boundaries. There is thus a possibility that C_2S inversion may play some contributory role in the development of defects in skeletal rhombohedral hematite (Patrick & Lovel 2001:133).

Figure 5 show grains of secondary hematite together with magnetite and the melt phase. The phases that are associated with high melt zones include silicate, ferrite and magnetite (Choudhary 2007:517). This sample was obtained from the Vanderbijl Park sinter plant.

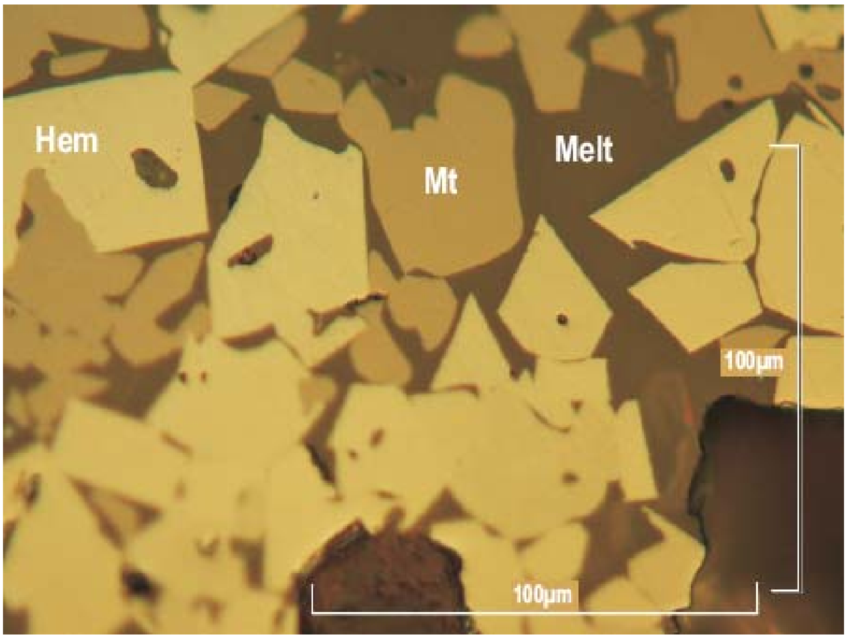

Figure 5: Optical micrograph of secondary hematite (Hem) with magnetite (Mt) and glass (Melt). Note the smooth crystal boundaries of the secondary hematite.

3.1.2 Spinel

Magnetite is an important component in the sinter and it is usually present in quantities approaching 20-30% by mass. It usually contains smaller quantities of MgO and Al_2O_3 and it is usually distinguished under the optical microscope from a spinel phase which contains approximately 6-12% MgO by mass. Figure 5 shows magnetite crystals occurring with hematite and glass under reflective light. Magnetite has an off white color and is isotropic.

Loo (1998:1301-1307) describes the involvement of magnetite during the sinter process as being part of two reaction stages namely “at calcination” and “during melting/reaction”. To start with it is well known that magnesia-bearing minerals have a large influence on sinter magnetite content. The reason is that magnesia stabilizes the formed spinel, forming a magnetite-magnesio-ferrite (Fe_3O_4 - $MgO.Fe_2O_3$) solid solution which is considered to be more stable than magnetite ($FeO.Fe_2O_3$) (Loo 1998:1301-1307). Compared to serpentine $(Mg,Fe)_3Si_2O_5(OH)_4$, dolomite ($CaMg(CO_3)_2$) greatly increases the sinter magnetite content. The MgO from dolomite after calcination is extremely mobile and quickly diffuses (in the solid state and probably as cations) out to surrounding areas. The diffusion of Mg^{2+} into hematite causes its transformation to magnetite/magnesio-ferrite. The mechanism involved could be explained as follows: the presence of Mg^{2+} lowers the decomposition temperature of hematite to magnetite because:

1. Diffusing Mg^{2+} in hematite causes a charge imbalance which can be alleviated by the hematite giving up O^{2-} i.e. converting to magnetite, and
2. The hematite structure can not accommodate the Mg^{2+} unless it transforms to magnetite.

The calcination of certain minerals in the ores can therefore cause the reduction of surrounding hematite to magnetite at lower temperatures (Loo 1998:1301-1307).

Secondly, under atmospheric conditions hematite decomposes to magnetite at around 1390ºC, but this temperature decreases by as much as 200ºC at an oxygen partial pressure of 0.002 atm. Increasing sintering temperatures, or lowering the pO_2 by carbon addition (decreased coke addition) will therefore increase hematite decomposition and increase the magnetite level in sinter (Loo 1998:1301-1307).

Another factor that could have an impact on sinter magnetite content is the properties of the melt. This relates particularly to the Fe^{3+}/Fe^{2+} value of the melt. It has so far been assumed that assimilation of magnetite will increase the Fe^{2+} content of the melt and that this will then result in increased magnetite precipitation during cooling, but this may not always be true. The Fe^{3+}/Fe^{2+} value of a melt can also vary depending on the chemical composition of the melt. It has been found that Ca^{2+} influences the equilibrium conditions of the iron oxides in the melt and increases the Fe^{3+}/Fe^{2+} ratio. It is possible that SFCA formation is enhanced by high basicity not just because lime is essential for its formation, but also because the Fe^{3+} content of melt is favoured over Fe^{2+}. It would also appear that the conversion of Fe^{3+} to Fe^{2+} is easier than from Fe^{2+} to Fe^{3+} as the former involves the evolution of oxygen from the melt, whereas the latter requires the dissolution of atmospheric oxygen into the melt, and the kinetics of this process can be expected to be slow. If this was the case, oxygen partial pressure would not greatly influence the Fe^{3+}/Fe^{2+} value (Loo 1998:1301-1307).

3.1.3 Dicalcium silicate

Dicalcium silicate occurs as discrete crystals interstitial to the oxide phases and along their grain boundaries. It is distinguished from the melt phase by a lamellar texture and light yellow colour. Figure 6 shows C_2S and magnetite under reflected light. The lamellar texture is apparent. The sample is from the Vanderbijl Park sinter plant.

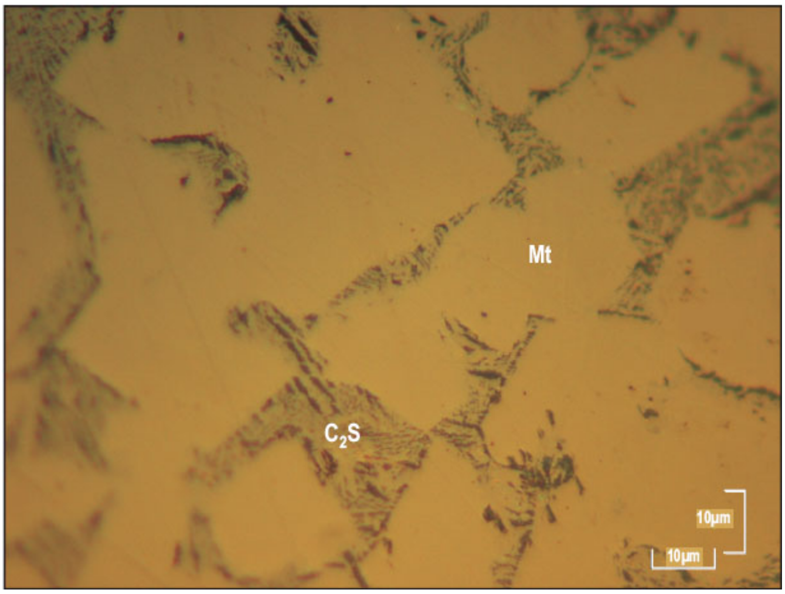

Figure 6: Micrograph of C_2S surrounding magnetite (Mt) crystals

The effect of C_2S in iron ore sinter is explained by Patrick & Lovel (2001:129). It has been recognized that the potential loss of sinter strength may be a result if the β to γ transition that dicalcium silicate undergoes during cooling. Some significant properties of C_2S include:

1. They are the only essentially Fe-free phases in sinter. Small amounts of Fe can substitute into dicalcium silicates in sinters but is usually <1 mass%.
2. They are relatively unstable, suffering from five temperature / composition / microstructure dependent phase transitions between α, α'_H, α'_L, β and γ polymorphs, which can be accompanied by significant volume changes that are known to cause the phase to break down or "dust" in some cases.
3. C_2S is known to incorporate a wide variety of impurities (Cr, K and P (Patrick & Lovel 2001:134)) in several different systems, including those relevant to the cement industry and steelmaking slags, where they preferentially concentrate undesirable components.
4. The incorporation of impurities in the crystal lattice can stabilize different polymorphs of C_2S and thereby inhibit phase transformations.
5. The theoretical basicity (CaO/SiO_2) of C_2S is 2.0.

At sintering temperatures the α'_H (orthorhombic) polymorph should be stable (1177-1425ºC) although it is also possible that thermal heterogeneities could result in local zones of stability for either the α (hexagonal; 1425-2150ºC) or α'_L (orthorhombic; 850-1177ºC) polymorphs. Another complication is that the sintering process (including air cooling) is relatively fast, and so kinetic effects may also play an important role in determining which phases will crystallize (Patrick & Lovel 2001:129).

3.1.4 CF and C_2F

CF and C_2F are minor phases in commercial sinters, and they probably form only during the early stages of sintering and were not present in the samples analyzed for this project. The CF concentration appears to increase in direct proportion to the amount of aluminium in the sample. The rate of hematite consumption decreases near the maximum CF concentration, but this decrease is more apparent with samples that contain less alumina. This may indicate the preferential consumption of hematite with increased alumina content (Scarlett *et. al*. 2004:365). CF commenced formation between T = 920°C and 1000°C. CF initially coexisted with C_2F, the latter declining as the amount of CF increased. The decomposition of C_2F is explained by the subsequent reaction of the first formed C_2F with the excess hematite still present in the mixture. The amount of CF reached a maximum when all of the C_2F had been consumed. The CF phase completely disappears at T = 1200°C to 1220°C (Scarlett *et. al*. 2004:932).

C_2F is stabilized by the presence of alumina. The measured hematite content in samples decrease as it reacts with lime in the formation of C_2F according to the following reaction: $2CaO + Fe_2O_3 \rightarrow Ca_2Fe_2O_5$ (Scarlett *et. al*. 2004:365). The fact that C_2F forms first between T = 750°C and 780°C indicates that the dominant reaction mechanism favoured at low temperatures is the solid state reaction between individual CaO and hematite particles (Scarlett *et. al*. 2004:932).

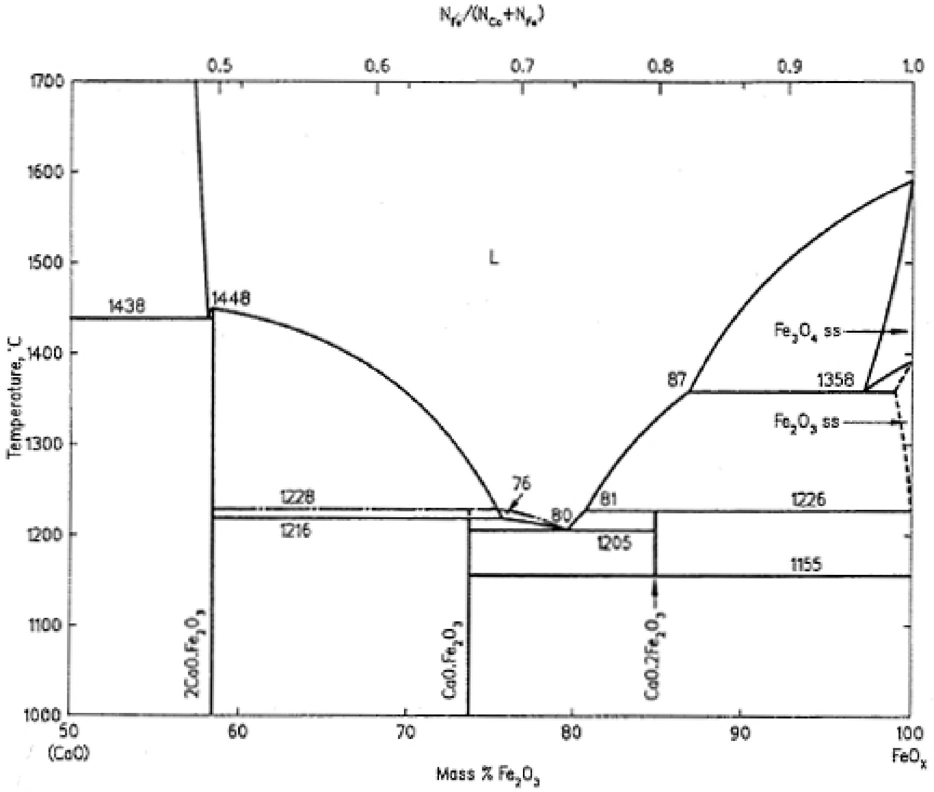

Figure 7: CaO-FeO$_x$ system in air. The dash-dot line represents the decomposition temperature of CaO-Fe_2O_3 (Verein Deutscher Eisenhuttenleute. 1995).

Figure 7 show the CaO-FeO_x system in air. It shows that C_2F is stable at 58% Fe_2O_3 at temperatures ranging from 1000 to 1448°C. CF is stable at 74% Fe_2O_3 at temperatures ranging from 1000 to 1228°C (Verein Deutscher Eisenhuttenleute. 1995).

3.1.5 SFCA phases

The calcium ferrites usually contain some silica and alumina and are thus referred to as silicoferrites of calcium and aluminium abbreviated to SFCA (Hamilton *et. al.* 1989; Mumme *et. al.* 1998; Mumme 2003). They form the main bonding phase in sinter (Scarlett *et. al.* 2004:362). Three different phases have been identified. A brief description of each will be given and followed by their formation reactions and characteristics.

Figure 8 (sample from the Vanderbijl Park sinter plant) shows the optical micrograph of the SFCA phase in association with numerous pores. SFCA is medium grey in colour and has three different textures corresponding to the three different types (see Table 4). These textures are only a practical guideline that were used and has not been proved yet.

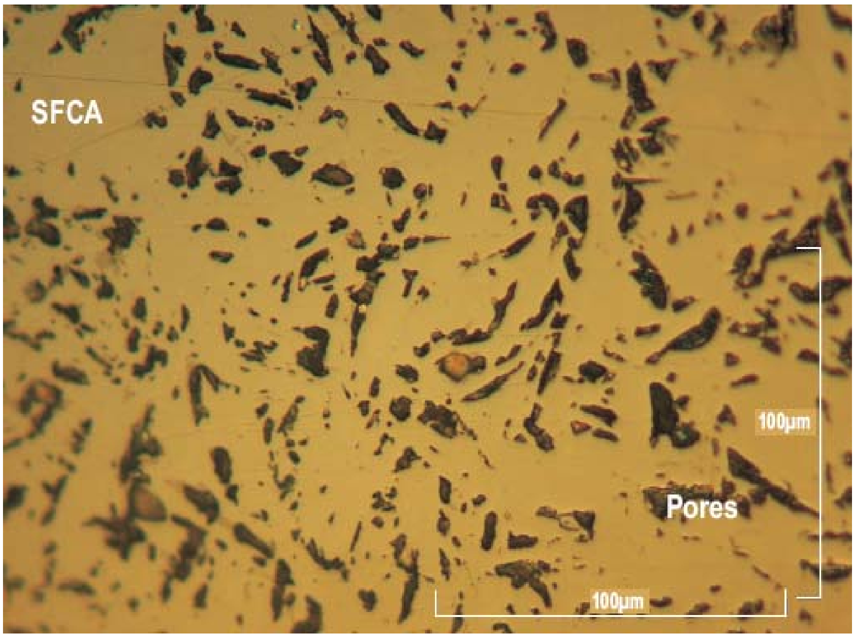

Figure 8: Optical micrograph of SFCA showing its columnar texture

Table 4: Correlation between SFCA phases and their associated textures (Mashao 2007)

Name	Texture
SFCA	Columnar
SFCA I	Acicular
SFCA II	Dendritic

According to Scarlett *et. al.* (2004:929) SFCA has a prismatic form, and its morphology can be referred to as columnar, blocky or lath shaped. SFCA I has a characteristic platy morphology and in cross section appears needle-like or acicular.

Bristow and Waters (1991:9) describe the importance of SFCA as follows: It promotes high-temperature reduction by stabilizing the fine porosity formed during the early stages of reduction and thereby influence granule design. The SFCA content of sinter will need to be increased to maximize the reducibility benefits it confers in combination with relict hematite. There will be an associated range of SFCA-hematite contents that will be associated with maximum reducibility.

SFCA has a layered structure with metal atoms occupying octahedral and tetrahedral sites within the layer framework of oxygen atoms (Hamilton *et. al.* 1989:1-14). Untwinned single crystals of SFCA were grown by these authors using a PbO/Bi_2O_3 flux-melt system. The single crystal X-ray diffraction data collected from one of them were used for crystal structure analysis. Chemical and structural data derived suggest that cation substitution in the SFCA phase $Ca_{2,3}Mg_{0,8}Al_{1,5}Si_{1,0}Fe_{8,3}O_{20}$ follow the mechanism $2(Al,Fe^{3+}) <-> Ca(Mg^{2+}) + Si^{4+}$for charge compensation. This mechanism is supported by EMPA results that showed that low lime fluxed pellets produced SFCA of low silica content and vice versa which corresponds to the proposed substitution mechanism (Hamilton *et. al.* 1989:1-14).

The almost ideal close packed nature of the layers in the SFCA structure is the reason for its good bonding characteristics. A “semi-epitaxial” overgrowth of hematite crystals occurs, thus providing stronger bonding that would normally exist between two unrelated crystal structures (Hamilton *et. al.* 1989:19).

Mumme *et. al.* (1998:94) then described the crystal structure of a new calcium ferrite phase that is called SFCA I and is related to SFCA by an increased width of the octahedral and tetrahedral walls in the alternating layers comprising its structure. SFCA I has a distinctive “platy” nature. The composition of the silica free SFCA I is $Ca_{3,18}Al_{1,34}Fe^{3+}_{14,66}Fe^{2+}_{0,82}O_{28}$. It was observed that the crystal structures and compositions of SFCA and SFCA I bear a homologous relationship to one another of the form $M_{14+6n}O_{20+8n}$ for values of n = 0 and 1. In SFCA I just as in SFCA, Ca octahedra are located at the edges and centres of the octahedral walls. However in SFCA I (probably to maintain the integrity of the widened walls) alternate pairs of octahedral rows contain additional distorted Fe^{2+} octahedra at the centre of the walls, edge-sharing with the central Ca octahedra, thus forming a continuous sub-chain of paired Ca and Fe^{2+} octahedra running down through the middle of each wall.

The structural characteristics determined for SFCA and SFCA I suggest there is a strong possibility of intergrowth structures forming at least between these two members of this group. Such an effect may tend to blur the compositions of any homologues of SFCA that form in this region of the phase diagram, making it difficult to assign them to lines of constant *n*, wherever solid solutions ranges may overlap. This is apart from the effect that the individual member substitution of Ca by Fe^{2+} has on the solid solution series. Therefore the composition lines defined by the substitution mechanism $2Fe^{3+} = Si^{4+} + Ca^{2+}$ will be displaced (Mumme *et. al* 1998:115).

According to Scarlett *et. al*. (2004:365) SFCA exists as a homologous series of the aenigmatite structure type. The type and morphology of the SFCA phase generated depends critically on the chemical composition of the sinter mixture as well as the processing conditions of sintering. The reactions for the formation of the SFCA phases (although unbalanced) are:

1. $CaFe_2O_4 + Fe_2O_3 + SiO_2$ $(+Al_2O_3)$ -> SFCA I + SFCA
2. SFCA I + $Fe_2O_3 + SiO_2$ $(+Al_2O_3)$ -> SFCA

Mumme (2003:309-332) completed a new attempt at preparing and identifying the true nature of a so-called ternary phase. Flux growth of single crystals at 1250°C from the composition CAF_2 resulted in the formation of a new calcium ferrite phase which is shown to have overall stoichiometry $M_{34}O_{48}$. This phase has a crystal structure which is a composite of the previously described homologues SFCA and SFCA I. This phase is composed of layers of octahedral walls with an intermediate width of 5 octahedra, alternating with tetrahedral layers in which the different components of this type of layer found in SFCA and SFCA I, themselves alternate, resulting in a composite unit-cell volume for the new structure and stoichiometry $M_{34}O_{48}$. This new structure is labelled SFCA II. Therefore the overall structure of SFCA II with its intermediate width in the octahedral wall layer and sequencing of ribbons in the tetrahedral layer represents a composite or mixture of SFCA and SFCA I structure types. Appropriately the unit cell volume of SFCA II is nearly the sum of the cell volumes of SFCA and SFCA I.

Figure 9 shows the three SFCA compositions (in wt%) in the CaO-Al_2O_2-Fe_2O_3 system.

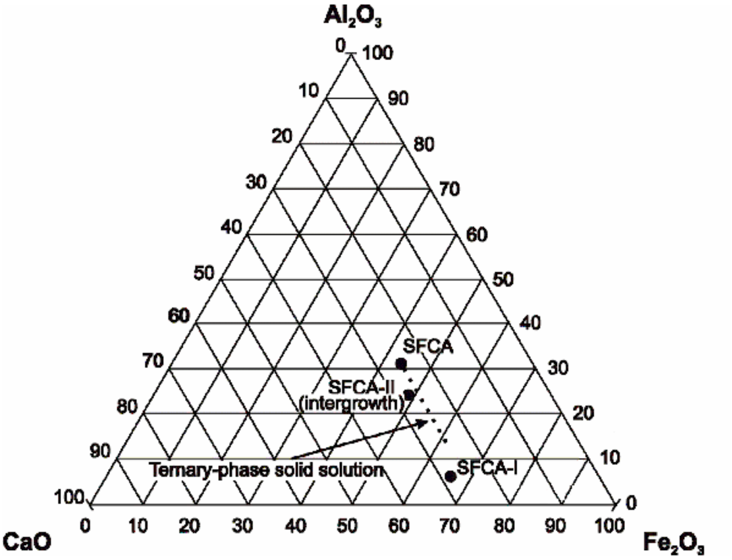

Figure 9: Compositional plot showing a section of the CaO-Al_2O_3-Fe_2O_3 phase diagram with SFCA, SFCA I and SFCA II types (Mumme 2003:319)

The near coincidence of the three unique phase points with the so-called solid-solution range, and the progressive variation in critical *d*-spacings in their individual powder X-ray data sets is the reason why there has been confusion with single-phase solid-solution formation in this part of the phase diagram. This effect would be compounded by any disorder and solid-solution (predominantly between Al and Fe) in each of the three homologues so far determined. In addition, the formation of further unique intermediate (intergrowth-like) phases cannot be discounted (Mumme 2003:333).

3.1.6 SFCA reaction characteristics

The study by Pownceby & Patrick (2000:461-464) involved the thermal stability and phase relationships of SFC in the FCS system. SFC_{ss} is a silicoferrite of calcium solid solution and Liq_{α} is a high iron melt phase) stabilized at low temperatures (T = 1240°C). At 1260ºC SFC is not a stable phase, but instead melts incongruently to produce the two-phase assemblages Hem+Liq. At 1250ºC the appearance of SFC as a stable crystalline phase occurs. The SFC solid solution range is very narrow at 1250ºC extending from approximately 8.0 to 11.5wt% C_4S_3 along the CF_3-C_4S_3 pseudobinary. At the high CF_3 end of the pseudobinary single phase SFC was not stable, but decomposed to produce the three-phase assemblage Hem+SFC+Liq.

This study (Pownceby & Patrick 2000:461-464) was done to determine the liquidus temperature for SFC. Melting appears to be asymmetric with the more CF_3-rich composition melting at slightly lower temperatures than the C_4S_3-rich member.

A decrease in equilibration temperature to 1250ºC results in a slight increase in the solid solution range of SFC. At 1240ºC the solid solution breadth is estimated to lie between about 7.0 and 11.5 wt%. The solid solution range between the 1240ºC SFC end-member compositions is slightly broader implying increased stability at lower temperatures. The compositional range measured at 1240ºC is also approximately equal to the ranges determined for all experiments within the interval 1225-1150ºC. This solid solution range therefore appears to be the maximum possible for SFC. Lowering the equilibrium temperature to 1150ºC results in all phases becoming subsolidus and there is a perceptible decrease in the kinetics of SFC formation. At all temperatures greater than 1192ºC, the gradient of single phase SFC data in the plots of wt%Fe_2O_3 versus wt%C_4S_3 are remarkably constant. Below 1192ºC there is a visible reduction in slope with compositions higher in C_4S_3 component having apparently higher Fe_2O_3 than for the same compositions equilibrated at higher temperatures (Pownceby & Patrick 2000:461-464).

Results from experiments conducted at the 1060ºC isotherm indicated that SFC remains as a stable crystalline phase at this temperature. In comparison, the 1050ºC isotherm is clearly below the lower temperature stability limit of SFC as indicated by the decomposition of SFC to the assemblage Hem+CF+C_2S in the breakdown experiments using pre-synthesized SFC compositions and the failure to produce any SFC phase in the oxide synthesis charges. Therefore the lower limit for low temperature breakdown of SFC phase is within the temperature interval 1050-1060ºC (Pownceby & Patrick 2000:461-464).

The ability to re-form SFC from the high temperature Hem+Liq assemblage also appears to be limited (see Figure 10). All compositions examined consistently record crystallization peaks at around 1187-1193ºC. If the temperature during sintering exceeds the liquidus of SFC and is followed by rapid cooling (i.e. $\geq$ 10ºC/min), the above results indicate that SFC will not form via a down-temperature precipitation reaction involving hematite and liquid. Low C_4S_3 compositions will produce a liquid phase which will evolve towards the ternary eutectic minimum at 1192ºC following the crystallization path shown in Figure 10 (heavy line). High C_4S_3 compositions will follow a crystallization path which first reaches an invariant point at T~1216ºC (Pownceby & Patrick 2000:461-464).

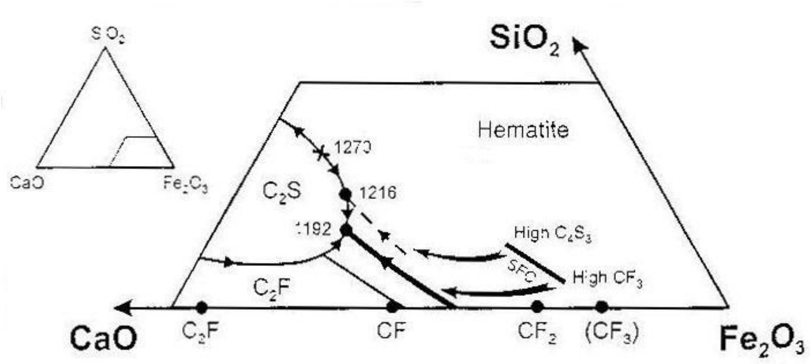

Figure 10: Schematic ternary phase diagram showing projected down-temperature liquid evolution paths: Liquids derived from the melting of high C_4S_3 SFC compositions follow the dashed path to the invariant 1216ºC point, then down to the 1192ºC eutectic. Low – C_4S_3 SFC compositions produce liquids which migrate directly towards the 1192ºC eutectic (heavy line). Point “X” at 1273ºC is a thermal maximum within the FCS system (Pownceby & Patrick 2000:465)

The phase diagram for the CF_3-rich part of the CF_3-C_4S_3 binary system in air is shown in Figure 11 by following the crystallization path for each experimental composition of the pre-synthesized SFC compositions prepared by Pownceby & Patrick (2000:461-464) for this study. Although constructed as a binary it is however, strictly classified as a pseudobinary because:

1. The end-member compositions CF_3 and C_4S_3 do not exist as discrete phases and,
2. The compositions of some of the crystalline and liquid phases can not be expressed in terms of the chosen components and therefore deviate from the binary plane.

This Figure shows a series of isothermal sections that predicts phase relationships within the expanded FCS ternary.

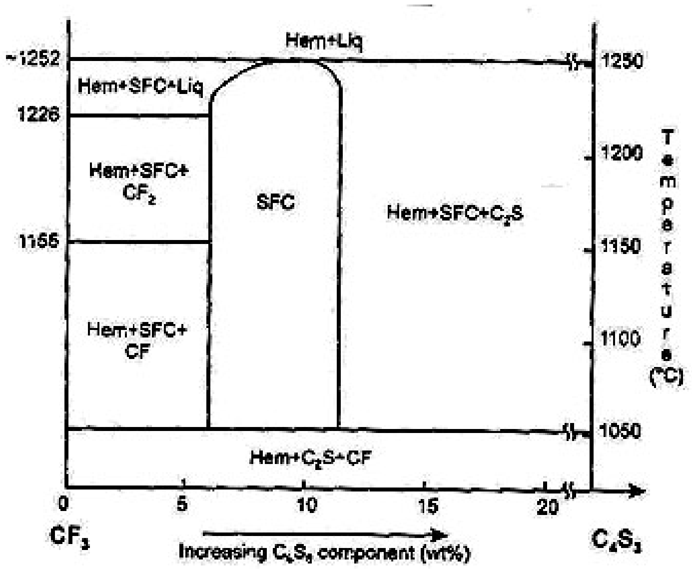

Figure 11: Diagram showing phase stability along the pseudobinary join CF_3-C_4S_3 in air (Pownceby & Patrick 2000:466).

Pownceby & Clout (2003:45-49) investigated the thermal stability of FCS system in air and at $pO_2 = 5x10^{-3}$atm. Results for the FCS system in air are shown in Figure 12*a-c*. At temperatures above 1270°C a continuous, liquid only, phase field extends from Fe_2O_3 rich to SiO_2 rich compositions. Below 1270°C, the liquid phase field segregates into two distinct melt regions: one at high Fe_2O_3 contents and basicities (CaO/SiO_2) greater than B = 2.0 and a second melt field at low basicities (B < 2.0) and high SiO_2 contents. The melt field at high basicities result in calcium ferrite(s) crystallizing upon cooling, while the low basicity melt field crystallises calcium silicate(s) and hematite. The composition of the first melt to develop in the FCS system therefore depends strongly on the basicity. At 1240°C, SFC is part of the crystallizing assemblage. However between 1240°C and 1255°C, SFC becomes unstable and breaks down to give the phase assemblage Hem + Liq or Hem + C_2S + Liq depending on temperature and composition. Further work on the stability of SFC indicated that SFC forms a solid solution along a line between the theoretical end members CF_3 and C_4S_3, within the range 7.0-11.5 wt%C_4S_3. The SFC was found to be stable between 1060°C and 1252°C. It has also been concluded that the maximum liquidus temperature for SFC is composition dependant with the highest melting point (T = 1252°C) corresponding to a sample containing 9.0wt%C_4S_3 (Pownceby & Clout 2003:45-49).

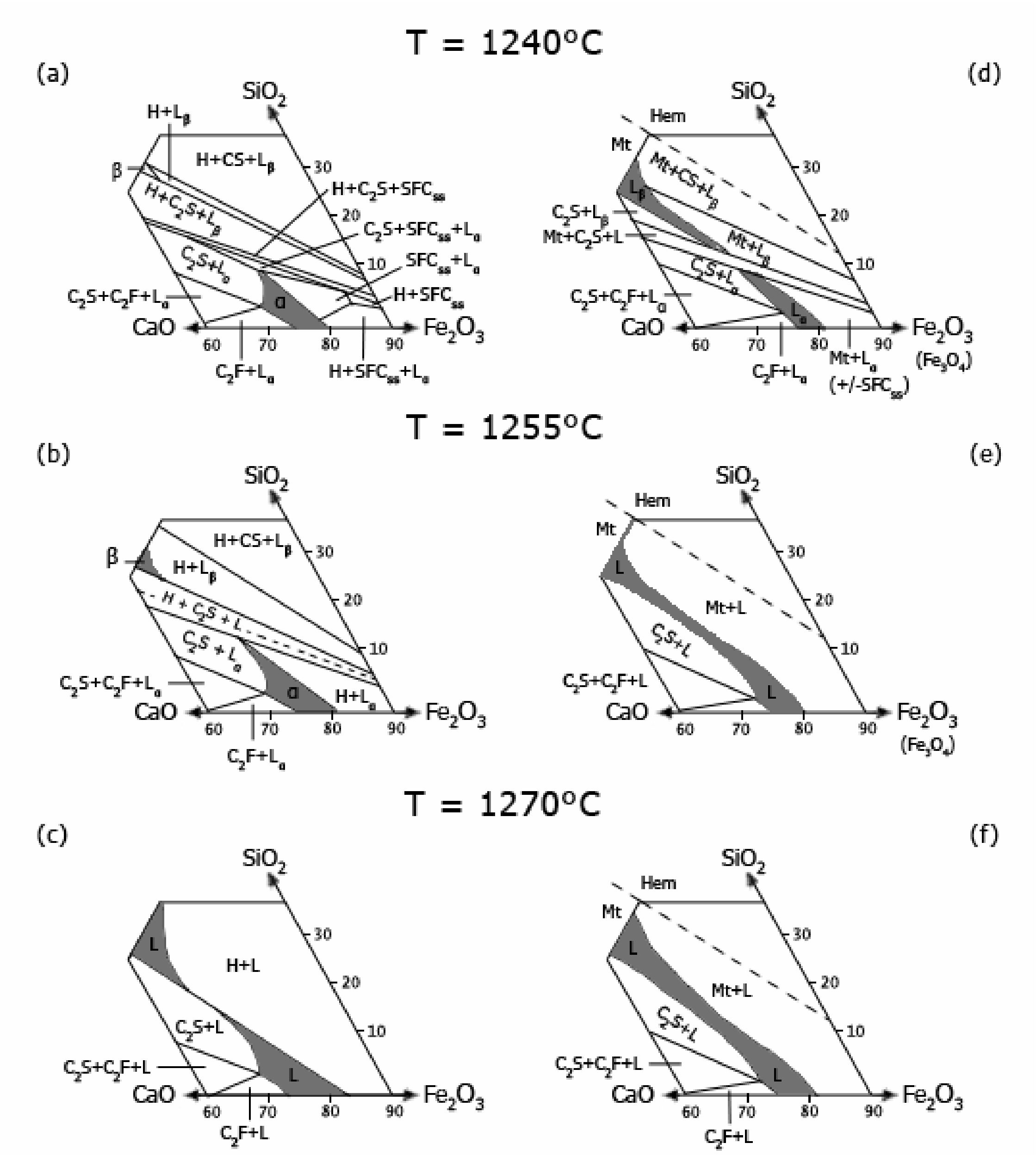

Figure 12: Summary of phase relations determined for the Fe_2O_3-CaO-SiO_2 ternary system between 1240°C and 1300°C (12*a-c* are from experiments conducted in air, while 12*d-f* are from experiments at $pO_2 = 5x10^{-3}$atm) (Pownceby & Clout 2003:46)

Results for FCS at $pO_2 = 5x10^{-3}$atm are shown in Figure 12*d-f*. The effect of lower oxygen partial pressures in the FCS system causes a number of significant changes compared with the equivalent system in air:

1. Effect on melt formation

At lower oxygen partial pressures, the liquidus temperature has been depressed with the single, liquid only field not segregating into two distinct fields until below 1255°C-1250°C. Moreover, at all temperatures examined, the lower oxygen conditions have significantly enlarged the field of silicate melt present, relative to that of calcium ferrite melt. As the pO_2 decreases, more Fe^{2+} is generated, which exerts a greater influence on melt region β, reflecting the presence of the silicate melt for Fe^{2+}.

2. Stability of magnetite

The field of magnetite stability has been greatly increased while hematite is limited to the low Fe, high SiO_2 regions of the diagram. The occurrence of any particular iron oxide phase is closely linked to the overall basicity of the charge with magnetite more likely to form at high basicities whereas hematite is stable at low basicities.

3. Stability of SFC

SFC can not be produced as a single, unique, crystalline phase under reduced oxygen partial pressures. The bulk composition lies within the partially reduced Fe_2O_3(-Fe_3O_4)-CaO-SiO_2 pseudoternary system with the three phase assemblage Mt + SFC_{ss} + Liq_{α} (where Mt is magnetite) (Pownceby & Clout. 2003).

In their paper Pownceby & Clout (2000:45-47) discuss the phase relations of the FCS system at a partial oxygen pressure of $5x10^{-3}$atm. Firstly the interpretations of reaction/crystallization sequences are discussed. In industrial iron ore sintering the raw material (dominated by Fe_2O_3, CaO, SiO_2 and minor amounts of Al_2O_3) is heated by the combustion of coke particles, which form a low-pO_2 environment initially, and is then cooled under high pO_2. If the results obtained for the Fe_2O_3-CaO-SiO_2-system in air and those reported in this study for the Fe_2O_3-Fe_3O_4-CaO-SiO_2 system at reduced oxygen partial pressure are taken as end-members of a model sinter system, the following can be proposed as a typical reaction sequence:

1. In the heating stage of sintering at low pO_2 a CaO-SiO_2-rich melt will form in reasonable quantities at temperatures of more than about 1200ºC. This initial melt reacts with hematite ore particles to form ferrite bonding phases, including SFC_{ss} (up to *ca* 1255ºC). As the temperature continues to rise the magnetite content will increase and the hematite content will decrease. Assimilation of hematite iron ore particles will proceed through reactions with the melt until either the temperature drops and the melt solidifies, or solidification occurs because of dissolution of solid iron oxide material into the melt that results in a change to the chemical composition of the melt.
2. During cooling, if the oxygen partial pressure is not maintained at low values, magnetite will at least partially reoxidize to secondary hematite. The phase that

will crystallize from the melt phase during cooling to less than 1270ºC are determined largely by a thermal maximum, which occurs in the system Fe_2O_3-CaO-SiO_2 at around 50.0% Fe_2O_3-32.0% CaO-18.0% SiO_2. Provided that the basicity is higher than about B = 1.8-2.0, once temperatures are less than *ca* 1270ºC the crystallization path will proceed down-temperature towards the Fe_2O_3-rich apex of the ternary and ultimately result in the precipitation of minor hematite, SFC_{ss} and calcium ferrite(s). Conversely, if the basicity is less than about B = 1.8, a decrease in temperature would follow a crystallization path that leads to precipitation of minor hematite and calcium silicate(s), particularly larnite, and in some cases Fe-rich clinopyroxene. Figure 13 is a schematic diagram that shows the projected crystallization paths at temperatures less than 1270ºC.

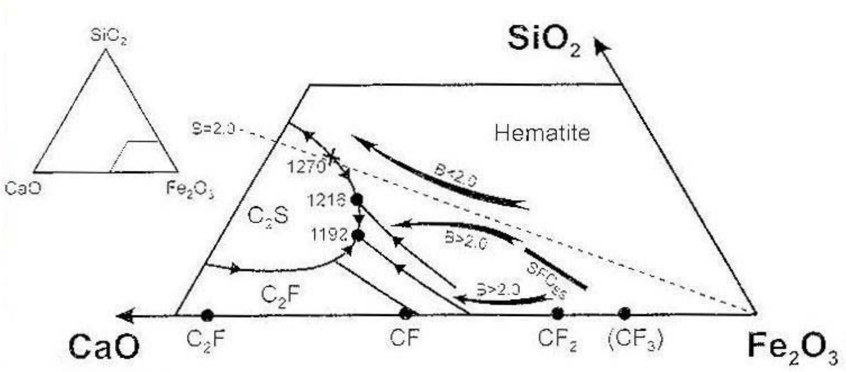

Figure 13: Schematic ternary phase diagram showing projected down-temperature, crystallization paths. Liquids derived from melting of high-basicity (B>2.0) compositions follow crystallization paths (depending on bulk composition) down toward 1192ºC eutectic resulting in precipitation of Fe-oxide (magnetite or hematite) and calcium ferrite(s). Low-basicity compositions follow crystallization path leading to precipitation of minor Fe-oxides and calcium silicate(s). Point *X* at 1270ºC is a thermal maximum within FCS system in air (Pownceby & Clout. 2000:46)

The interpretation of the formation of ferrite bonding phases is described as follows: The combined studies of the simple FCS system in air and at a reduced partial pressure of oxygen have significant implications for maximization the stability of SFC_{ss} (and therefore also SFCA) the phase that imparts considerable strength to iron ore sinter. For example, to maximize the production of SFC_{ss} two approaches may be employed. One is to generate the SFC_{ss} initially and to avoid its transformation to hematite and/or magnetite and silicate melt during the heating stage by ensuring that the reacting temperature is not too high but that the oxygen partial pressure remains quite high. The other is to provide high melt basicity and a favourable cooling regime that will produce SFC_{ss} from the reaction of hematite, melt and oxygen. No matter which method is employed, a low heating temperature is necessary for the formation of SFC_{ss}. The first scheme, of low temperature and high pO_2 during heating, is attractive in that lower fuel rates (i.e. less coke in the initial sinter mix) would be required. Lower temperatures are important since SFC_{ss} melts at around 1255-1260°C. The second approach, of a high basicity and a more favourable cooling regime, is probably less attractive to sinter producers since higher slag volumes will ultimately be obtained from the blast furnace and a more regulated cooling environment would need to be maintained in the sinter plant (Pownceby & Clout 2000:45-47).

At present, iron ore sinter is simply allowed to cool in air, but the foregoing results indicate that reactions will continue to occur during the cooling process, with the possibility of formation of a Fe-rich SFC_{ss} at temperatures less than 1250-1255°C via precipitation from Fe-rich liquid. The formation of SFC_{ss} is, however, strongly influenced by the kinetics of the down-temperature precipitation reaction and if quench rates are high, SFC_{ss} formation is not favored, i.e. the melt does not have sufficient time to react with the hematite to reform SFC_{ss} and the liquid composition will evolve, therefore, along a crystallization path towards the 1192°C invariant point shown in Figure 18. Thus, to ensure maximum production of SFC_{ss} within iron ore sinter the cooling rate needs to be carefully controlled (Pownceby & Clout 2000:45-47).

In the study by Scarlett *et. al*. (2004:929-930) the *in-situ* X-ray diffraction method was used to determine the sequence of reactions involved in the formation of SFCA and SFCA I. Experiments were conducted on synthetic sinter mixtures within the temperature range of T = 22°C to 1260°C and using a maximum heating rate of 10°C/min. This heating rate is significantly lower than those operating during industrial sintering processes where heating rates of more than 1000°C/min are typical. The slower rate used in the study was necessary to ensure accurate identification and quantification of all phases formed/consumed.

The results indicate that SFCA and SFCA I both started to form at $T < 1200°C$. The formation of these SFCA phases coincided with the first evidence of a decrease in the amount of quartz present (quartz is consumed in the SFCA forming reactions). The results indicated that SFCA I and SFCA formation is more rapid in the higher alumina containing mixture compared to the lower alumina containing and alumina free mixtures. The alumina appears to increase the stability range of SFCA phases by lowering the temperature at which they begin to form (Scarlett *et. al*. 2004:933-934).

Phase formation is dominated by solid-state reactions, mainly in the system $CaO-Fe_2O_3$. Hematite initially reacts with CaO at low temperatures (T ~ 750°C to 780°C) to form the calcium ferrite phase C_2F. The C_2F phase then continues to react with hematite, producing CF (T ~ 920°C to 1000°C). The CF is stable up to T ~ 1200°C. The presence of alumina increases the temperature at which both ferrite phases initially form. Quartz does not react at all with CaO and hematite, remaining essentially inert until SFCA and SFCA I begin to form around T = 1050°C. The formation of both SFCA types proceeds initially via a solid-state reaction mechanism (Scarlett *et. al*. 2004:936).

Many authors have attempted to describe the compositional variation and solid solution behavior of SFCA. The compositions were plotted on ternaries such as shown in Figure 14. The diagram on the left in Figure 14 shows a shaded area which represents the region where most SFCA compositions form in industrial iron ore sinters. The ……. line represents previous work by Inoue & Ikeda (1982/68), _._._ work by Dawson *et. al.* (1983/27) and ----- work by Hamilton *et. al.* (1989/161). The ternary used by (Patrick & Pownceby. 2002:80) shown on the right side of Figure 14 indicates the compositional variation on the $Ca_4Si_3O_{20}$ – $CaFe_6O_{20}$ – $CaAl_6O_{20}$ ternary diagram. In shorthand notation: C_4S_3 – CF_3 – CA_3 as shown on the right side of Figure 14 with the shaded area representing the region where most SFCA compositions form in industrial iron ore sinters.

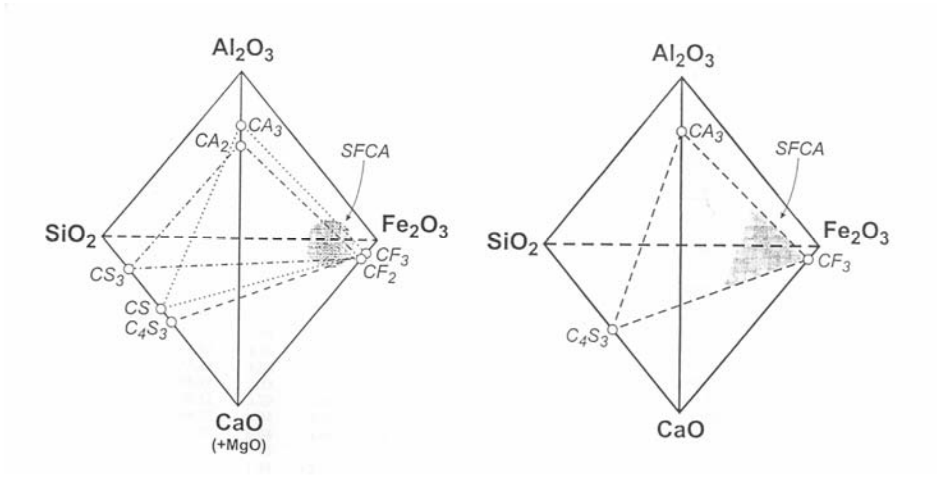

Figure 14: The ternary system which portrays the composition of SFCA (Patrick & Pownceby 2002:80)

In the study by Patrick & Pownceby (2002:79-80) their previous work were expanded to systematically resolve the solid-solution range and thermal stability of SFCA within the four component Fe_2O_3-CaO-Al_2O_3-SiO_2 (FCAS) system. Assuming the ternary solid-solution along the CF_3-C_4S_3 pseudobinary is valid for SFCA, as well as SFC, and that Al^{3+} directly substitutes for Fe^{3+} in four component SFCA, the SFCA solid solution was anticipated to lie in the CF_3-CA_3-C_4S_3 (CCC) plane as shown in Figure 15.

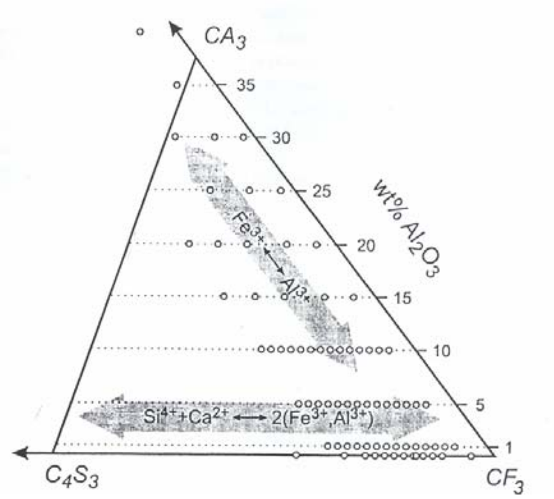

Figure 15: Representation of the two substitution mechanisms in SFCA. The unfilled circles indicate synthetic compositions prepared by Patrick & Pownceby (2002:80)

The SFCA solid solution is characterized by two main substitution mechanisms:

1. Al^{3+} substituting for Fe^{3+}
2. Si^{4+} + Ca^{2+} substituting for $2Fe^{3+}$

The Al-Fe substitution is much more extensive than the Si/Ca-Fe substitution. Figure 15 is plotted in such a way as to show the CA_3 component in terms of wt% Al_2O_3. Therefore if more Al_2O_3 is present then Al^{3+} <-> Fe^{3+} will be the dominant substitution reaction, whereas if very little Al_2O_3 is present then Si^{4+} + Ca^{2+} <-> $2(Fe^{3+},Al^{3+})$ will be the dominant substitution reaction (Patrick & Pownceby 2002:80).

The SFCA solid solution is most extensive at low temperatures, (≥30wt% Al_2O_3). As shown on Figure 16 the stability field for SFCA at 1240ºC is much larger compared to at 1480ºC where the field is very small.

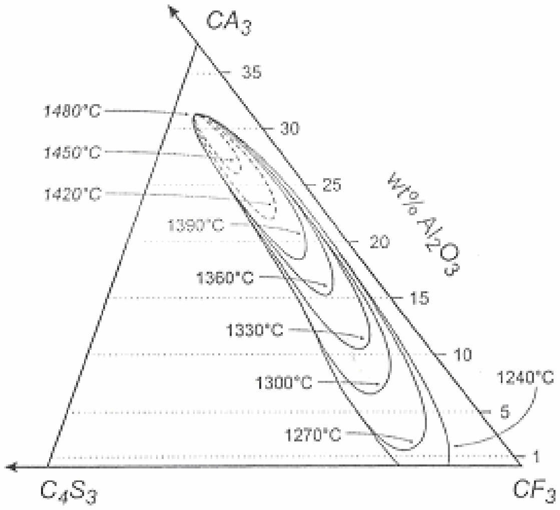

Figure 16: Solid solution limits and thermal stability for SFCA in the FCAS system (Patrick & Pownceby 2002/33B:85)

Figure 16 shows that the greatest range of solid solution exhibited by SFCA occurs in the direction of the $Al^{3+} \Leftrightarrow Fe^{3+}$ exchange, extending between 0 wt% Al_2O_3 and ~31,5 wt% Al_2O_3. The high Al_2O_3 compositional limit of SFCA is fixed at ~31,5 wt% and the range of $Al^{3+} \Leftrightarrow Fe^{3+}$ substitution decreases and contracts toward this upper limit with increasing temperature as the lower Al_2O_3 portions of the SFCA solid solution series become progressively unstable. The rate of SFCA breakdown is approximately constant with increasing temperature, and by extrapolating this trend (dashed lines) it is estimated that the SFCA solid solution will entirely decompose at 1480ºC (Patrick & Pownceby 2002:85).

In comparison, the substitution for $Si^{4+} + Ca^{2+} \Leftrightarrow 2(Fe^{3+},Al^{3+})$ is more limited, having a maximum range between 3-11 wt% C_4S_3. This maximum occurs at 1240ºC for bulk compositions containing around 10 wt% Al_2O_3. The low temperature stability limit for SFCA was not determined since the reaction kinetics were expected to be sluggish below 1240ºC making equilibrium difficult to attain. Previous studies did show that SFCA is likely to be stable down to at least 1050ºC to 1060ºC (Patrick & Pownceby 2002:85).

Figure 17 shows that the Mittal sinters (from the Vanderbijl Park sinter plant) do not fall in the expected phase assemblage for SFCA as classified by Patrick & Pownceby (2002:85). Some Mittal sinters may form SFCA at 1270°C, others will form hematite + SFCA + liquid, and others will form hematite + liquid. Variations of ~2% Al_2O_3 are enough to substantially change the phase assemblage (see Figure 18 for a more detailed view of the location of the Mittal sinters). Note that the Mittal sinters data represent the bulk composition of the sinter and not single phase SFCA. The Vanderbijl Park plant operates at temperatures ranging from 1190 to 1370°C and is therefore comparable with the diagram proposed by Patrick & Pownceby (2002:85). It should also be noted that the samples contain appreciable magnetite, and their presence can only be explained if the sinters are at a high temperature or a lower pO_2.

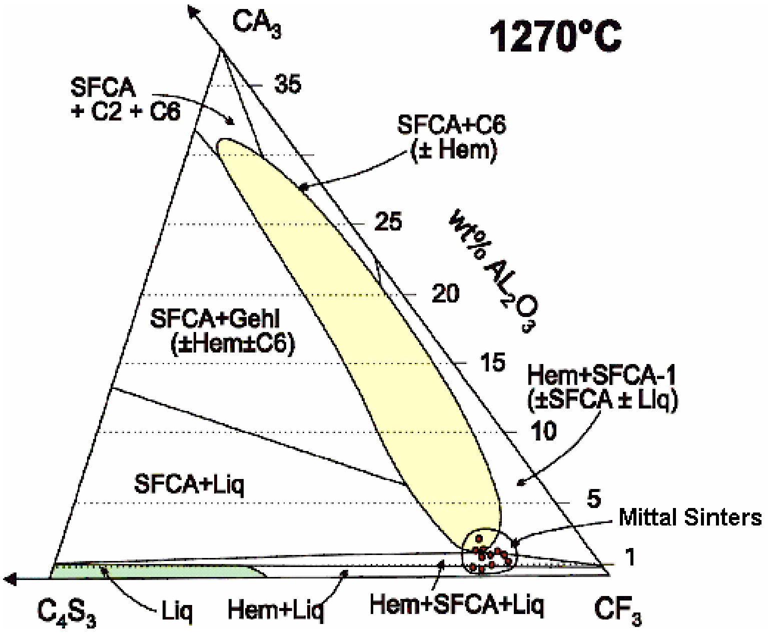

Figure 17: Location of Mittal sinters at 1270ºC projected onto the phase diagram and the SFCA phase field as determined by Patrick & Pownceby 2002:87 (C6 = $CaO(Al_2O_3,Fe_2O_3)_6$ or $Ca(Al,Fe)_{12}O_{19}$ and C2 = $CaO(Al_2O_3,Fe_2O_3)_2$ or $Ca(Al,Fe)_4O_7$)

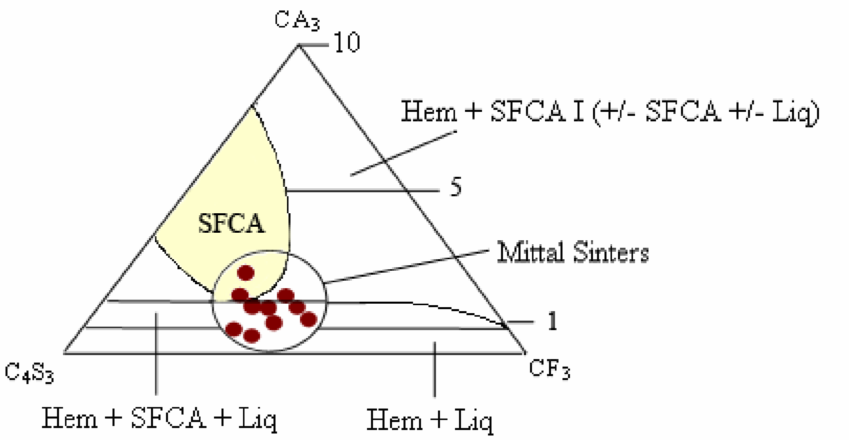

Figure 18: Enlarged area from Figure 17 showing the location of the Mittal sinters at 1270ºC

In Figure 19 it is apparent that at 1360ºC the Mittal sinters all should fall within the magnetite + liquid field. The presence of SFCA is therefore unexplained. The SFCA, if present, contains appreciable amount of Al_2O_3, which could affect its reducibility. An increase in silica content will increase the amount of liquid formed. This is apparent if you apply the lever rule.

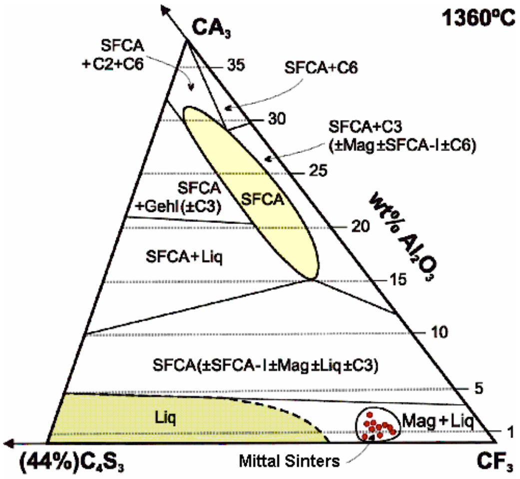

Figure 19: Location of Mittal sinters at 1360ºC (after Patrick & Pownceby 2002)

According to Figures 17 and 19 the ability of Mittal sinters to form pure phase SFCA is rather small. Lowering the alumina content allows SFCA to be stabilized at lower temperatures whereas increasing the SiO_2 content moves the phase assemblage toward phase regions dominated by silicate phases such as C_2S.

3.2 Sintering reactions

The first phase in the sintering reaction as described by Ponghis & Leroy (1971:18) states that the lime attacks the other oxides according to their acid nature and their degree of fineness and forms a silicate which is contaminated by iron and aluminum oxides. This new phase is formed in a liquid phase. With the exception of the Al^{3+} ion, there is no solid diffusion in the original hematite crystals. The presence of magnetite promotes the dissolution of the iron. It has been concluded that magnetite is attacked more easily by the molten silicates and silico-aluminates of lime. This justifies the disappearance of a major part of the magnetite formed by gaseous reduction.

The liquid slag thus formed then attacks the larger grains in the mixture by penetrating through the boundaries and dissolves them. This dissolving effect reaches its maximum at the moment at which the flame front coincides with the layer concerned. At this stage the dissolution of the ore grains is great if not complete (Ponghis & Leroy 1971:18-23).

When combustion reaches its limit, the layer of the sinter bed receives air which has to pass through the liquids that have formed. Depending on the porosity of the top portion of the bed, the viscosity and surface tension of the liquid phase, a certain number of channels will be formed and will allow the passage of air. This causes a solidification of the material located in the vicinity of these passages which is in contrast with the remainder of the sinter bed which, since the cooling effect is less prominent, will remain in a liquid state. This non-uniformity of temperature at different points in the bed continues throughout the cooling process and may, when it is very marked and the contraction of the material is sufficient, bring about the formation of round pores. Sinters which have a porous and fissured texture have poor mechanical properties. Observations lead to the conclusion that the characteristics of the finished product will depend on the one hand on the lack of uniformity in the cooling and composition of the bed and on the other hand on the composition of the liquid formed (Ponghis & Leroy 1971:18-23).

During what has been referred to as the "sintering reaction" the liquid is charged with Fe^{3+} and Fe^{2+} ions. As soon as the cooling stage begins, these ions are in a state of over-saturation and are precipitated. Depending on the ratio of Fe^{3+} to Fe^{2+} in solution the phase which is precipitated will be hematite or magnetite or both simultaneously. This precipitation tends to occur on the grains of original hematite which initiate grain growth. Where such grains are absent, precipitation takes place in the mass of liquid. Parallel with these two types of precipitation mechanisms, the liquid is oxidized by the air and the precipitation of hematite becomes predominant (Ponghis & Leroy 1971:18-23).

The next stage depends solely upon the basicity of the material and the rate of cooling at various locations within the sinter bed. Silicates are able to form glasses. Basic oxides and CaO particularly prevent this phenomenon to occur. Depending on the CaO content, another phase may precipitate after hematite and or magnetite, in which case calcium ferrites are produced. These are formed in a similar manner to the magnetite. Finally the remaining mass, from which most of the iron and calcium have been eliminated, solidifies in the form of a glass (Ponghis & Leroy 1971:18-23).

3.3 Variation in sinter mineralogy

The temperature of the sintering process has a significant influence on the microstructure of the sinter produced. The fuel content of the mix essentially determines the thermal parameters. Sinters produced at low temperatures contain fine acicular calcium ferrite. At higher process temperatures, columnar and dendritic types of calcium ferrite are found in the sinter. The presence of higher Al_2O_3 and TiO_2 contents leads to the stabilization of the calcium ferrite and hematite respectively (Pimenta & Seshadri 2002:173).

The effect of flame front speed (FFS) according to Choudhary & Nandy (2006:613) can have the following effects:

1. A trend can be seen in the phases present in sinter at different FFS. The hematite content increases at higher FFS. This is an evidence of faster oxidation of the melt.

2. The hematite phase in sinter contains much higher Ca and Mg than the original materials. This indicates that this hematite has formed by dissociation of SFCA and is of secondary type. Evidence was found of higher diffusion of Al and Si into hematite.
3. The composition of the SFCA was affected by the FFS. At higher FFS, SFCA was having higher Fe and lower Si contents and at lower FFS, it contained lower Fe and higher Si concentrations.
4. Based on the results a modified flow chart of formation of phases in high alumina sinter is proposed (see Figure 20).

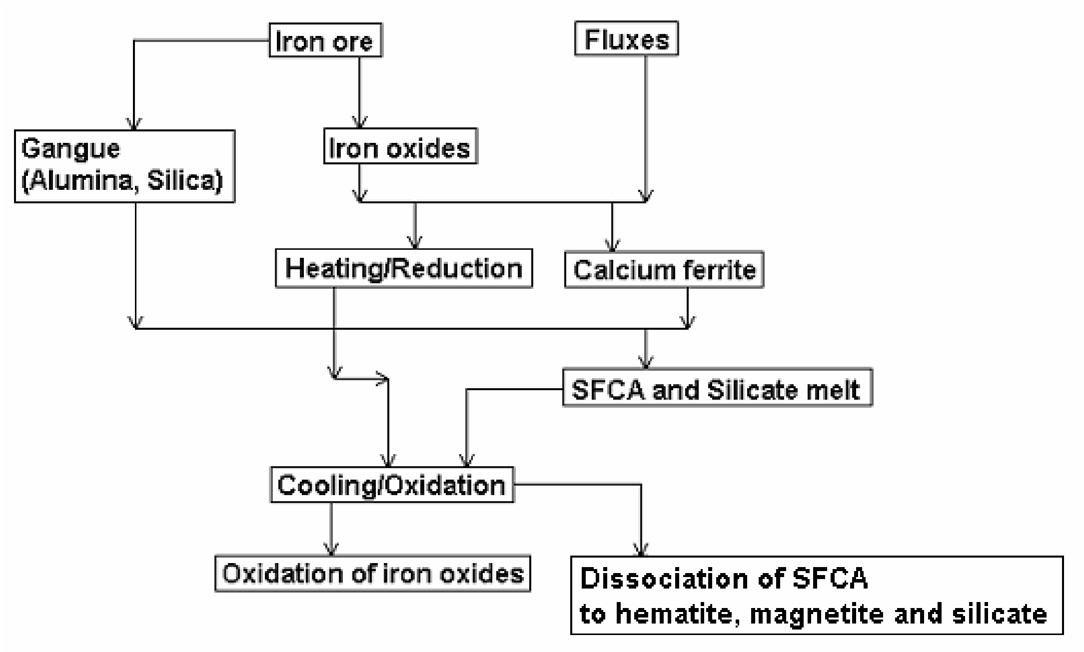

Figure 20: Flow chart showing the formation of phases during sintering of iron ore (after Choudhary & Nandy 2006:613)

4. Experimental procedure

4.1 Description of the steel plant

The Vanderbijl Park steel plant consists of the following units (Mittal Steel South Africa 2007):

1. Six coke oven batteries
2. One sinter plant (two strands, A-line and B-line, producing approximately 2000-4000t daily)
3. Two blast furnaces
4. Direct reduction plant (four kilns)
5. Three electric arc furnaces
6. Three basic oxygen furnaces
7. Three continuous casters
8. 3,650 mm plate mill
9. 2,050 mm hot strip mill (seven strand)

4.2 Sample descriptions

Two groups of samples were obtained from the Vanderbijl Park sinter plant. The first comprised of four samples taken during the year 2005. They represented the different sinter products that are produced, namely accretion material adhering to the moving hearth ("sticker"), normal sinter (sinter that proceeds to the blast furnace), internal fines (screened and returned before sinter product is transported to the blast furnace) and external fines (screened just before the sinter product enters the blast furnace).

The second group was taken in the year 2006. The samples comprised of approximately 50 samples that were taken at 4 hour intervals over a time period of three days from 14 to 16 April. Samples were taken at both the A and B production lines, and consisted of normal sinter, internal fines and external fines. The detailed description can be found in Appendix 1.

4.3 Homogeneity tests

The samples taken in 2005 were sent to Australia to be analyzed with a mineral analyzer. The analyses show that the material is extremely heterogeneous, as can be seen in Figure 21 (a scale is not available since the image is only to illustrate the heterogeneity of the sample). Analytical results and a brief description of the mineral analyzer are in Appendix 2. Therefore great care had to be taken in preparing the samples in order to ensure that reproducible samples were used for analysis. Taking representative samples was also a challenge due to the high production capacity of the sinter plant.

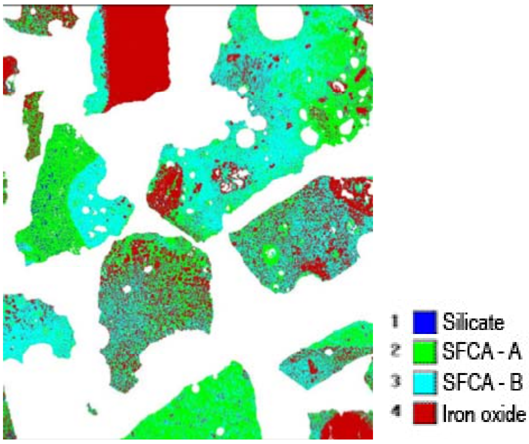

Figure 21: MLA image of iron ore sinter. Note the inhomogeneity of the sample in which different particles can consist of entirely different phases. SFCA – A and SFCA – B are two different SFCA phases identified. The white areas in the figure represent a combination of epoxy resin mounting media as well as pores within the individual particles.

The samples taken at the plant varied in size between two to three kilograms each. These samples were taken with the plant sampler after the sinter has cooled down. The samples were then screened into two groups. Normal sinter was comprised of material >5mm and the fine fraction of material <5mm. The samples were placed in a jaw crusher and upon exit into a gyratory crusher. They were then milled in a ball mill for thirty minutes. The samples were then split into two parts using Eriez Hi-Vi Vibratory Equipment (Model 15A, 230 volts, 50 cycles, 0.25 amps). The one half was discarded and the other milled in the ball mill for another ten minutes. The above described split process was repeated and then the sample was milled for five minutes. The final weight of the sample was approximately half a kilogram from which samples were taken for analyses.

In order to ensure that the above described sample preparation was adequate, XRD and XRF analyses were conducted on the normal sinter sample. The sample was prepared for XRD analysis by first adding 20% Si powder (Aldrich 99% purity) as a standard in order to confirm the presence of amorphous material and to verify correct quantification. It was then micronized in a McCrone micronizing mill, and then prepared for analysis using a back loading preparation method. It was analyzed using a PANalytical X'Pert Pro powder diffractometer with X'Celerator detector and variable divergence- and receiving slits each set at 15mm, scanned from 10 to 60 °2θ at a scanning speed of 9 sec/step. The radiation was Fe filtered Co-Kα radiation. One sample was analyzed by the XRD machine ten times (without removing it from the machine) in order to test the reproducibility of the machine itself. The same sample was then removed from the sample holder, remounted (using a back loading preparation method) and tested. This procedure was repeated ten times in order to determine the impact of remounting on the results. Ten sub samples were then taken from the half kilogram sample and tested in order to test the homogeneity of the milled sample. Phases were identified using X'Pert Highscore plus software and quantification was accomplished with Autoquan/BGMN software (GE Inspection Technologies) employing the Fundamental Parameter Approach (Kleeberg & Bergmann, 1998 & 2002). For the homogeneity tests, the amount of amorphous phase was not determined since this is prone to large errors due to its dependence on the errors of all the phases. It was decided to treat the silicon as one of the phases and to use its deviation from the measured value (16.67%) as a measure of the accuracy of the measurement. The Autoquan software uses the parameter Rwp which is displayed as a function of the iteration steps to illustrate the calculation progress. This parameter (the weighted residual square sum) allows the user to assess the quality of fitting of the measured and calculated diagram. A smaller value stands for better fitting. The minimum possible value of Rwp is the value Rexp, which is equivalent to ideal fitting. Thus, Rexp can serve to assess Rwp but is also a measure for the quality of the measurement.

XRF analyses were conducted on 5 sub samples from the sample used in the XRD analyses. The apparatus consisted of an ARL 9400XP+ Wavelength dispersive XRF Spectrometer with Rh tube, LiF200, LiF220, GER, AXO6 and PET analysing crystals and flow proportional and scintillation detectors. Sample preparation included drying and roasting at 1000ºC to determine % loss on ignition. Major element analyses were executed on fused beads, following the standard method used in the XRD & XRF laboratory of the University of Pretoria, as adapted from Bennett & Oliver (1992). This involves the following, a 1g pre-roasted sample + 6g Lithium Tetra borate flux mixed in a 5%Au/Pt crucible and fused at 1000ºC in a muffle furnace with occasional swirling. A glass disk was prepared with the liquid flux poured into a pre-heated Pt/Au mould and the bottom surface was analysed. Trace elements were analysed on pressed powder pellets, using an adaptation of the method described by Watson (1996), using a saturated polyvinyl alcohol 40-88 solution as binder. The XRF Spectrometer was calibrated with certified reference materials, specpure oxides and some in-house standards. Some examples are: Specpure AL2O3, AGV, BCR1, BEN, BHVO1, BR, Specpure $CaCO_3$, Specpure CaO, DRN, FECA (in-house), FeSi(in-house), GA, GSN, GSP1, Specpure SiO_2, JB1, JG1, Lithium Tetraborate blank, MAN, MICAFE, MICAMG, MRG1, NIMD, NIMG, NIMN, NIMP, NIMS, PCC1, SARM 8, SARM9, SARM32, SARM34, SARM39, SARM40, SARM42, SARM44, SARM45, SARM46, SARM47, SARM49, SY2, SY3, UBN, UREM3, UREM4, UREM7, W2. The NBSGSC fundamental parameter program was used for matrix correction of the major elements as well as Cl, Co, Cr, V, Sc and S. The Rh Compton peak ratio method was used for the other trace elements. As part of ongoing quality control, a blank and two certified reference materials are run with each batch of samples. Each tenth sample is run in duplicate. The XRF laboratory participates in the International Association for Geoanalysts' GeoPT proficiency test where geological materials are analysed three times a year, and results reported after statistical treatment with "z" values for each element from each laboratory. To evaluate sample preparation errors, an in-house standard is monthly submitted with a batch of unknowns and prepared in the same manner as unknowns. Reported standard deviations are expressed as the standard deviation of a calibration curve, set up with an average of 20-30 standards, as this method best approximates the entire calibration range. Detection limits were also calculated from calibration standards.

After completion of the homogeneity tests on the samples taken in 2005 the same sample preparation procedure was performed on the samples taken in 2006.

4.4 Microprobe analysis

A Cameca SX100 Microprobe of the University of Pretoria was used for all micro-analytical work. The counting times on peak positions are 20 seconds and 10 seconds on background positions. The electron beam is defocused to a 10 micron diameter for feldspars. Certified standards that are used for analyses include:

1. A Wollastonite ($CaSiO_3$) Standard is used for Si and Ca.
2. Pure Oxide Standards are used for Mg, Al, Mn and Fe.
3. A Fe_2O_3 Standard is used for O.

The PAP and ZAF correction procedures were applied on the material analyzed and the results showed no differences. Therefore the ZAF procedure was used throughout the analyzing process.

Electron microprobe analyses were performed on both groups of samples (all samples taken in 2005 and 4 representative samples were selected from the samples taken in 2006). Elements that were analyzed included O, Mg, Al, Si, Ca, Mn and Fe (thus O is to be analyzed separate and not as oxides). The phases that were analyzed included C_2S, hematite, magnetite and SFCA (all phases identified with an optical microscope). Approximately 65 analyses were made on each sample.

The results were recalculated to determine the compositions of the different phases present. The data was then statistically analyzed using the Microsoft SPSS Statistical Program. The results were clustered according to the elemental analyses and the results recalculated to fit the phases present (hematite, magnesioferrite, magnetite, C_2S and SFCA). These clusters were then used to compare the phase chemistry of the samples (specifically the different SFCA phases) with that described in the literature.

4.5 XRD and XRF

Both groups of samples were analyzed with XRD and XRF in order to examine the differences between normal and fine sinter. The samples prepared using sinter pot tests and samples synthesized using the sol gel technique was also investigated with these two analytical tools. XRD and XRF analyses were also used to compare sinter produced in lines A and B of the sinter plant.

4.6 Samples synthesized using the Sol gel technique

The data obtained from microprobe analyses showed that the SFCA phases present in the Vanderbijl Park samples did not correspond well to those described in the literature. It was therefore decided to synthesize one of the SFCA phases found in the Vanderbijl Park samples that closely corresponded to the SFCA phase in the literature. The first synthesis was conducted by using oxides (the grain sizes of the materials used was approximately 45µ) that were pelletized and sintered at 1000°C for 24 hours. It was then regrind and sintered at 1000°C for 24 hours. This method did not give homogeneous results and therefore the sol gel method was used to synthesize the SFCA phase.

The first method used (named sol gel 1) is based on the work of Gaki *et. al*. (2007:1781-1784). Molar ratios were calculated on the basis of the cluster analysis done with the microprobe data. $Al(NO_3)_3.9H_2O$, $Mg(NO_3)_2.6H_2O$, $Ca(NO_3)_2.4H_2O$, $Fe(NO_3)_3.9H_2O$, TEOS, Citric Acid and Ethylene Glycol were used as reagents. The nitrate salts were dissolved in just enough distilled water, citric acid was then added with a molar ratio of Citric acid: Cations = 1. The mixture was then magnetically stirred until a clear solution was present. Ethylene glycol was then added with the molar ratio Ethylene glycol: Citric acid = 2. The solution was then stirred magnetically at 80ºC for the excess water to evaporate and for the necessary polyesterification reactions to take place. When a viscous gel was formed the sample was placed in a 150ºC oven for twenty four hours. It was then transferred to a furnace and kept at 1250ºC for two days.

Another method for sol gel synthesis (named sol gel 2) based on the work of Chrysafi *et. al*. (2007:1707-1710) was then used to produce C_2S, CF and SFCA. TEOS was mixed with ethanol with the molar ratio C_2H_5OH:TEOS = 1.5. The nitrates were dissolved in just enough ethanol. The two mixtures were then mixed and ten drops of glacial acetic acid was added. Water was then added with the ratio H_2O:TEOS = 6. The mixture was then left overnight at room temperature. It was then heated to 80ºC for four hours until a gel was formed. This gel was then heated at 10ºC/minute up to 1250ºC. Half of the sample was sintered at this temperature for three hours and the other half for twenty four hours to determine any differences.

SEM and XRF analyses were completed for the first and second SFCA sol gel synthesized. XRD analyses were used to test C_2S and CF sol gels that were made as control tests (See Appendix 3, Tables 27 and 28).

4.7 Point counting

Point counting was performed by Mashao (2007) on four of the bulk samples taken in 2006 (same four samples as used for microprobe analyses, 500 counts per sample were done). The reasoning behind this method of analysis is the following: Since the start of the project Kumba Iron Ore was involved since they are responsible for the research work done for Mittal at Vanderbijl Park. They primarily use point counting for quantification of phases. This project on the other hand focused on XRD analyses both quantitative and qualitative. This procedure was therefore undertaken to compare the two methods.

4.8 Sinter Pot tests

Samples from pot tests formulated with approximately the same basicity and chemistry as the bulk plant samples taken in 2006, were obtained from Kumba Iron Ore. There were slight variances present due to the basicity and chemical nature of the sinter used at the plant compared to those used for the pot tests. The basicity was comparable; the only major difference is that the ore used in the pot tests contained more silica. There were two samples; a +5mm fraction representing normal sinter and a -5mm fraction representing fine sinter. Sample preparation was conducted in the same manner as described in the homogeneity section. XRD analyses were completed on these samples.

4.9 Statistics

All statistical procedures in this project were calculated with the "significance test" method, where a $\boldsymbol{P}$-value for the given data is calculated. The following interpretations were taken as benchmarks: $\boldsymbol{P} < 0.01$: Strong evidence against $\boldsymbol{H}_0$, $0.1 < \boldsymbol{P} < 0.05$: Moderate evidence against $\boldsymbol{H}_0$, $\boldsymbol{P} > 0.10$: Little or no evidence against $\boldsymbol{H}_0$ ($\boldsymbol{H}_0$ is the hypothesis of "no difference" also known as the null hypothesis) (Berry & Lindgren 1990:461-474).

5. Results

5.1 Homogeneity test results

The standard deviation based on XRD results for the 2 samples that were taken 4 hours apart is shown in Figure 22. The standard deviation is a measure of how widely values are dispersed from the average value (the mean).

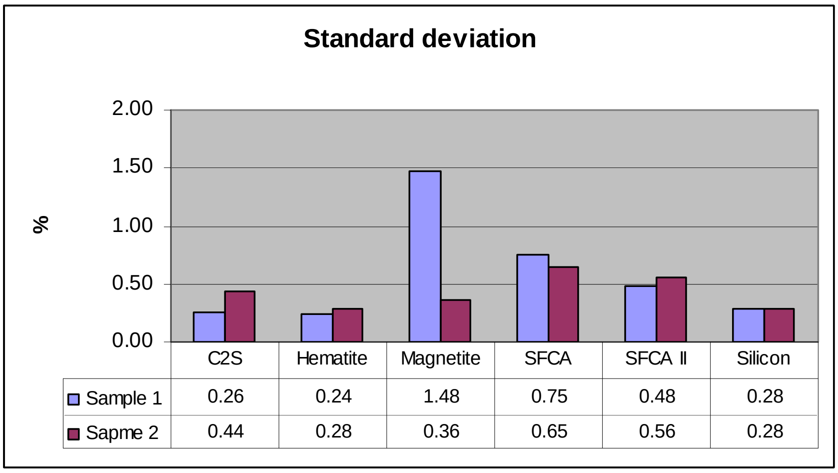

	C2S	Hematite	Magnetite	SFCA	SFCA II	Silicon
□ Sample 1	0.26	0.24	1.48	0.75	0.48	0.28
■ Sapme 2	0.44	0.28	0.36	0.65	0.56	0.28

Figure 22: Standard deviation based on the error in the mineral percentages (deviation from the mean) for the XRD results. Sample 1 consists of the average of T1 and T48, Sample 2 consists of the average of T3 and T47 as defined in Appendix 1.

The standard deviation based on XRF results for the 2 samples that were taken 4 hours apart is shown in Figure 23.

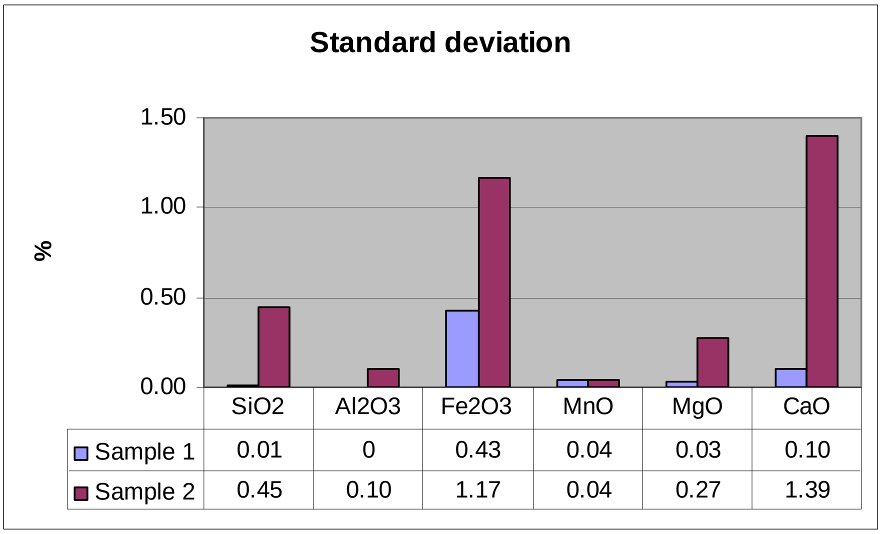

	SiO2	Al2O3	Fe2O3	MnO	MgO	CaO
□ Sample 1	0.01	0	0.43	0.04	0.03	0.10
■ Sample 2	0.45	0.10	1.17	0.04	0.27	1.39

Figure 23: Standard deviation based on XRF results. Sample 1 consists of the average of T1 and T48, Sample 2 consists of the average of T3 and T47 as defined in Appendix 1.

Both XRD and XRF results show standard deviations of no more than 1.48%, although the overall percentages are closer to 0.5%.

Figure 24 shows the results for the XRD reproducibility test. The individual XRD results are given in Appendix 3, and the XRF results in Appendix 4. For this analysis the following values were obtained: Rwp=2.70% Rexp=2.22%. The repeats on the same subsample mount, remounts of the same subsample and sub samples of the same sample never varied more than 1%. It is evident from this graph that the sampling and sample preparation procedure was successful. It should be noted that during the Rietveld analyses distinction can be made between the three SFCA phases. The combination that produced the best results (Rwp value) for these samples included only SFCA and SFCA II. Though it is not the perfect result due to the fact that the Autoquan software uses the standard formulae for the phases as described in the literature and it has been concluded that the Vanderbijl Park SFCA phases do not correspond to those formulae. (Please note that the silicon was only added as a standard in all XRD analyses.) Note also that the magnetite contents represent both magnetite and magnesioferrite.

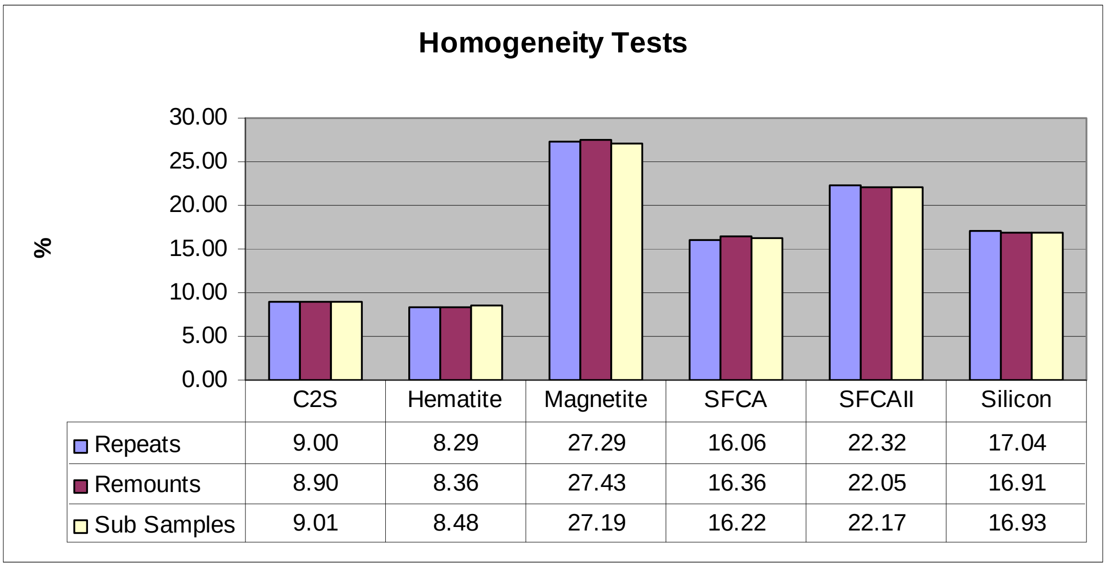

	C2S	Hematite	Magnetite	SFCA	SFCAII	Silicon
☐ Repeats	9.00	8.29	27.29	16.06	22.32	17.04
■ Remounts	8.90	8.36	27.43	16.36	22.05	16.91
☐ Sub Samples	9.01	8.48	27.19	16.22	22.17	16.93

Figure 24: XRD reproducibility test of one sinter sample. The values given are the average of 10 repeat XRD analyses. The blue column represents measurements of the same sample mount, the brown represents measurements of different sample mounts, and the yellow, measurements of 10 different sub samples of the same sample

The standard deviation expressed as a percentage of the concentration of the phases shown in Figure 25 shows that the sub samples have the largest standard deviation (except for C_2S) which is due to the fact that the most variance is present due to the nature of the experiment. It must be noted that the standard deviation for all analyses is below 1% as shown in Figure 25.

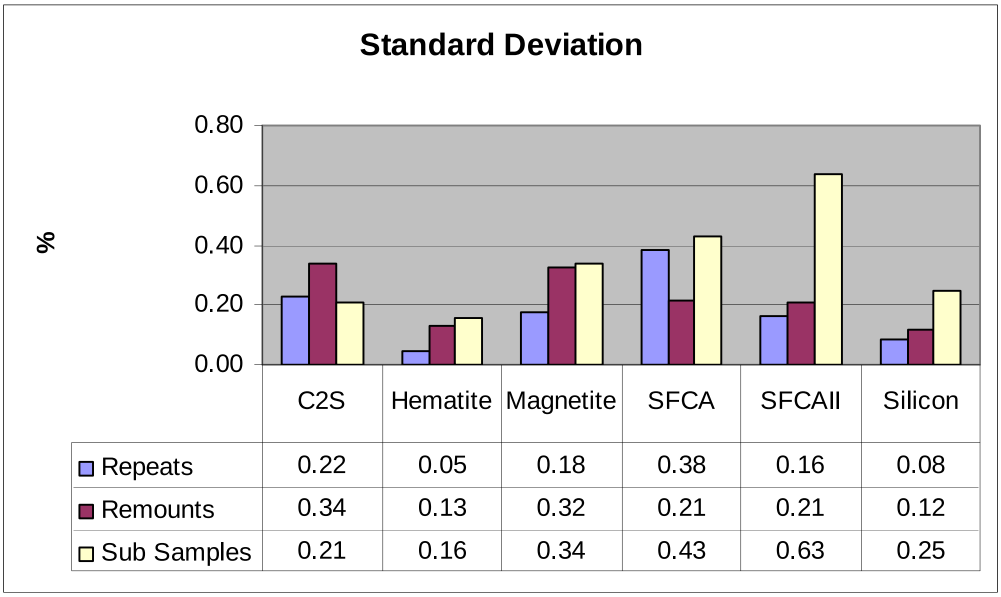

	C2S	Hematite	Magnetite	SFCA	SFCAII	Silicon
▢ Repeats	0.22	0.05	0.18	0.38	0.16	0.08
■ Remounts	0.34	0.13	0.32	0.21	0.21	0.12
▢ Sub Samples	0.21	0.16	0.34	0.43	0.63	0.25

Figure 25: Standard deviation for XRD results expressed as the deviation from the mean of ten determinations

For the XRF reproducibility test five sub samples from the sample used in the XRD analyses were taken and fused beads and pressed powders were prepared. The results only show approximately 1% difference between the sub samples. Therefore the XRF results also show that the sample preparation procedure was successful. Data can be viewed in Figure 26 (statistical data in Table 5 and LOI values for all analyses can be found in Appendix 4).

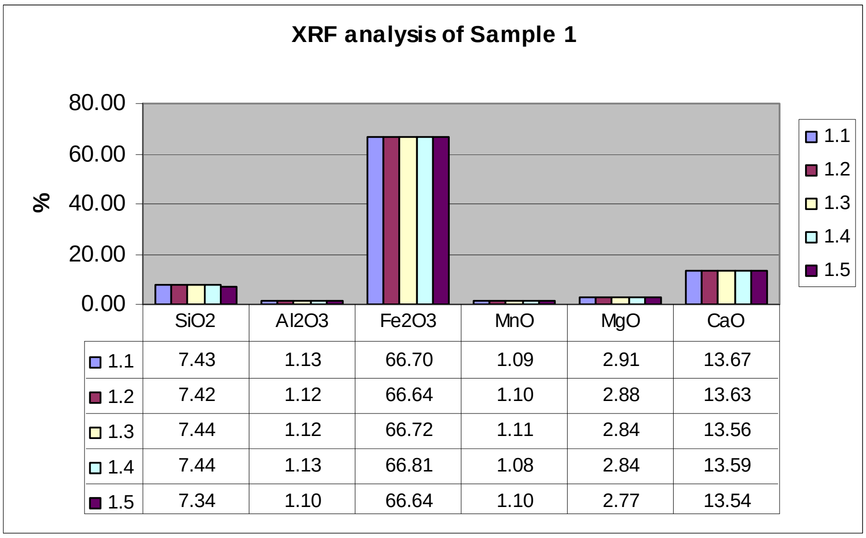

	SiO2	Al2O3	Fe2O3	MnO	MgO	CaO
▢ 1.1	7.43	1.13	66.70	1.09	2.91	13.67
■ 1.2	7.42	1.12	66.64	1.10	2.88	13.63
▢ 1.3	7.44	1.12	66.72	1.11	2.84	13.56
▢ 1.4	7.44	1.13	66.81	1.08	2.84	13.59
■ 1.5	7.34	1.10	66.64	1.10	2.77	13.54

Figure 26: XRF reproducibility test on five sub-samples using fused beads

In Table 5 the standard deviation and limit of detection values for the XRF analyses are shown (Table 5 includes the values for the analyses done on all the samples that were taken in 2006). The standard deviation values are low with the largest value at 0.4%. The limit of detection values also represents good analyses.

Table 5: Standard deviation expressed as a percentage of the elemental concentrations and limit of detection for samples analyzed (Loubser 2007)

Oxides	**std dev.(%)**	**LOD**
SiO_2	0.4	0.02
TiO_2	0.03	0.0032
Al_2O_3	0.3	0.01
Fe_2O_3	0.3	0.0097
MnO	0.007	0.0013
MgO	0.1	0.0118
CaO	0.07	0.01
Na_2O	0.11	0.0265
K_2O	0.06	0.005
P_2O_5	0.08	0.01
Cr_2O_3	0.005	0.0006
NiO	0.01	0.0013
V_2O_5	0.002	0.0008
ZrO_2	0.005	0.0009
CuO	0.004	0.0003

For comparison the Rwp values for these samples are shown in Table 6. This can be compared to Figure 25 and Table 5. The values in Table 6 do show higher values than the XRD and XRF standard deviation, but represent good Rwp values.

Table 6: Rwp values for the XRD analyses which shows that the XRD refinement produced good results

Sample description	**Rwp value**
Repeats	3.28
Remounts	3.23
Sub samples	3.30

5.2 Microprobe data and cluster analysis

The samples taken in 2005 were analyzed with an electron microprobe. Hematite, magnetite, magnesioferrrite, C_2S and SFCA were observed. The different phases present were analyzed specifically to determine which SFCA phases are present. It was not possible to distinguish between them optically and it was hypothesized that the microprobe data would solve this problem. Unfortunately that was not the case. Cluster analysis was then performed on the samples and representative results are shown in Figure 27. In Figure 28 only part of the diagram is shown for optimum presentation. All the individual microprobe and cluster analyses are given in Appendix 5. Note that the bulk compositions have been normalized in order to present the data on a ternary diagram.

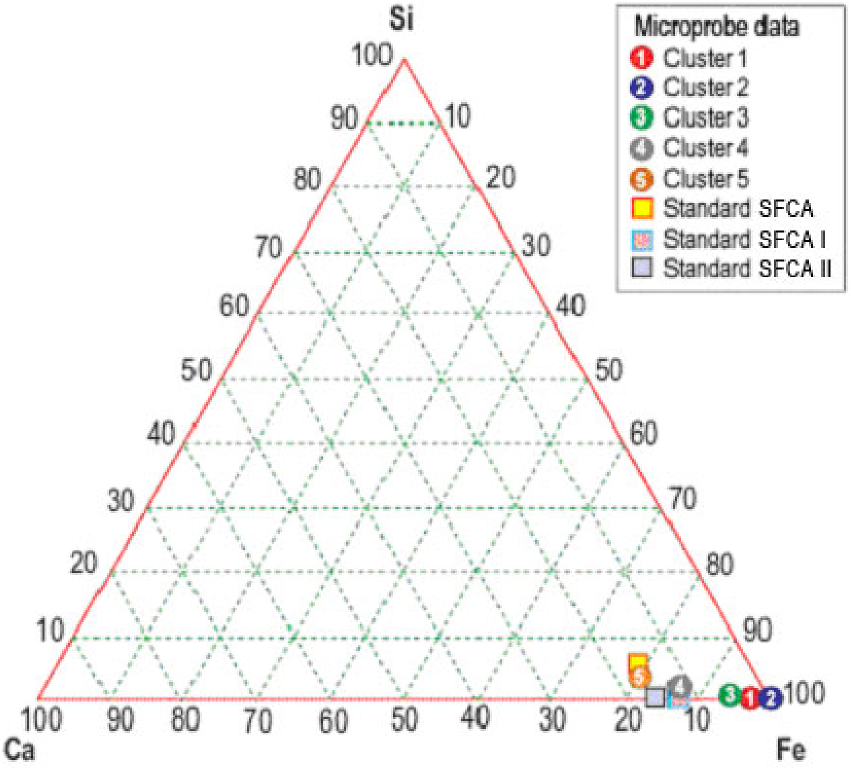

Figure 27: Compositional diagram comparing standard SFCA and microprobe data. The compositions of the standard SFCA samples are those described by Hamilton *et. al*. 1989, Mumme *et. al*. 1998 and Mumme 2003.

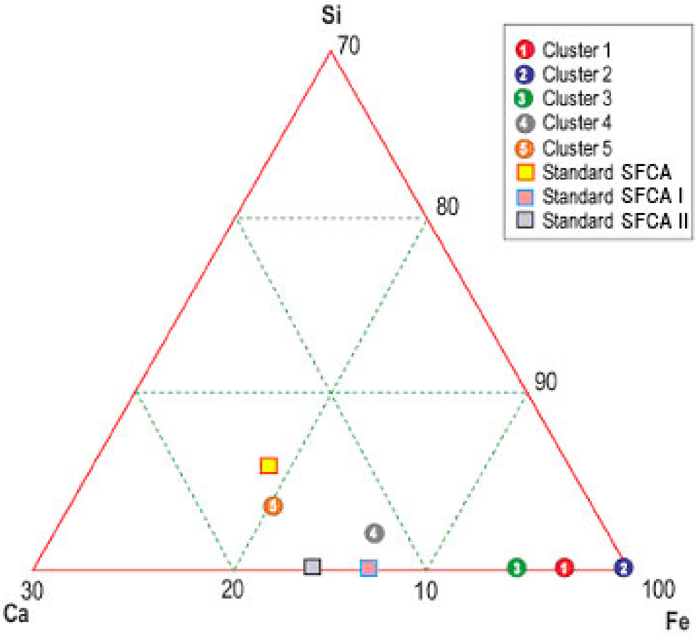

Figure 28: Area of interest showing cluster compositions. The compositions of the standard SFCA samples are those described by Hamilton *et. al*. 1989, Mumme *et. al*. 1998 and Mumme 2003.

In Figures 27 and 28 cluster two represents hematite, cluster one magnetite and clusters four and five represent the different SFCA phases. It is evident that the compositions of clusters 4 and 5 do not correspond with the three standard SFCA phases as described by (Patrick & Pownceby 2002:80). They rather seem to represent the extent of the SFCA solid solution. Cluster 5 was used to synthesize the sol gel that is discussed in section 5.4. Cluster 3 could indicate a partial solid solution between Fe_3O_4 and $MgFe_2O_4$ but is closer to the Fe_3O_4-rich side of the binary system.

Figure 29 shows the composition of the phases analyzed by microprobe, on the diagram of Patrick & Pownceby (2002:87). Note that the samples that were analyzed in 2005 represent sinter and not just the single SFCA phase.

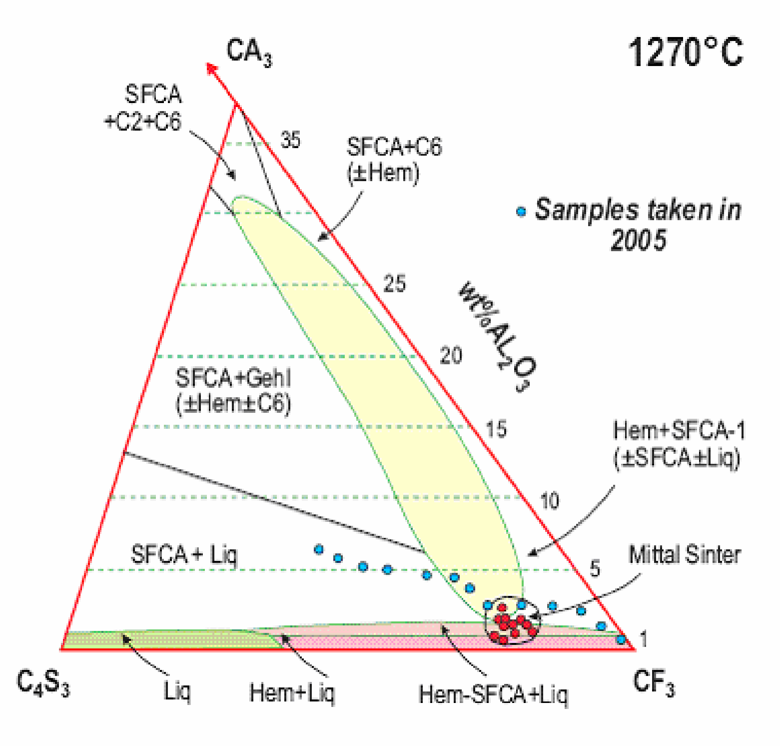

Figure 29: Composition of phases analysed in samples taken in 2005. These are represented by the blue dots on the diagram

Microprobe analyses on the samples taken in 2006 showed different compositions to those present in the samples from 2005. Figure 30 shows the analyses of phases in fine sinter and Figure 31 for phases in normal sinter. Note that the cluster numbers represent different phases in the different diagrams. The numbers were taken directly from the individual cluster analyses.

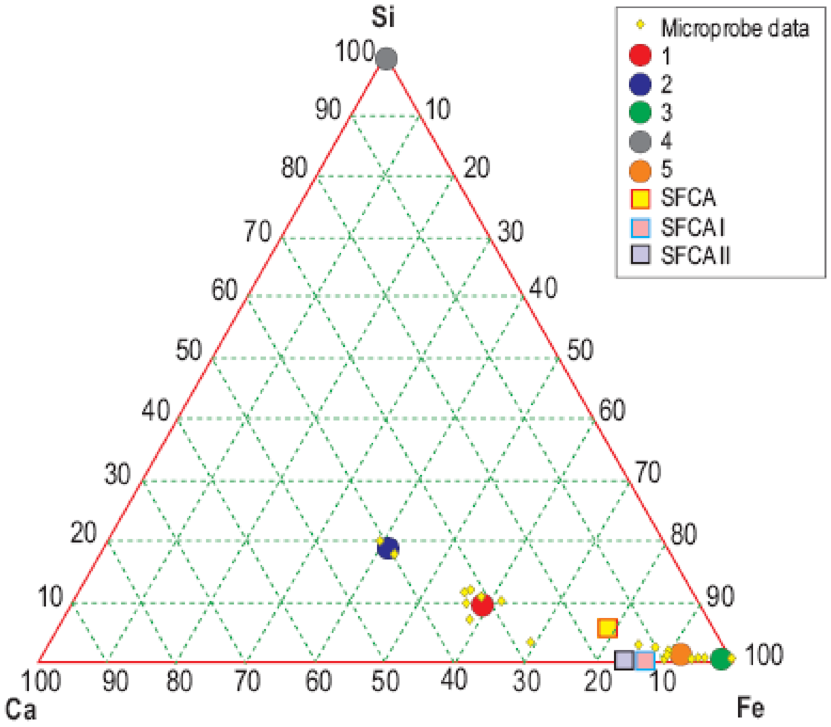

Figure 30: Microprobe analyses on a fine sinter sample taken in 2006. The compositions of the standard SFCA samples are those described by Hamilton *et. al*. 1989, Mumme *et. al*. 1998 and Mumme 2003.

In Figure 30 cluster 3 represents hematite, cluster 5 magnetite/magnesioferrite, cluster 4 unreacted SiO_2 and clusters 1, 2 are probably liquid compositions.

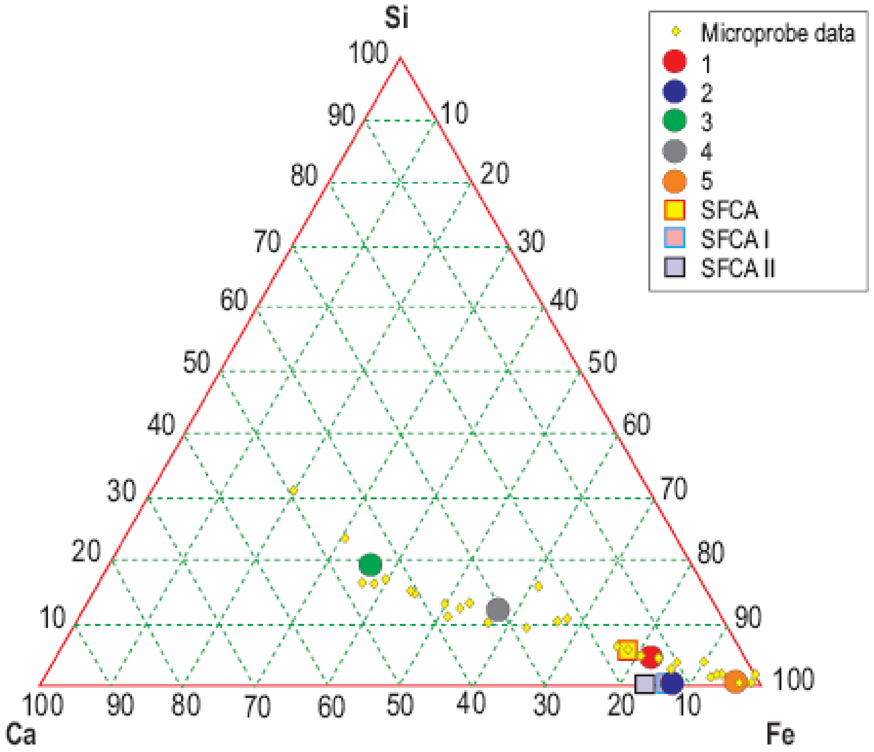

Figure 31: Microprobe analyses on a normal sinter sample taken in 2006. The compositions of the standard SFCA samples are those described by Hamilton *et. al*. 1989, Mumme *et. al*. 1998 and Mumme 2003.

The yellow dots representing the microprobe data show all the compositions of the points analyzed. The clusters were statistically calculated according to the density of the compositions in certain areas. In Figure 31 cluster 5 represents hematite/magnetite, cluster 1 SFCA and clusters 3 and 4 are melt phases.

Figures 30 and 31 are combined in Figure 32, in order to show the different cluster compositions of fine and normal sinter. There are small differences in the composition of the clusters, but they are not noteworthy.

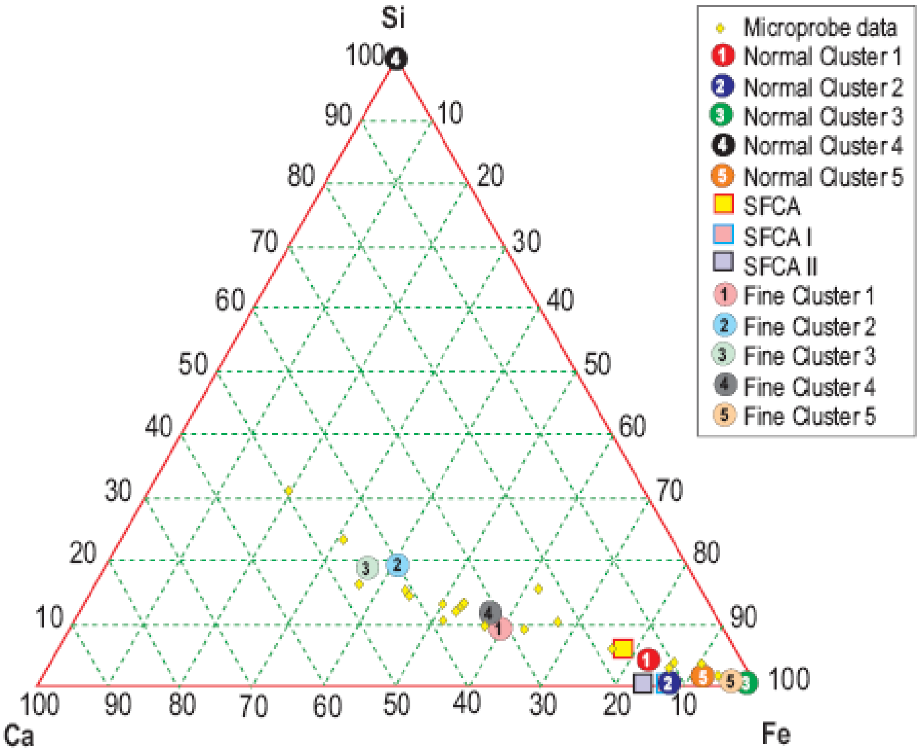

Figure 32: Combination of Figures 29 and 30. The compositions of the standard SFCA samples are those described by Hamilton *et. al*. 1989, Mumme *et. al*. 1998 and Mumme 2003.

Microprobe analyses showed that the magnesioferrite spinels found in Vanderbijl Park samples contain between 6-9% MgO which may be due to the fact that the hematite/magnetite equilibrium becomes more magnetite rich as reducing conditions increase. Magnesioferrite ($Mg^{2+}Fe^{3+}{}_2O_4$) on average contain 20.15% MgO. Magnesioferrite is more stable than magnetite under oxidizing conditions since it contains no Fe^{2+}. The a-cell dimension values for magnetite/magnesioferrite (as determined by XRD analyses) are compared to the standard values for pure magnetite and magnesioferrite in Figure 33 (it should be noted that XRD analyses can not distinguish between magnetite and magnesioferrite). Figure 33 shows that the magnesioferrite spinel phase in Vanderbijl Park sinters have a relatively constant unit cell dimension, and therefore MgO content. The values correspond closer to that of magnetite and not to magnesioferrite. These two phases are however distinct and the latter is not a Mg-containing magnetite. The higher values could be due to Ca substitution since the microprobe data showed that this phase also contains 3% Ca.

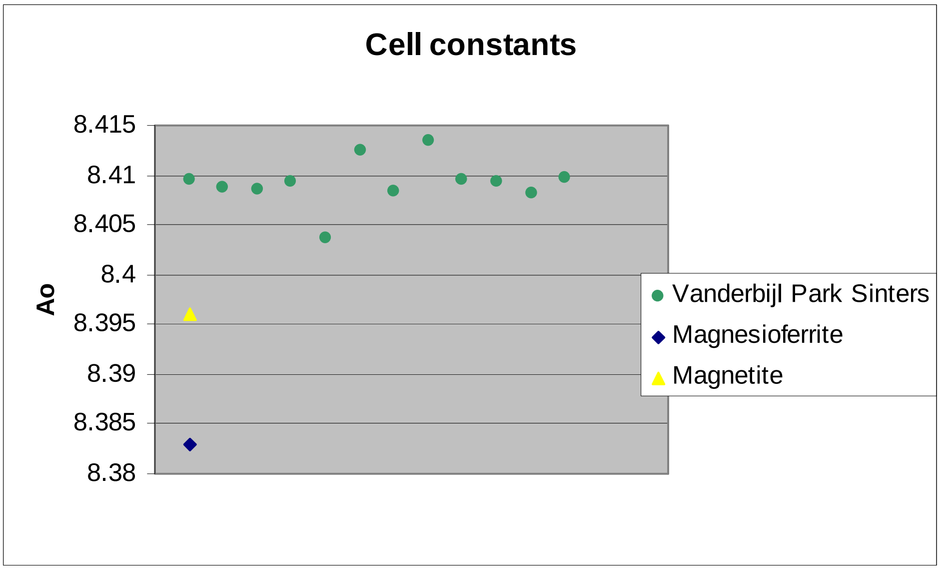

Figure 33: The a-cell dimension values for pure magnetite and magnesioferrite (Deer *et. al*. 1992:558) compared to the spinel mixture in Vanderbijl Park sinters values for magnetite and spinel determined by XRD analysis

Figure 34 (Vanderbijl Park sinter plant sample) shows the optical micrograph of a magnesioferrite, magnetite, hematite mixture. Magnesioferrite has a reflectance between hematite and magnetite and is therefore regarded as a distinct phase.

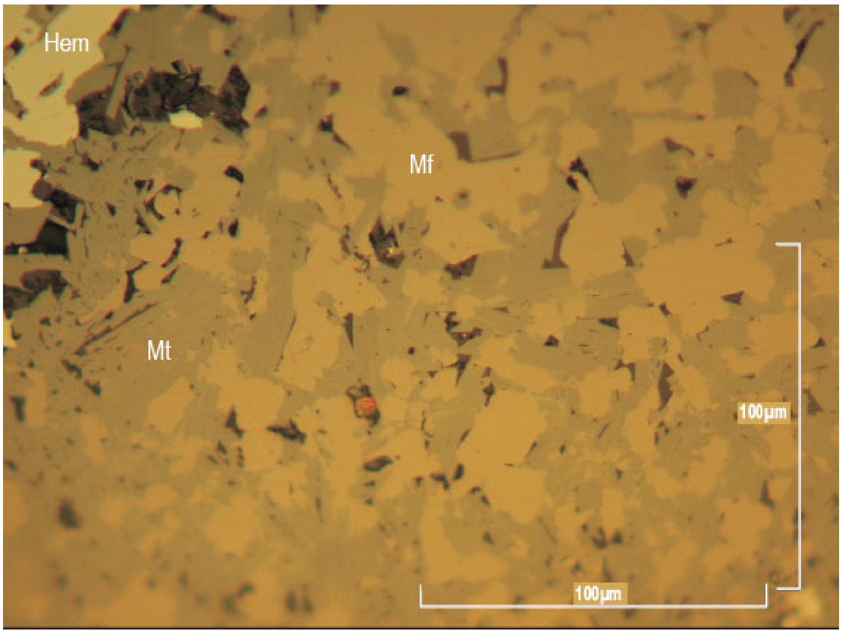

Figure 34: Optical micrograph showing hematite (Hem), magnetite (Mt) and magnesioferrite (Mf)

Two distinct spinel phases are therefore present in the Mittal sinters, magnetite and a Mg-Fe spinel with 6-12% Mg. The determined unit cell constants are for the mixture of magnetite and magnesioferrite, and the spinel peaks of the mixture show no splitting.

5.3 XRD and XRF results of plant sinters

The sinters from the two production lines (termed A and B), are compared in Figure 35. The normal and fine sinters for the two production lines are shown (averages for normal sinter A-line (blue), averages for normal sinter B-line (brown), averages for fine sinter A-line (yellow) and averages for fine sinter B-line (green). The individual XRD analyses are given in Appendix 3.

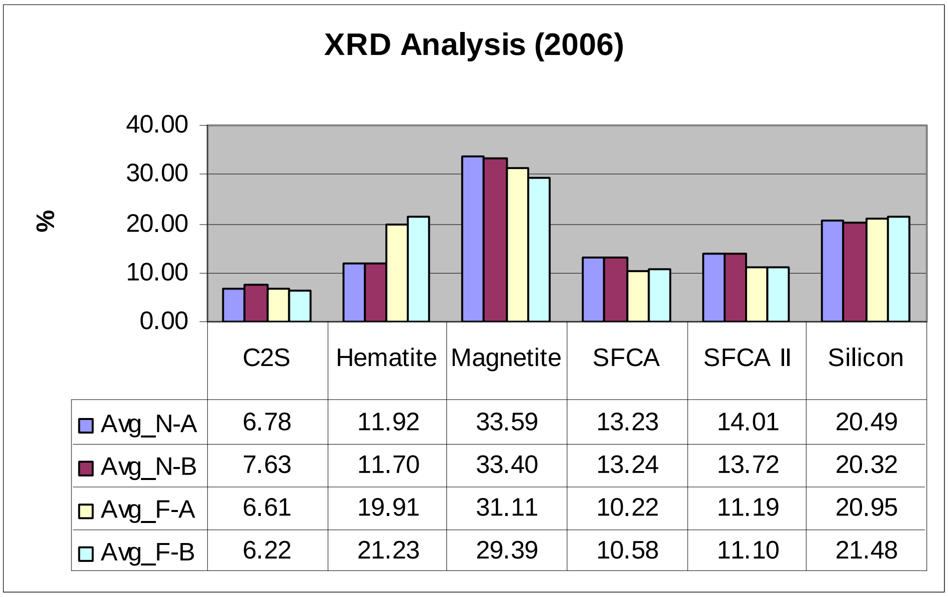

	C2S	Hematite	Magnetite	SFCA	SFCA II	Silicon
Avg_N-A	6.78	11.92	33.59	13.23	14.01	20.49
Avg_N-B	7.63	11.70	33.40	13.24	13.72	20.32
Avg_F-A	6.61	19.91	31.11	10.22	11.19	20.95
Avg_F-B	6.22	21.23	29.39	10.58	11.10	21.48

Figure 35: XRD results comparing sinter from Lines A and B (Avg_N-A = Average normal sinter A-line, Avg_N-B = Average normal sinter B-line, Avg_F-A = Average fine sinter A-line and Avg_F-B = Average fine sinter B-line)

Seven samples were analyzed for each section (7 A-line normal, 7 A-line fine, 7 B-line normal and 7 B-line fine). The comparison between lines A and B based on the XRD results for normal sinter yielded ***P*** = 0.042 which indicates a moderate significant difference. The fine sinter comparison yielded ***P*** =0.035 which indicates a moderate significant difference between the two sinter production lines.

The XRF comparison between normal sinter and fine sinter combining lines A and B is shown in Figure 36. The individual XRF analyses are given in Appendix 4.

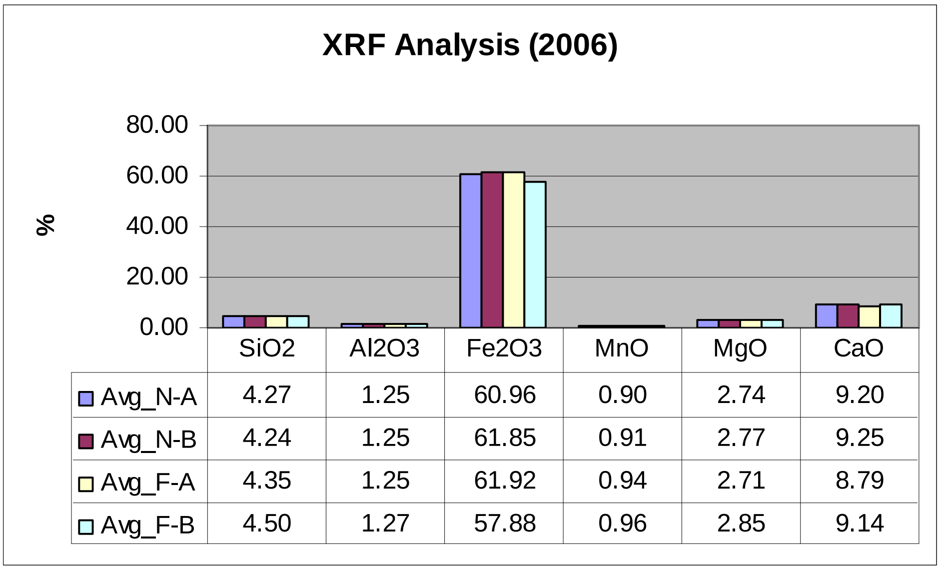

	SiO2	Al2O3	Fe2O3	MnO	MgO	CaO
Avg_N-A	4.27	1.25	60.96	0.90	2.74	9.20
Avg_N-B	4.24	1.25	61.85	0.91	2.77	9.25
Avg_F-A	4.35	1.25	61.92	0.94	2.71	8.79
Avg_F-B	4.50	1.27	57.88	0.96	2.85	9.14

Figure 36: XRF results comparing Lines A and B (Avg_N-A = Average normal sinter A-line, Avg_N-B = Average normal sinter B-line, Avg_F-A = Average fine sinter A-line and Avg_F-B = Average fine sinter B-line)

The statistical comparison between lines A and B based on the XRF results for normal and fine sinter yielded ***P*** = 0.163 which indicates no significant difference. The only visible difference is in the Fe_2O_3 content of the fine sinter. It should be noted that the largest variances for both XRD and XRF results are present in the fine sinter samples and is associated with the iron content. Since moderate to no differences exist between the two production lines according to XRD and XRF results the two lines will be combined as an average for the rest of this report.

Figure 37 shows the XRD analyses for the samples taken in 2006.

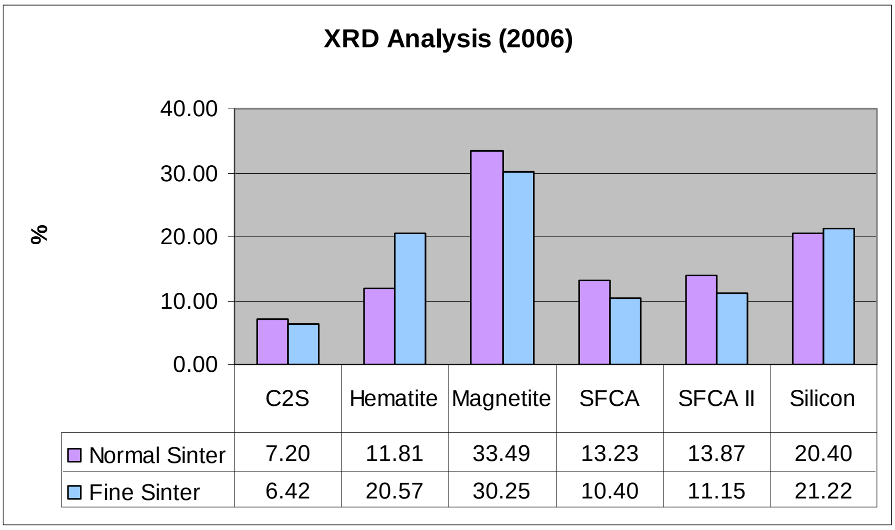

Figure 37: XRD analyses for the 28 samples taken in 2006

Statistical comparison between normal and fine sinter based on the XRD results for samples taken in 2006 yielded ***P*** = 0.042, which indicates a moderate significant difference.

Figure 38 shows the XRD analyses for the samples taken in 2005.

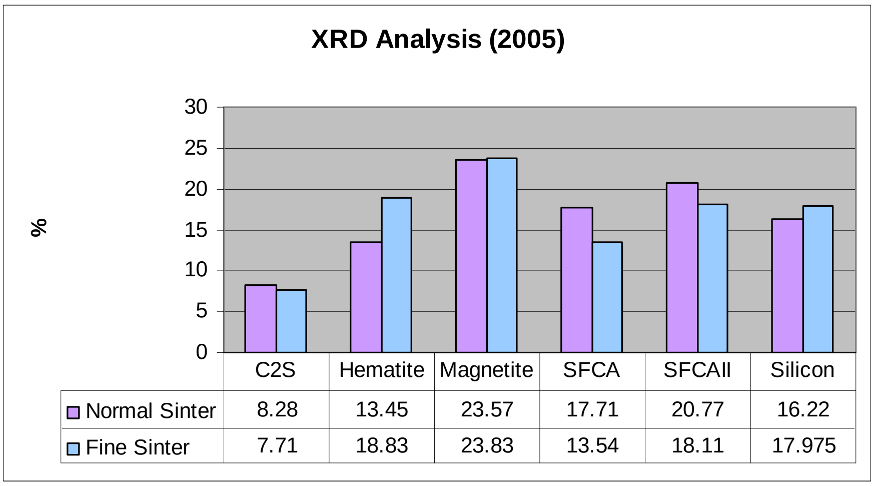

Figure 38: XRD analyses of the 4 samples taken in 2005

Statistical comparison between normal and fine sinter based on the XRD results for samples taken in 2005 yielded ***P*** = 0.004, which indicates a strong significant difference.

The differences between the samples taken in 2005 and 2006 can be simplified as is shown in Table 7.

Table 7: XRD differences between samples taken in 2005 and 2006

Phase	**2005 Normal sinter**	**2005 Fine sinter**
C_2S	1% more than 2006	1% more than 2006
Hematite	2% more than 2006	2% less than 2006
Magnetite	10% less than 2006	7% less than 2006
SFCA	4% less than 2006	3% more than 2006
SFCA II	4% less than 2006	5% more than 2006

The XRD results for both groups of samples indicate that there is a significant difference between normal and fine sinter. The general differences between normal and fine sinter are as follow: C_2S content is fairly small and therefore not noteworthy. The differences between hematite and SFCA are important. The fines contain almost 10% more hematite than the normal sinter. The magnetite content for the samples taken in 2005 is fairly similar whereas the samples taken in 2006 show a small difference. The SFCA content is about 5% less in the fines.

The results for the XRF analysis of samples taken in 2006 can be seen in Figure 39. There is no obvious difference in the chemistry between the normal and fine sinter.

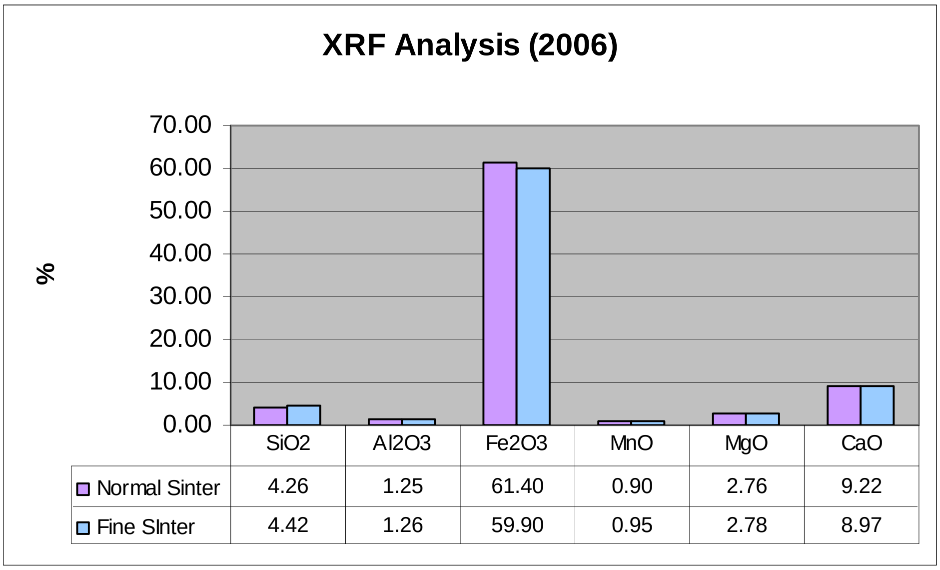

	SiO2	Al2O3	Fe2O3	MnO	MgO	CaO
▨ Normal Sinter	4.26	1.25	61.40	0.90	2.76	9.22
▨ Fine SInter	4.42	1.26	59.90	0.95	2.78	8.97

Figure 39: XRF comparison of normal sinter versus fine sinter of the 28 samples taken in 2006

Statistical comparison between normal and fine sinter based on the XRF results for samples taken in 2006 yielded ***P*** = 0.163, which indicates no significant difference.

The XRF analyses for the samples taken in 2005 are shown in Figure 40.

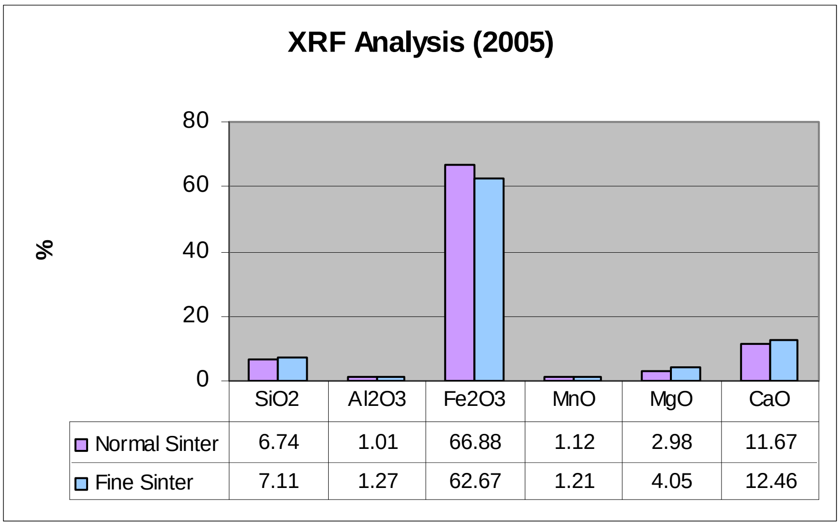

Figure 40: XRF analyses of the 4 samples taken in 2005

Statistical comparison between normal and fine sinter based on the XRF results for samples taken in 2005 yielded ***P*** = 0.163, which indicates no significant difference.

The differences between the samples taken in 2005 and 2006 can be simplified as is shown in Table 8.

Table 8: XRF differences between samples taken in 2005 and 2006

Chemistry	**2005 Normal sinter**	**2005 Fine sinter**
SiO_2	2% more than 2006	3% more than 2006
Al_2O_3	No difference	No difference
Fe_2O_3	5% more than 2006	3% more than 2006
MnO	No difference	No difference
MgO	No difference	2% more than 2006
CaO	2% more than 2006	3% more than 2006

The XRF results for both groups of samples indicate that there is no significant chemical difference between normal and fine sinter. This indicates that the only difference between normal and fine sinter is in the phase chemistry.

In comparison the XRD and XRF results for the samples taken in 2005 and those taken in 2006 differ. The reason for this is due to the chemical differences in the mixture that changed with time, but the differences between normal and fine sinter show the same trend.

Comparison of XRF results of samples taken in 2005 and 2006 is shown in Figure 41.

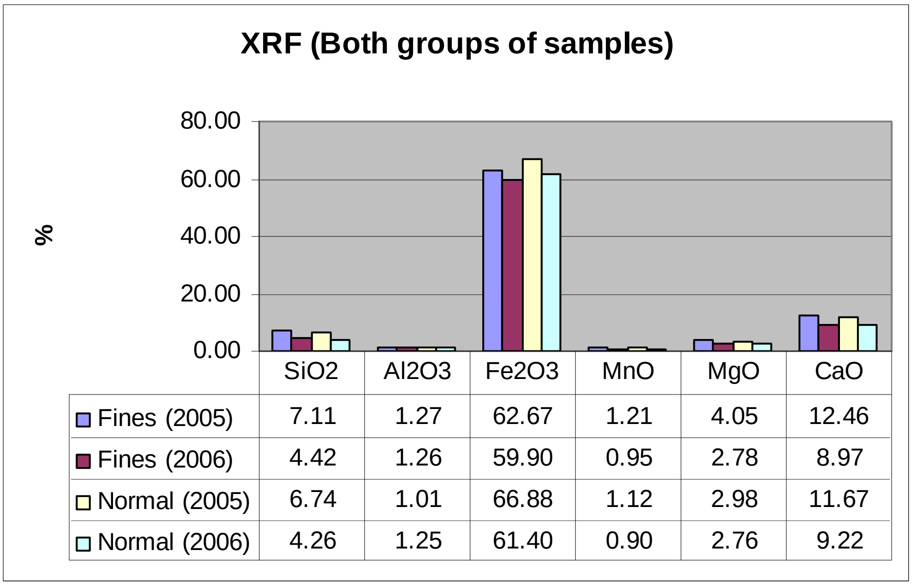

	SiO2	Al2O3	Fe2O3	MnO	MgO	CaO
Fines (2005)	7.11	1.27	62.67	1.21	4.05	12.46
Fines (2006)	4.42	1.26	59.90	0.95	2.78	8.97
Normal (2005)	6.74	1.01	66.88	1.12	2.98	11.67
Normal (2006)	4.26	1.25	61.40	0.90	2.76	9.22

Figure 41: Chemical comparison between samples taken in 2005 and 2006

The ***P*** value for the comparison between fine sinter of the samples taken in 2005 and 2006 is ***P*** = 0.621 which indicates no significant difference. The P value for the normal sinter equivalent is ***P*** = 0.601 which indicates no significant difference. This indicates that even though there is a slight chemical difference between the samples taken in the 2005 and 2006 it is not noteworthy.

5.4 Sol gel results

The first attempt to synthesize SFCA (with the composition determined by the microprobe data as shown in Figures 27 and 28 as cluster 5) was done by using oxides which were pressed into a pellet and then sintered at 1000ºC for three days. When analyzed with XRD it was found that the sample was very heterogeneous and did not react completely. It was then decided to use the sol gel method to synthesize the SFCA since this would give a more homogeneous product (all sol gels were synthesized at 1250ºC in air with the methods described in section 4.6).

Sol gel 1 was made with the sol gel method described in section 4.6 and presented the following results when analyzed with XRF (see Table 9):

Table 9: XRF results for SFCA prepared using sol gel method 1

Oxides	XRF	Weighed
SiO_2	4.94	3.34
Al_2O_3	3.06	3.04
Fe_2O_3	76.52	76.6
MgO	0.88	1.05
CaO	14.68	15.9

Statistical comparison between the weighed material and results after synthesis yielded ***P*** = 0.172 which indicates no significant difference.

It is shown in Table 7 that the greatest dissimilarity between the weighed amount and the XRF results is in the silica content. It was expected that this was due to the fact that the TEOS used as the source for silica, evaporated during synthesis.

The compounds CF and C_2S were then prepared to test this theory. The CF was synthesized using the first sol-gel method and the results were as follows.

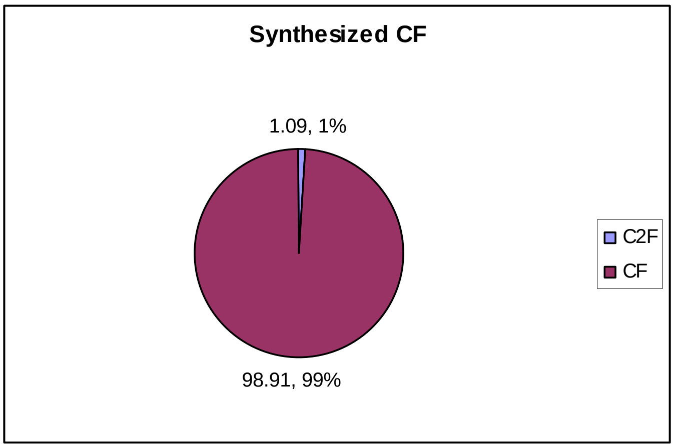

Figure 42: XRD results for synthesized CF

This shows that the technique does work well if no silica is present. In the case of the C_2S the first sol gel method resulted in 50% un-reacted lime, 48% C_3S and only 2% of the desired C_2S. These results can be seen in Figure 43. The reason for the large percentage unreacted lime is the fact that there was not enough silica to complete the reaction.

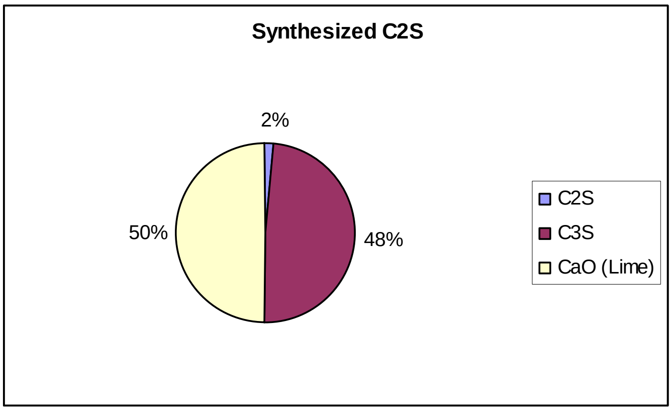

Figure 43: XRD results for C_2S

The XRF results for the C_2S made with the second method shows that $CaO/SiO_2 = 2.02$ instead of the acquired 2 (see Table 10). This is extremely close and shows that this method does not allow the TEOS to evaporate and is therefore the preferred method for synthesis if silica is present in the compound.

Table 10: XRF results for C_2S made with second sol-gel method

%	XRF	Weighed
SiO_2	33.25	34.89
CaO	67.25	65.11

The second sol-gel method was then used to synthesize SFCA. The results for that method can be seen in Table 11. It should therefore be expected that this method will result in improved synthesis compared to the first method used.

Table 11: XRF results SFCA prepared using sol-gel method 2

Oxides	XRF	Weighed
SiO_2	4.68	4.94
Al_2O_3	2.97	3.06
Fe_2O_3	75.16	76.52
MgO	0.71	0.88
CaO	15.59	14.68

Statistical comparison between the weighed material and results after synthesis yielded ***P*** =0.172 which indicates no significant difference.

The results in Table 11 conclude that the second sol gel method results in more precise synthesis for the desired SFCA phase.

SFCA prepared using sol gel methods 1 and 2 were analyzed with the SEM, using polished sections. SFCA prepared using method 1 will be referred to as sol gel 1 and the SFCA prepared using method 2 will be referred to as sol gel 2. Figure 44 indicates the location of SEM analyses of sol gel 1 and Figure 45 for sol gel 2 on a CaO-SiO_2-Fe_2O_3 compositional diagram to show the difference between the sol gels, standards and cluster value composition (the cluster represents the phase composition that was synthesized, i.e. cluster 5 from Figures 27 and 28).

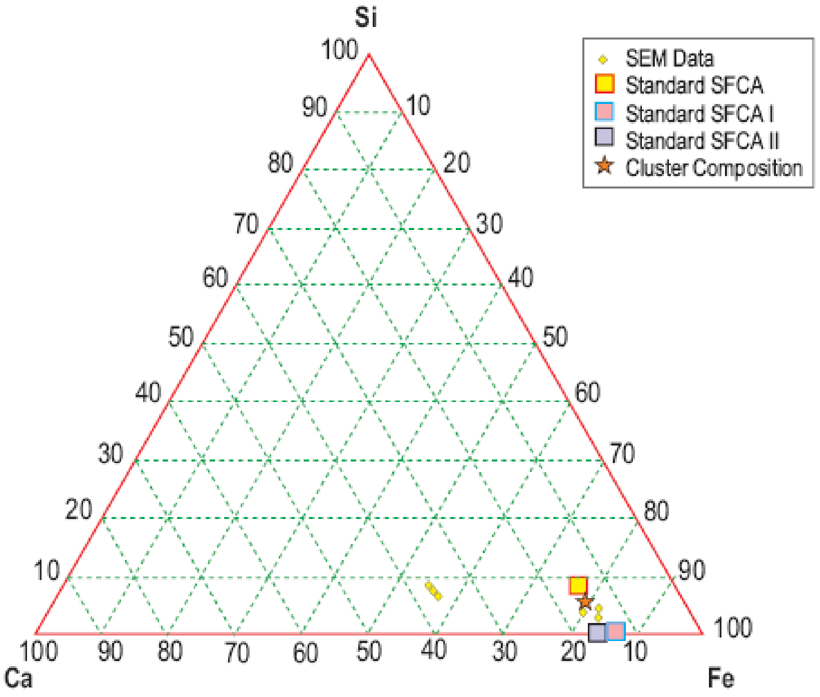

Figure 44: SEM analysis of sol gel 1. The compositions of the standard SFCA samples are those described by Hamilton *et. al*. 1989, Mumme *et. al*. 1998 and Mumme 2003.

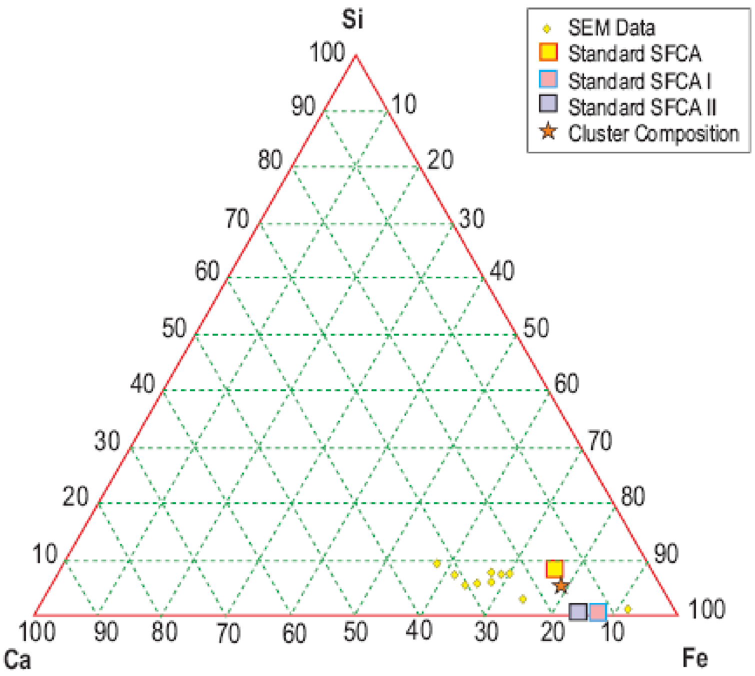

Figure 45: SEM analysis of sol gel 2. The compositions of the standard SFCA samples are those described by Hamilton *et. al.* 1989, Mumme *et. al.* 1998 and Mumme 2003.

In Figures 44 and 45 there are compositions present with higher CaO content than is associated with SFCA. In the following Tables where the SEM results are shown there are no analyses that can be compared to the prepared compositions. It might be due to unreacted material because the SEM analyses were mainly focused on well defined crystals.

Figure 46 shows the SEM image (EBI) that was taken for sol gel 1. It shows a heterogeneous mixture that contains two distinct phases. In Table 10 the chemical data for the two phases is given. Note that all sol gels were once-only synthesis. The reaction times were prolonged up to 3 days with no difference in the compositions. The SEM images that follow (Figures 46-49) each show one grain illustrating a light and dark phase. Tables 10-13 show the average data for each light and dark phase for the specific sol gel that was synthesized.

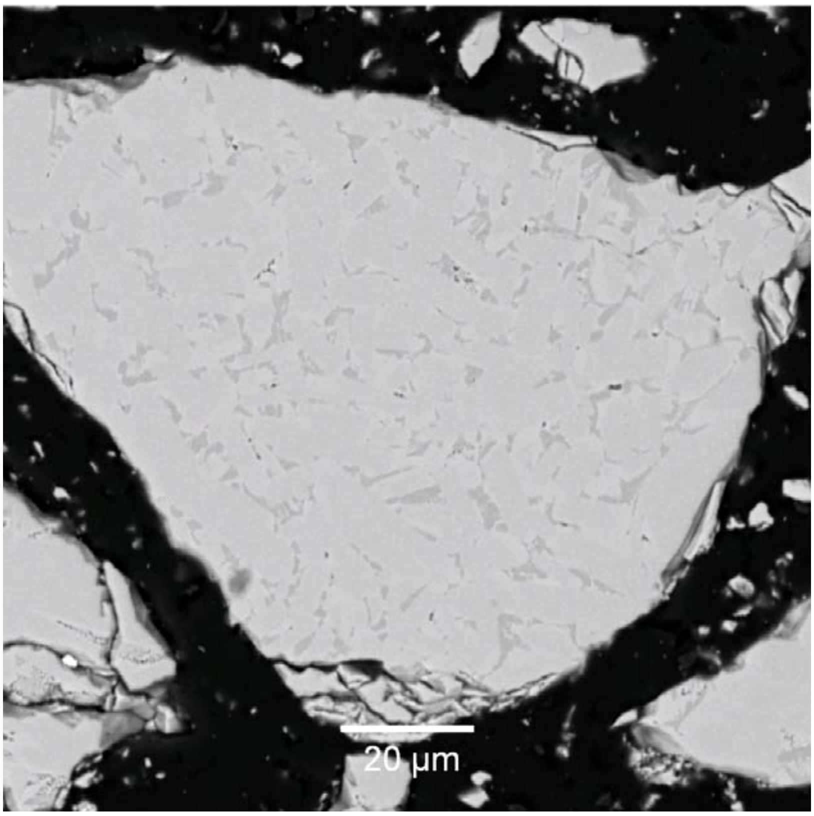

Figure 46: SEM image (EBI) of sol gel 1 showing light and darker colored phases. The crystal is heterogeneous which would not be expected from synthesis with the sol gel method

Table 12: Chemical data of the phases shown in Figure 45

Description	Fe_2O_3	SiO_2	CaO	MgO	Al_2O_3
Dark coloured area	54.9	7.6	36.8	0	0.6
Light coloured area	82.3	2.4	13.3	0	2.0

From Table 12 it is evident that neither of the two phases corresponds to the cluster composition, but that their average composition would be closer to the desired composition. This could be due to incomplete reaction, although the sample was subjected to lengthy reaction times and it appeared that the phase relationships did not change with longer reaction times. The composition of the light coloured area indicated in Table 12 is comparable to the C2 phase described by Patrick & Pownceby (2002).

Figure 47 depicts a grain from sol gel 2 taken with the SEM as an EBI.

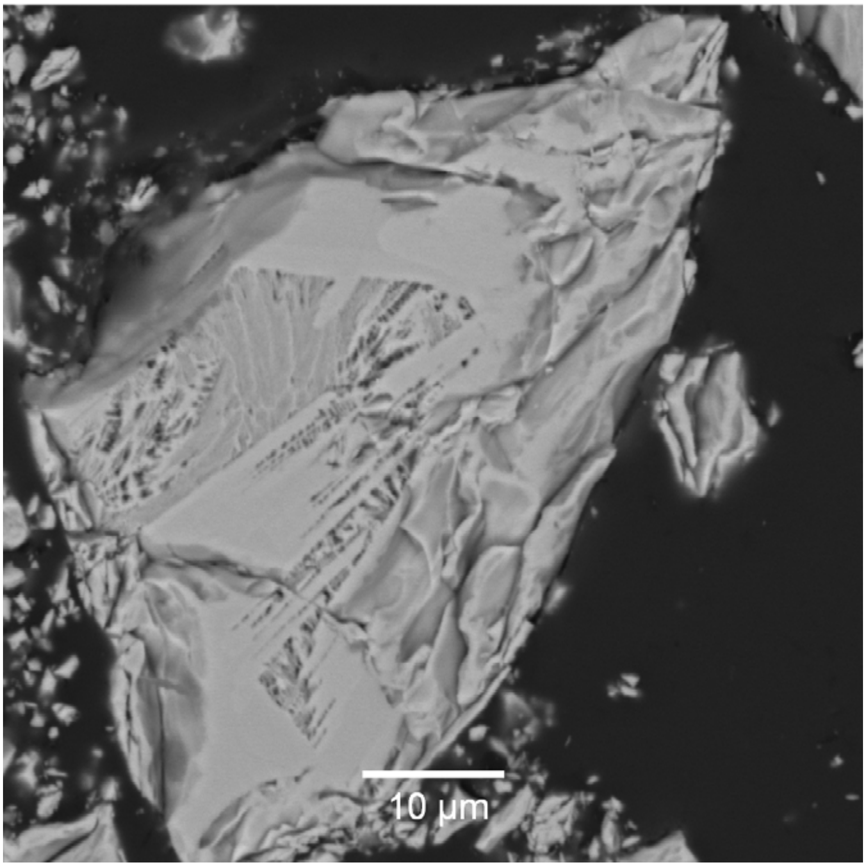

Figure 47: Sol gel 2 grain 1 showing the different textures and phases present

Chemical analysis of grain 1 revealed the following:

Table 13: Chemical data for Figure 46 showing the two distinct phases present

Description	**Fe_2O_3**	**SiO_2**	**CaO**	**MgO**	**Al_2O_3**
Dark coloured area	65.6	5.2	24.7	0.9	3.5
Light coloured area	83.7	0.2	6.8	7.7	1.3

Table 13 shows that there is a significant chemical difference between the two phases, and that a homogeneous SFCA has not yet been synthesized. Further work on different compositions and methods needs to be done.

Figure 48 depicts another grain from sol gel 2 taken with the SEM as an EBI.

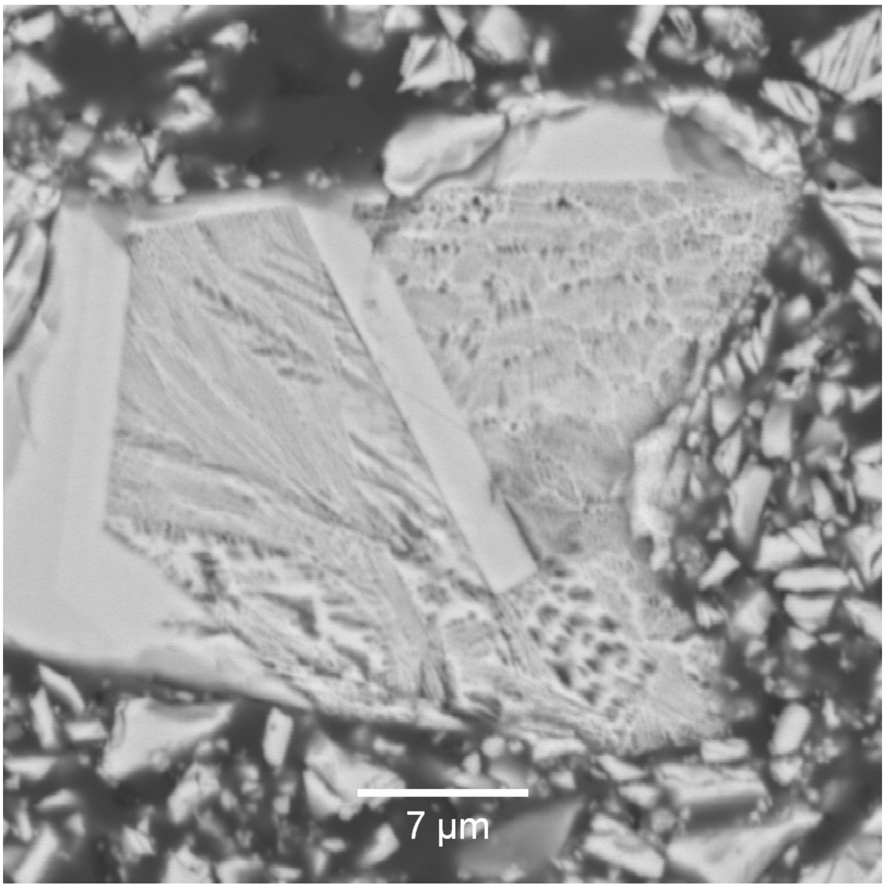

Figure 48: EBI of grain 2 from sol gel 2 depicting the different textures present. Note the smooth grain boundaries and lamellar texture on the left side of the grain.

Analyses of grain 2 revealed the following:

Table 14: SEM data for Figure 47 showing the compositional differences between the three phases

Description	**Fe_2O_3**	**SiO_2**	**CaO**	**MgO**	**Al_2O_3**
Needle like phase	56.3	8.4	32.0	0.0	2.7
Dark coloured area	63.1	6.6	23.1	1.0	6.0
Light coloured area	72.5	2.2	22.4	0.5	2.3

The composition of the light coloured area in Table 14 can be compared to that of CF.

Figure 49 depicts another grain from sol gel 2.

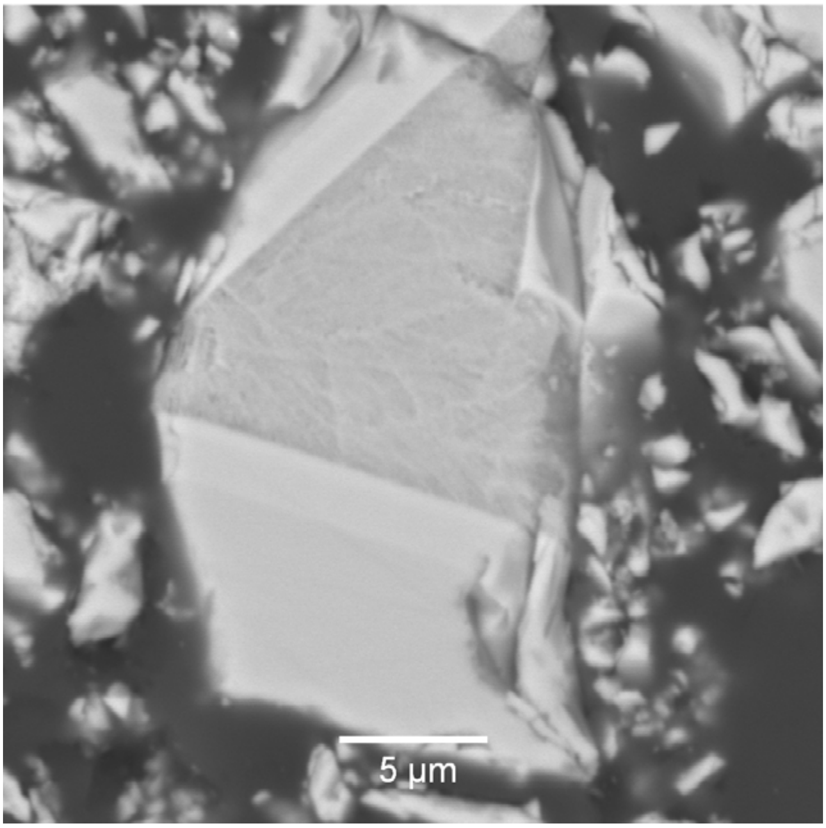

Figure 49: EBI of sol gel 2 grain 3 shows the light and darker coloured phases, note the smooth grain boundaries

Analyses of grain 3 revealed the following:

Table 15: SEM data for Figure 48 showing the compositions of the phases present 51

Description	Fe_2O_3	SiO_2	CaO	MgO	Al_2O_3
Dark coloured area	66.1	6.8	24.2	0.0	2.5
Light coloured area	73.4	2.1	22.3	0.4	1.7

The composition of the light coloured area in Table 15 can be compared to that of CF.

In Figure 50 the differences between the two SFCA phases prepared by the two sol gel methods are illustrated. This suggests that further experimental work is necessary in order to develop the preferred sol gel method by which homogeneous SFCA can be synthesized.

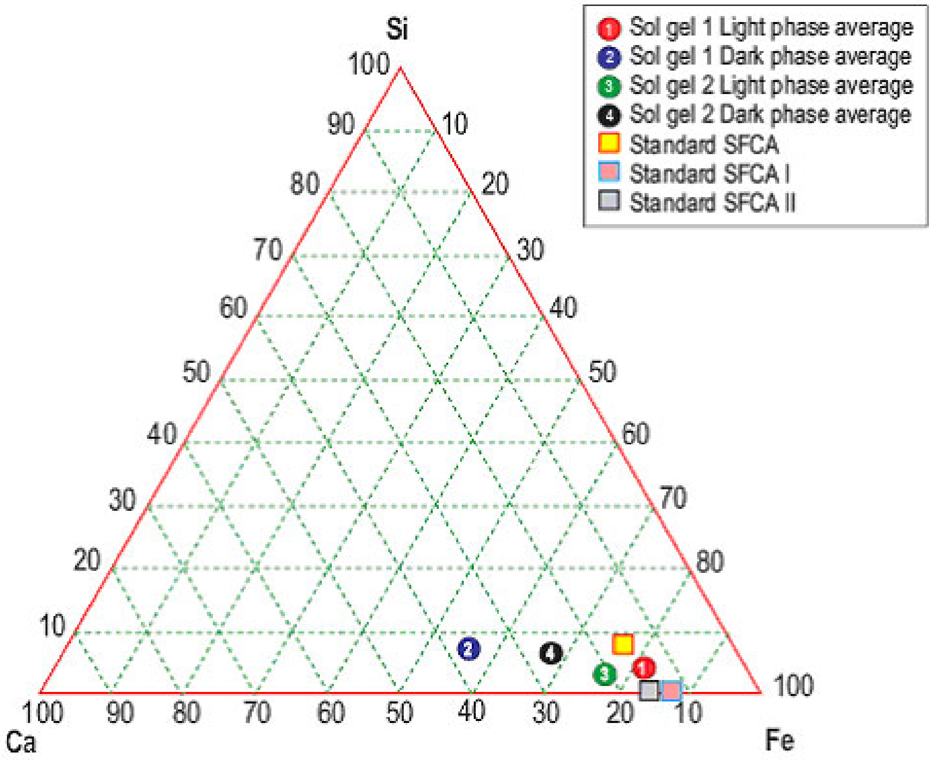

Figure 50: The light and dark coloured phases present in the two sol gels. The compositions of the standard SFCA samples are those described by Hamilton *et. al*. 1989, Mumme *et. al*. 1998 and Mumme 2003.

5.5 Point Counting

Figure 51 depicts the point counting results completed on one normal and one fine sinter from the samples taken in 2006. The data are shown in Appendix 6.

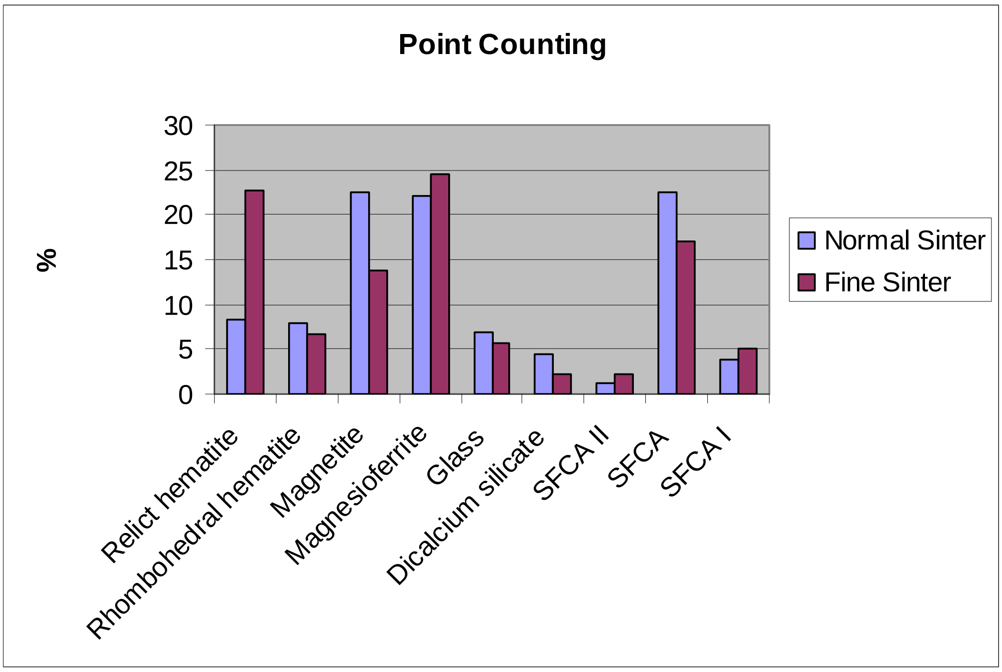

Figure 51: Point counting results. The spinel phase that contains both Fe and Mg is shown here as "magnesioferrite". The SFCA phases were distinguished by their morphology.

Fine sinter contains almost 15% more relict hematite than the normal sinter. This is an indication that all the hematite did not take part in the sintering reactions, therefore it can be concluded that the fine sinter did not react as completely as the coarse sinter to form the desired phases. The normal sinter contains only 1% more rhombohedral hematite than the fine sinter. This shows that both fine and normal sinter contains the same amount of reacted hematite. Normal sinter contains 10% more magnetite than the fine sinter, and it could be proposed that the ideal sinter would rather have more magnetite than hematite. Differences in the amounts of glass and C_2S are insignificant. The overall SFCA content is higher in the normal sinter which corresponds with the fact that SFCA is a bonding phase.

The comparison between the XRD analysis and point counting results can be seen in Figures 52 and 53. It should be noted that for comparison the different SFCA phases are grouped together as SFCA. Magnetite and "magnesioferrite" determined by point counting are combined and shown as magnetite for comparison purposes with the XRD results.

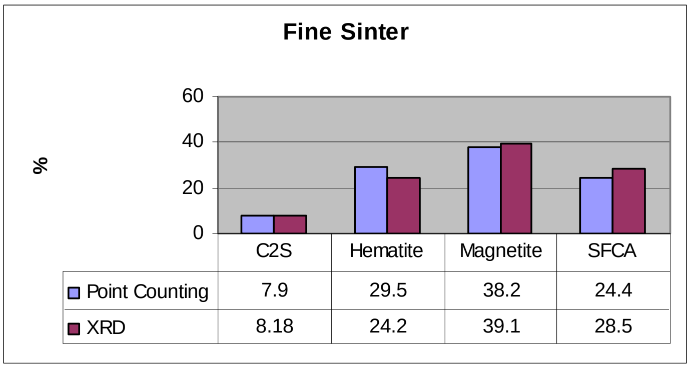

Figure 52: Comparison of the differences between Point counting and XRD in fine sinter

Statistical comparison between the quantification of the phases with point counting vs. XRD analyses for fine sinter taken in 2006 yielded ***P*** =0.037 which indicates a moderate significant difference.

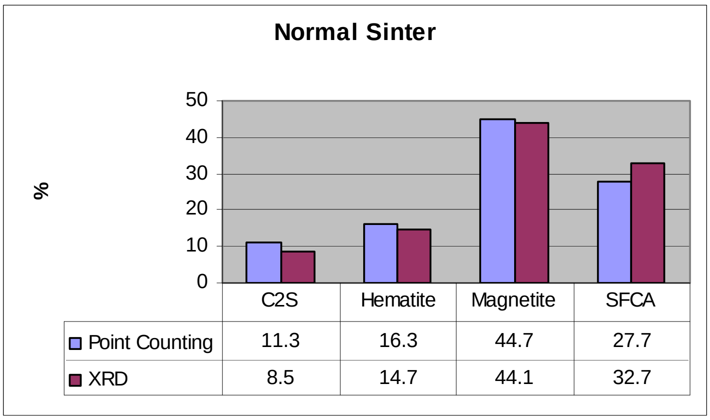

Figure 53: Comparison of the differences between Point counting and XRD in normal sinter

Statistical comparison between the quantification of the phases with point counting and XRD analyses for normal sinter taken in 2006 yielded ***P*** =0.057 which indicates no significant difference. According to the statistical data there is little significant difference between the XRD and point counting techniques. It should be noted that the largest differences present are in the fine sinter. Although variances exist they are small enough that XRD analysis can be compared to, or replace the point counting method if required since it is not as labour intensive.

5.6 Pot test results

XRD and XRF analyses were performed on the pot test samples. The samples were received as two fractions, +5mm represents the normal sinter and -5mm the fine sinter.

XRD results show that the hematite content is higher, and the SFCA is lower in the fine sinter. This corresponds to the trends found on all samples taken at the Vanderbijl Park sinter plant.

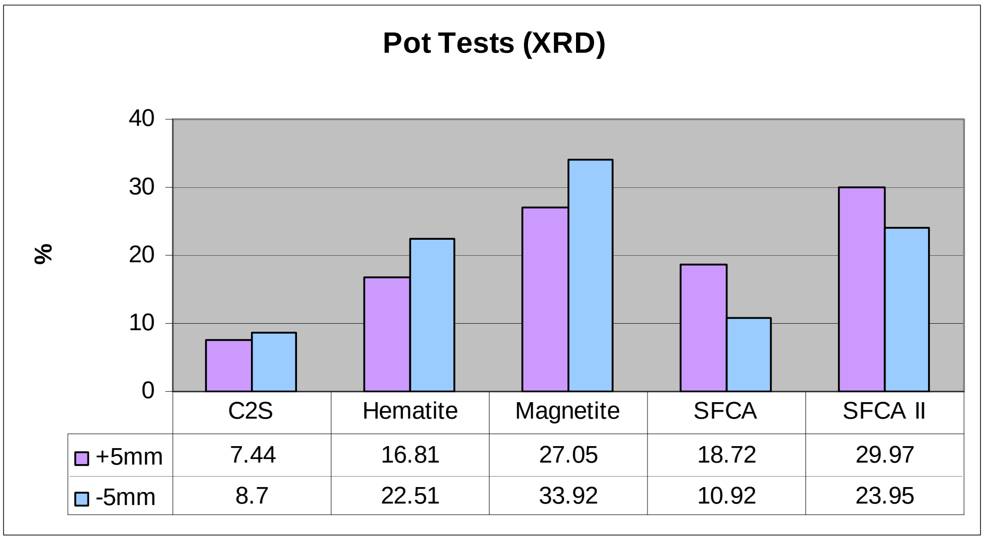

	C2S	Hematite	Magnetite	SFCA	SFCA II
▫ +5mm	7.44	16.81	27.05	18.72	29.97
▫ -5mm	8.7	22.51	33.92	10.92	23.95

Figure 54: XRD analysis showing the difference between normal and fine sinter produced in pot tests

Statistical comparison between normal and fine sinter according to the XRD analysis yielded ***P*** =0.028 which indicates a moderate difference in phase composition. This data show that the same trends visible in the plant samples are present in the pot tests. This may indicate that the fine sinter production is not only due to plant specific parameters.

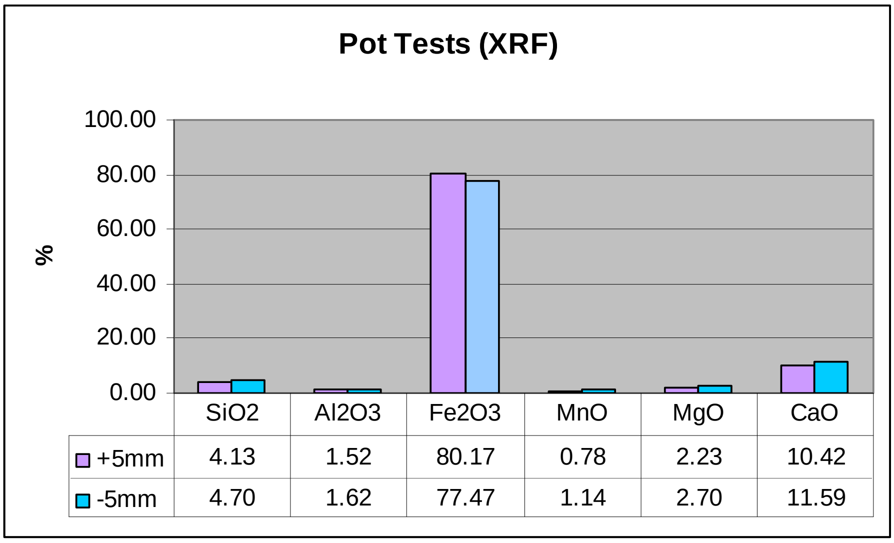

	SiO2	Al2O3	Fe2O3	MnO	MgO	CaO
▫ +5mm	4.13	1.52	80.17	0.78	2.23	10.42
▫ -5mm	4.70	1.62	77.47	1.14	2.70	11.59

Figure 55: XRF analysis showing the difference between normal and fine sinter produced in pot tests

XRF results show a lower Fe_2O_3 content in the fine sinter which corresponds with the plant samples. Statistical comparison between normal and fine sinter according to the XRF analysis yielded ***P*** =0.172 which indicates no significant difference in the chemistry of normal and fine sinter.

5.7 Plant factors

Statistical analyses were done on the samples taken during the three days of sampling (XRD analyses from the A-line were used) in order to determine if the various plant parameters had any influence on the phase chemistry of the sinter product. The plant circumstances associated with sampling instances can be viewed in Appendix 1. These short delays in the sinter plant strand operation include the following: pallet cars that need to be replaced, problems with gas pressure and blocked shutes. For 14/04/2006 and 15/04/2006 the calculations yielded ***P*** = 0.042 which indicate a moderate significant difference. For 16/04/2006 it was calculated as ***P*** = 0.057 which indicates no significant difference. These values indicate that the various interruptions that occurred during production have little to no effect on the product formed. The interruptions on 15/04/2006 were the least of all days and yet did not have the lowest ***P*** value, whereas the lowest ***P*** value for 16/04/2006 had approximately the same amount of factors as on 14/04/2006.

6. Discussion

6.1 Homogeneity tests

The samples taken at the plant were taken directly from the conveyer belts. This type of sampling from a flowing stream is the easiest, cheapest, most satisfactory and reliable method of sampling (Gy 1979:363). Sampling was carried out by fully qualified operators (Gy 1979:350).

In section 4.3 of this paper the sample preparation procedure was discussed. The stationary feeder sectorial splitter is one of the most unbiased methods that can be used for sample splitting. The only source of bias would be a non-uniformity of the revolving motion of the tray on which the containers are placed (Gy 1979:301).

The samples that were compared to determine if the plant sampling was representative showed relatively low standard deviations. The XRD average standard deviation is 0.43% and for the XRF 0.29%. This concludes that the sampling process produced samples which reflected the characteristics of the population.

The homogeneity tests that were completed with XRD illustrated the following: That the machine itself is capable of generating reproducible results. That the manner in which samples is mounted on the sample holder does not affect the analysis significantly. That smaller sub samples taken from the sample for analyses represent the sample satisfactorily. The XRF results all show less than 1% difference between the 5 samples analyzed which indicates that the results in connection with sample preparation and machine capability are reproducible with no significant differences.

The homogeneity tests therefore conclude that it is possible to scale down a large sample into manageable proportions for laboratory analyses. It is also evident that it is possible to sample a large production plant and obtain a representative sample.

6.2 Microprobe results

The microprobe data of the samples taken in 2005 indicated that the phases hematite, magnetite and C_2S are present as expected. The results showed that the SFCA phases were not present in the compositions by which they are described in the literature. Note that all microprobe data represent the sinter sample and not the single phase SFCA. Note that the bulk compositions have been normalized to show the Ca-Si-Fe ternary diagram.

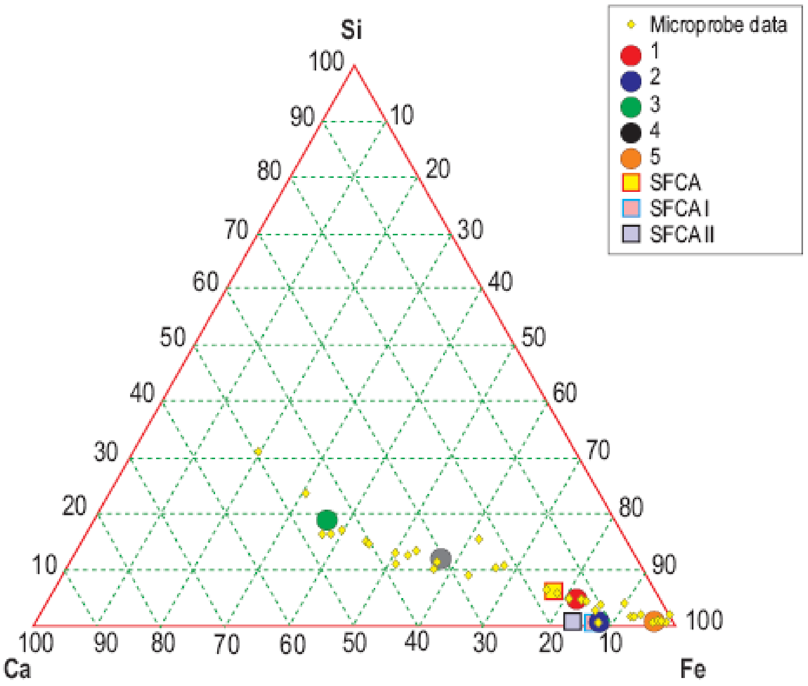

Figure 56: Microprobe analyses of phases present in normal sinter samples taken in 2006. The compositions of the standard SFCA samples are those described by Hamilton *et. al*. 1989, Mumme *et. al*. 1998 and Mumme 2003

The calculations completed on the analyses did not result in any perfect fit to the $M_{14+6n}O_{20+8n}$ formula. This is also visible on the compositional diagram presented (Figures 56 and 57). It has not been resolved if these phases have these stoichiometries that deviate from $M_{14+6n}O_{20+8n}$ because they did not react completely or if they are new SFCA phases.

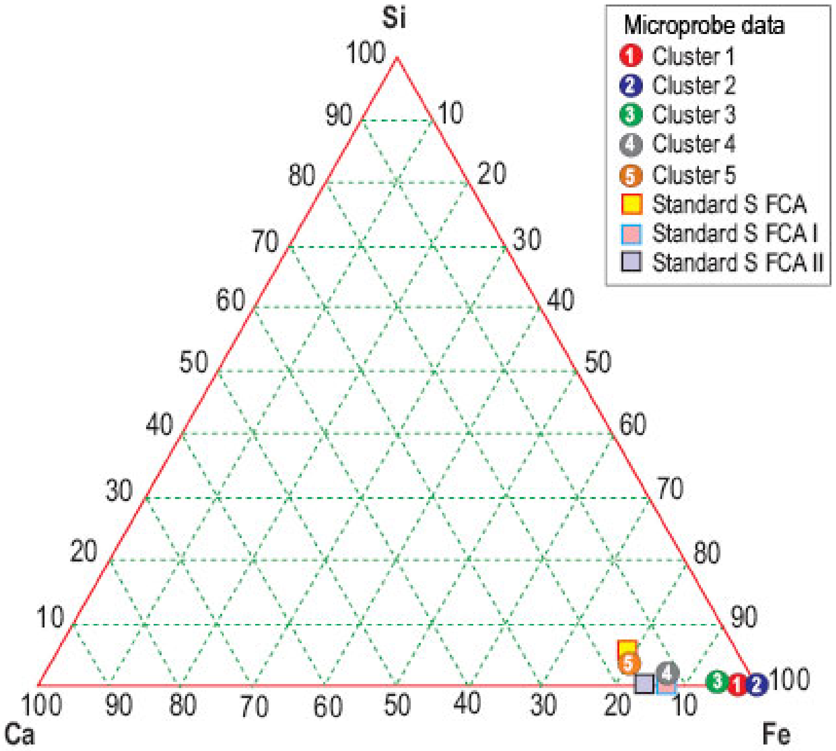

Figure 57: Compositional diagram comparing standard SFCA and microprobe data (elemental analysis) from samples taken in 2005. The compositions of the standard SFCA samples are those described by Hamilton *et. al*. 1989, Mumme *et. al*. 1998 and Mumme 2003.

The samples taken in 2006 showed different results when compared to the 2005 samples due to the difference in chemistry as explained in section 5.3. It has been shown that this difference is not significant. The hematite, magnetite and C_2S phases were similar to the samples taken in 2005, but the SFCA phases did not correspond closely to the standards defined in the literature.

When the analysed phase compositions are presented on the diagram by Patrick & Pownceby (2002:87) they plot in the hematite + SFCA I (+/-SFCA +/- liquid), SFCA + C6 (+/-hematite) and SFCA + liquid phase fields.

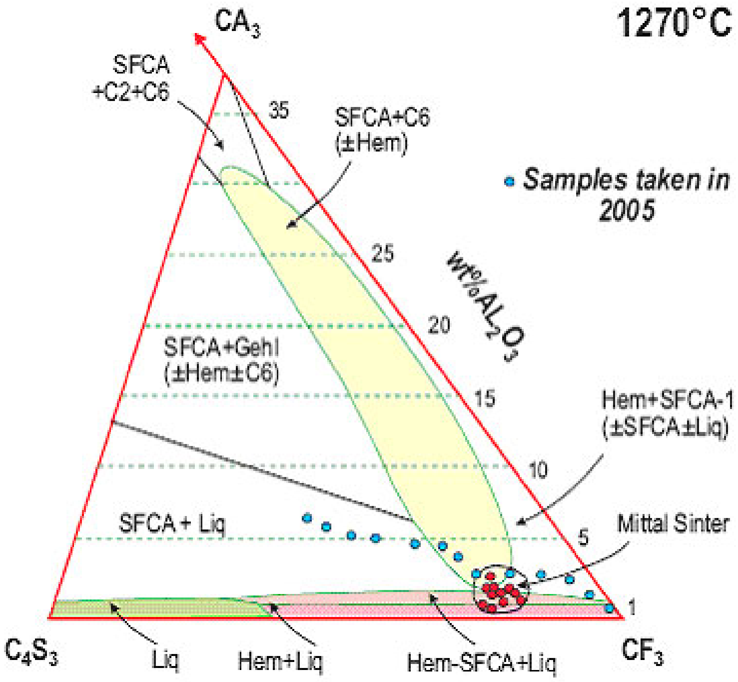

Figure 58: Phase compositions of samples taken in 2005 projected on the C_4S_3 – CA_3 – CF_3 ternary at the 1270ºC isotherm (Patrick & Pownceby 2002:87)

In Figure 58 the blue dots represents the samples that were taken in 2005 and illustrates the different phases that are present in the Vanderbijl Park sinter samples. Figure 58 shows that the compositions of the phases do not fall in the compositional range of the SFCA solid solution. These phases need to be synthesized and examined further to determine their relation to the SFCA phases.

6.3 Comparison between samples taken in 2005 and 2006 (XRD and XRF)

The XRD results showed that the same trends are apparent in both groups of samples. The proposed reason why the fine sinter contains more hematite is that it is unreacted material (due to the fact that it is largely relict hematite) that therefore did not completely take part in the desired crystallization sequence of sinter. The presence of secondary hematite may point to high reaction temperatures since small amounts can be associated with these conditions (Pimenta & Seshadri 2002:170). The relatively high magnetite content in the samples may be due to too high temperatures present during formation. At low pO_2 the magnetite stability field is increased while hematite is limited and single phase SFCA can not be produced as a crystalline phase under reduced pO_2 conditions (Pownceby & Clout. 2003) (Refer to Figure 12d-f for the SFCA stability field under reduced oxygen pressures).

The above mentioned high temperatures associated with magnetite and to a small extent secondary hematite could also result in less SFCA formation. The SFCA stability field is large at 1240°C compared to 1480°C. When Figures 59 and 60 are considered it is evident that too high temperatures will result in less SFCA formation especially when low amounts of Al_2O_3 are present.

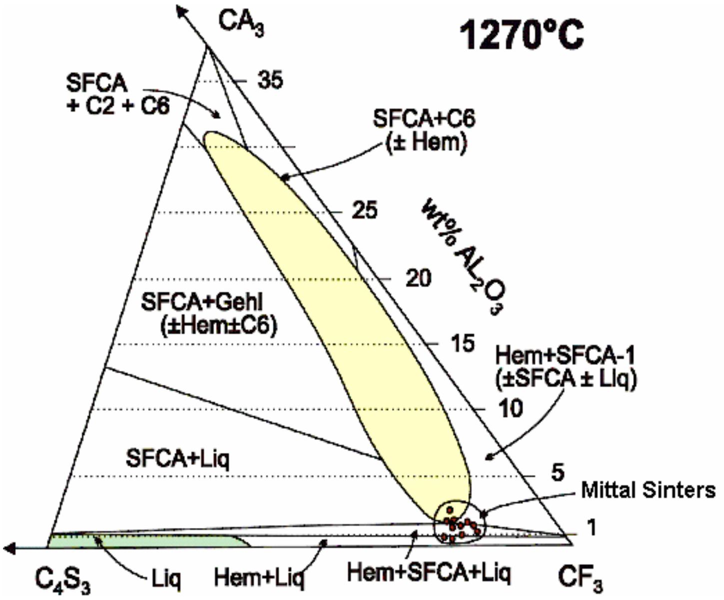

Figure 59: Compositions of Mittal sinters projected onto the 1270ºC isotherm as determined by Patrick & Pownceby (2002:87)

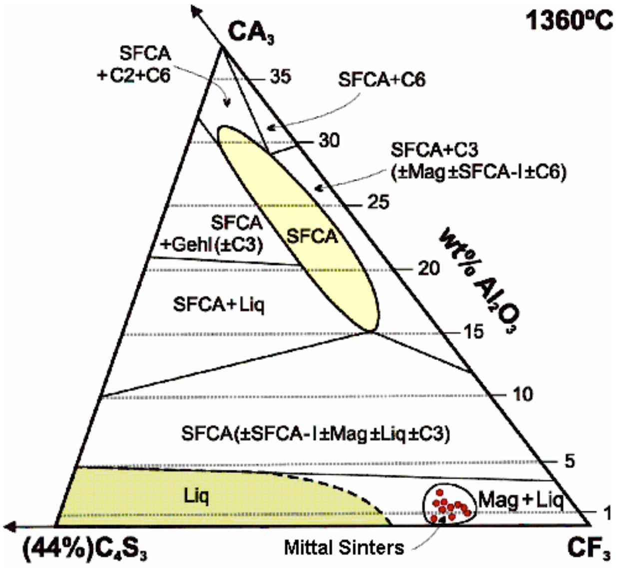

Figure 60: Compositions of Mittal sinters projected onto the 1360ºC isotherm (after Patrick & Pownceby 2002)

The Al_2O_3 content will have to be raised if high temperatures (T > ~1200°C) are present at the sinter plant. It should be noted that this may dilute the ore meaning that this is not the perfect solution to the problem. Since reactions continue during cooling, the possibility of SFCA formation via the precipitation of Fe-rich liquid could be attained if the cooling rate is controlled efficiently. The melt field at high basicity will result in crystallization of SFCA upon cooling, whereas low basicities will crystallize calcium silicates and hematite. Therefore the composition of the first melt will control the ability of SFCA to form. Since Vanderbijl Park operates at a high basicity of B = 2.1 the dependence of SFCA formation on such a high basicity is not well defined at this point.

A compositional diagram was constructed based on the XRD results to illustrate the differences between the fine and normal sinter (Figure 61). It depicts the distinct difference in phase relationships between the normal and fine sinter for the samples taken in 2006 (the same trend is present in the samples that were taken in 2005). The fine sinter contains more hematite and less SFCA than normal sinter. SFCA is the main bonding phase in sinter and the deficiency thereof will result in the production of fine material. The amount of SFCA in sinter will therefore have to be increased in order to decrease the amount of fine sinter that forms during production. This Figure also includes the pot test results which will be referred to in the pot test discussion section of this paper.

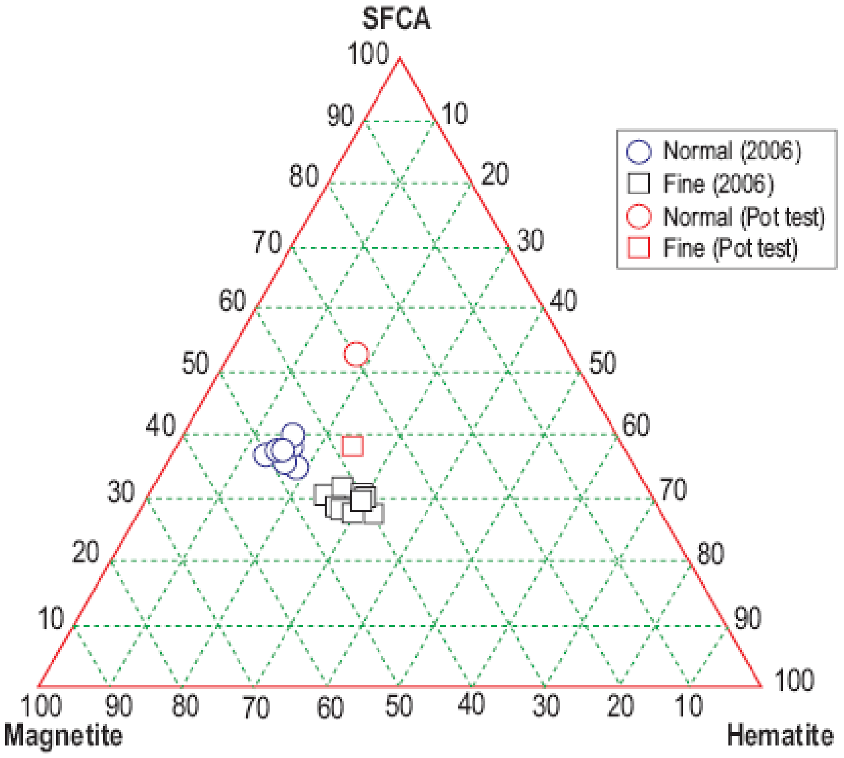

Figure 61: Compositional diagram showing differences in proportions of SFCA, magnetite and hematite between normal and fine sinter. The fine plant sinters contain

significantly more hematite than the normal sinters. The pot test results indicate a decrease in SFCA in the fine sinter.

XRF results indicated that the chemistry of the normal and fine sinter do not vary significantly (Figures 39 and 40). This indicates that the only the only difference between the normal and fine sinter is due to differences in phase relationships. This may rule out previous statements with regard to the microprobe analyses that the starting mixture does not allow the correct phases to crystallize. It rather indicates that the conditions under which the reactions take place are not suitable, therefore not providing the necessary temperature – time related conditions for crystallization.

6.4 Sol gels

The XRD and XRF analysis proved that the second method for preparing sol gels is more applicable to SFCA's chemistry than the first. The question that arises is if the end result of the second method is the appropriate synthesized phase due to the fact that the chemistry only fluctuates slightly. The answer lies in the SEM analyses of the gels. Although the chemical analyses of the sol gel 2 show almost no variance from the weighed material (which should indicate accurate synthesis) the SEM data does not support this. The first sol gel method provides a closer relationship to the desired composition (see Figures 44 and 45). The SEM images depicts that the sample is not homogeneous as would be expected from sol gel synthesis. The SEM analyses of the samples indicate that there is a distinct difference between the phases present on the EBI. Due to the preparation method this phenomenon could not be due to reaction time as mentioned above. It is unfortunately not clear why sol gel 1 plot so close to the cluster composition on the composition diagram. This could also be related to the XRD and XRF results determined for the samples taken in 2005 and 2006. In their analyses it was shown that great differences may be present in the XRD results (phase relationships) whereas the XRF analyses showed almost no variation. Further work is necessary in order to successfully synthesize the SFCA phases present in the Vanderbijl Park samples.

6.5 Point counting

The point counting results showed that it is possible to compare this technique with XRD analyses although significant variances were detected. The point counting results indicate that the hematite present in the fine sinter is largely relict hematite which suggests that unreacted material is present in the sinter sample.

The fact that spinel ("magnesioferrite") is abundant in both normal and fine sinter can be ascribed to the dolomite present in the starting mixture. This could lead to an increased MgO content of the mixture because the presence of Mg^{2+} decreases the decomposition temperature of hematite to magnetite and thus increases the magnetite and spinel content. The fact that fine sinter contains considerably less magnetite and slightly more magnesioferrite may be attributed to reduced partial oxygen pressures that leads to hematite decomposition at lower temperatures than in air.

This supports the conclusion that the reactions have not been completed in the preferred temperature – time related reaction conditions. According to the point counting results normal sinter contains more columnar SFCA (standard SFCA) than fine sinter. Microscopically the fine sinter contains more SFCA I and SFCA II which does not correspond with the XRD results that showed that fine sinter contains less SFCA (all phases included) than normal sinter (see Figures 37 and 38). In addition these results demonstrate the value of point counting since it is not possible to distinguish between the different forms of hematite with XRD analysis. Nevertheless, it could contain sampling errors due to the two-dimensional nature of the polished sample and the subjective phase recognition. XRD analyses would be less prone to sampling and interpretational errors.

6.6 Pot tests

It should be noted that there are certain differences between the conditions present at the plant and during pot tests. The pot tests are designed to represent plant conditions without the varying parameters that exist at the plant. Nevertheless there are certain parameters associated with the pot tests that introduce differences that are not present at the plant. They include the following: During pot tests the temperature can be controlled precisely, but at the plant it ranges between 1190 and 1370ºC. At the plant there is suction at the sides of the pallet car that is not present during the pot tests. These factors will therefore result in different sinter being produced during the pot tests than if the same starting material is used at the plant.

The comparison between plant samples and pot tests prove that there is a noteworthy difference. These include the following: Pot test samples show higher hematite content in the normal sinter and higher C_2S content in the fine sinter than is present in the plant samples. The important aspect to note is that the same trends are visible in both the plant samples and pot tests (fine sinter contains more hematite and less SFCA than normal sinter). This confirms that the reaction conditions should be changed in order to produce less fine sinter.

The large amounts of rhombohedral hematite in the fine sinter could be ascribed to its association with liquid or C_2S which can cause volume changes during sinter reactions. This may then lead to crack formation and subsequent production of fine material (Patrick & Lovel 2001:133). Crack formation decreases the cold strength of the sinter and may thereby lead to the formation of fine sinter.

In Figure 61 the location of the pot test compared to the samples taken at the plant is illustrated on a compositional diagram. Pot test results show that the fine sinter also contains more hematite and less SFCA than normal sinter resembling the composition of the samples that were taken at the plant. Both normal and fine sinters from the pot tests contain more SFCA than the plant samples. This can be ascribed to the fact that the starting material for the pot tests differed slightly from the plant starting material. It is also evident that the greater SFCA content in the pot test samples are directly related to the magnetite content. According to these results higher SFCA contents, decrease the magnetite content, but has no effect on the hematite content.

6.7 Plant factors

The statistical analyses for the samples taken in 2006 showed that the plant factors (interruptions due to replacement of damaged material etc.) do not have a direct influence on the sinter product. This implies that these pauses in the production process do not interrupt the reactions that produce the sinter material. This proves to be beneficial for the Vanderbijl Park sinter plant because it would be extremely difficult if not impossible to completely avoid these factors.

6.8 Economic considerations

At the Vanderbijl Park sinter plant the sinter product is sold at R260/t. An average of 10% fines is produced daily, which then have to be recycled back into the production line at a recycling cost of R140/t. If the amount of fines is reduced the recycling cost will decrease and result in greater revenue for the company. There are certain factors that may prevent the decrease in fine sinter produced. These factors include the following: The blast furnace operates at a certain basicity which might restrict any changes necessary to decrease the amount of fine sinter produced. The cost of changing the plant operations (new technology to control cooling regime) may be too high compared to the effect it will have on the fine sinter production.

7. Conclusions

The primary aim of this project was to investigate why fine sinter is produced at the Vanderbijl Park sinter plant, from a phase chemical point of view. Differences between normal and fine sinter as determined in this project are as follows.

According to the microprobe analyses there are small chemical variations between the phases in normal and fine sinter, however not substantial. The important data obtained from the microprobe results is that the composition and therefore the stoichiometry of SFCA in the Vanderbijl Park sinter do not agree with those described in the literature. This may indicate that the reaction conditions at the plant are not ideal for the formation of SFCA and could therefore explain the small amount of SFCA present in the fine sinter. Nevertheless the results show that the sinter does not contain pure SFCA the problem therefore might be that it does not contain the right type of SFCA i.e. acicular SFCA versus columnar SFCA. For the most part the Vanderbijl Park sinter plant produce sinter that contain Hem+SFCA+Liq (+ other minor phases) that is strong enough for commercial blast furnaces. The problem might be that the various variations within the sinter strand (T, pO_2), cause variation in the mineralogy (more relict hematite and therefore less SFCA) resulting in a loss of overall strength.

XRD results show that fine sinter contains more hematite and less SFCA than normal sinter, which is therefore the primary reason why fine sinter form. The results also show that there are no significant differences in the C_2S and magnetite content of normal sinter and fine sinter.

XRF data indicate that there are slight differences in the chemical composition between fine and normal sinter but it is insignificant. This indicates that there are no chemical differences between normal and fine sinter and that the difference is only due to the phases present. This then implies that the chemistry of the starting material is not the reason why fine sinter form.

Point counting results reveal that the hematite present in fine sinter is largely relict hematite which proves that the reactions were incomplete. The bulk SFCA content is higher in normal sinter which corresponds with the XRD results. The point counting and XRD results therefore confirm the difference between fine and normal sinter.

The comparison of pot tests and plant samples indicate that the fine sinter from pot tests also contains less SFCA and more hematite than normal sinter. This indicates that the scale of production at the plant is not the only cause for the creation of fine sinter.

It can therefore be concluded that the production of fine sinter is a direct function of the amount of hematite present in the sinter. This finding can be explained according to two hypotheses: The first proposed hypothesis is that the higher hematite content is a result of the inherent chemistry of the sinter material. The second proposed hypothesis involves the incomplete reaction of the sinter material during processing.

When investigating the validity of the first hypothesis there is no evidence that supports it. Evidence against this hypothesis is the XRF and microprobe analyses of all the samples that show there is no chemical difference between fine and normal sinter. The first hypothesis could therefore not be valid.

The second hypothesis is supported by the microprobe results that indicate that there is unreacted material present in both samples. The XRD results show that fine sinter contains more hematite than normal sinter. Another supporting factor is the point counting results that indicated that the hematite present is largely relict hematite.

The recommendations for minimizing the formation of fine sinter can be summarized as follows (see Table 16) and will then be described in detail:

Table 16: Summary of the recommendations for minimizing the production of fine sinter

Effect	**Recommendation**
Reduction of hematite	Uniform heat distribution during ignition
Reduction of hematite	pO_2 alteration by reductant addition
Increase the amount of SFCA	Lower ignition temperature
Increase the amount of SFCA	Regulate cooling regime
Increase the amount of SFCA	Decrease grain size of lime

The reduction of the amount of hematite in fine sinter could be achieved by various methods. The ignition and burning process should be investigated. The ignition temperature is one of the physical parameters that can influence sinter composition. At the Vanderbijl Park sinter plant this temperature is between T = 950 to 1050°C and the burn through temperatures vary between 1190 and 1370°C. These temperatures are in the stability field of SFCA under normal conditions and therefore do not seem to be the factor that limits SFCA formation. It should be noted that when examining the plant it was observed that as the pallet exited the ignition flame there were distinct sections across the bed that were not ignited. This could therefore lead to uneven heat distribution, which may then lead to the formation of round pores and which in turn may lead to the formation of fine sinter. If this phenomenon could be eliminated and even ignition attained it could lead to decreased fine sinter production.

Another physical parameter involved in the burning process is the FFS. When considering FFS it should be noted that at higher FFS the SFCA formed contained higher Fe and lower Si values compared to lower FFS where it contained lower Fe and higher Si. This could be an attributing factor since the microprobe analyses for all samples showed that all SFCA phases present (although they do not completely correlate with the standard SFCA's listed in the literature) do contain Si. The FFS at Vanderbijl Park and the effect it has on SFCA formation should therefore be investigated.

To decrease the amount of hematite the pO_2 content could be altered by reductant addition. This would then also increase the amount of magnetite formed. Unfortunately this could increase the temperature and create an environment in which SFCA can not be produced because it is stabilized at low temperatures ($T < 1240°C$). Another way is to provide high melt basicity and a favorable cooling regime that will produce SFCA from the reaction of hematite, melt and oxygen.

The amount of SFCA formed could be increased by decreasing the particle size of the lime (CaO) added as part of the starting mixture. This will result in larger surface areas available for reaction.

A proposed manner in which the SFCA production can be maximized is to generate this phase initially, and by doing so avoid its transformation to hematite/magnetite or silicate melt during the heating stage. In order to achieve this the reaction temperatures should not be too high, while the pO_2 should remain quite high. This will also decrease the amount of coke needed.

8. Suggestions for future work

More experimental data is needed in order to synthesize SFCA with the sol gel method which can then also be combined with increased temperature synthesis. When this is perfected single crystals can be grown and analyzed in order to determine the crystal structure of the SFCA phases identified in the Vanderbijl Park sinter plant samples. It can then be compared to the SFCA phases presented in the literature. It should then be possible to determine if these are new SFCA phases or part of the SFCA solid solution series. It would also improve the quality of the phase quantification.

There is still work to be completed on the kinetics of SFCA formation to determine its reactions in relation with time, temperature and formation transformations.

Investigation into the chemistry of the starting mixture is advised since it is possible that it could be altered to enhance the formation of SFCA.

9. References

Baffinland Iron Mines Corporation. 2005. Iron ore industry trends and analysis. Also available at: http://www.baffinland.com (accessed 20 February 2007).

Bennett, H. & Oliver, G. 1992. Proposed methods in XRF Analysis of Ceramics. Minerals and Applied Materials. John Wiley & Son. P. 67-93.

Berry, D.A. & Lindgren, B.W. 1990. *Statistics: Theory and Methods*. California: Brooks/Cole Publishing Company.

Bristow, N.J., & Waters, A.G. 1991. Role of SFCA in promoting high-temperature reduction properties of iron ore sinters. *Mineral Processing & Extractive Metallurgy, Section C*. vol. 100. p. 1-4.

Choudhary, M.K. 2007. Evolution of sinter structure along bed height of quenched test pot. *ISIJ International*. vol. 47. no. 3. p. 516-518.

Choudhary, M.K. & Nandy, B. 2006. Effect of Flame Front Speed on Sinter Structure of High Alumina Iron Ores. *ISIJ International*. vol. 46. no. 4. p. 611–613.

Chrysafi, R., Perraki, TH. & Kakali, G. 2007. Sol–gel preparation of $2CaO{\cdot}SiO_2$. *Journal of the European Ceramic Society*. vol. 27. p. 1707-1710.

Deer, W.A. Howie, R.A. Zussman, J. 1992. An introduction to the rock-forming minerals. 2nd Edition. Pearson Prentice Hall. China.

Dawson, P.R., Ostwald, J. & Hayes, K.M. 1983. *BHP Tech. Bull*. vol. 27. p. 47-51.

Gaki, A., Chrysafi, R. & Kakali, G. 2006. Chemical synthesis of hydraulic calcium aluminate compounds using the Pechini technique. *Journal of the European Ceramic Society*. vol. 27. p. 1781-1784.

Gy, P.M. 1979. *Sampling of particulate materials – theory and practice*. Elsevier. Amsterdam.

Hamilton, J.D.G., Hoskins, B.F., Mumme, W.G., Borbidge, W.E. & Montague, M.A. 1989. The crystal structure and crystal chemistry of $Ca_{2.3}Mg_{0.8}Al_{1.5}Si_{1.1}O_{20}$ (SFCA): solid solutions limits and selected phase relationships of SFCA in the SiO_2-Fe_2O_3-CaO(-Al_2O_3) system. *Neues Jahrbuch Miner. Abh*, vol. 161, no.1, p. 1-26.

Hayes, P. 1993. *Process principles in minerals and materials production*. Australia: Hayes Publishing Co.

Hoogovens Technical Services. (1997). The sintering process: Inland Steel Flat Products Company. Technological and Operational Assistance Inc.

Inoue, K. & Ikeda, T. 1982. *Tetsu-to-Hagane*. vol.68. p.2190-2199.

Ishikawa, Y., Shimomura, Y., Sasaki, M & Toda, H. 1983. Improvement of sinter quality based on the mineralogical properties of ores. *Ironmaking Proceedings*. vol. 42. p. 17-29.

Kama, M., Miyazaki, T., Ito, K., Hida, Y & Sasaki, M. 1984. Morphological analysis of calcium ferrite and hematite in sintered ore. *Transactions ISIJ*. vol. 24.

Kleeberg, R., & Bergmann, J. 1998. Quantitative Röntgenphasenanalyse mit den Rietveldprogrammen BGMN und AUTOQUANT in der täglichen Laborpraxis. *Ber. DTTG Greifswald.* Vol. 6. p. 237-250.

Kleeberg, R. & Bergmann, J. 2002. Quantitative Phase Analysis Using The Rietveld Method and a Fundamental Parameter Approach. In: S.P. SenGupta & P. Chatterjee (Eds.) Powder Diffraction. Proc. II Int. School on Powder Diffraction, IACS, Kolkata, Allied Publishers Ltd. p. 63-76.

Lecomte, P. 1971. Study on the structure of iron-ore sinters: The porosity of high-grade sinters. *C.R.M.* no. 28. p. 25-29.

Loo, C.E. (1998). Some progress in understanding the science of iron ore sintering. ICSTI/Iron Making Conference Proceedings. p. 1299-1315.

Loubser, M. 2007. Personal communication

Mashao, M. 2007. Personal communication.

Mittal Steel South Africa. Also available at: www.mittalsteel.com/Facilities/Rest+of+World/Mittal+Steel+South+Africa/ (accessed 25 May 2007).

Meunier, G. 1971. Study on the structure of iron-ore sinters: Sintering in an experimental pot-grate. *C.R.M.* no. 28. p. 5-16.

Mumme, W.G., Clout, J.M.F. & Gable, R.W. 1998. The crystal structure of SFCA-I $Ca_{3.18}Fe^{3+}_{14.66}Al_{1.34}Fe^{2+}_{0.82}O_{28}$, a homologue of the aenigmatite structure type, and new structure type, and new crystal structure refinements of β-CFF, $Ca_{2.99}Fe^{3+}_{14.30}Fe^{2+}_{0.55}O_{25}$ and Mg-free SFCA, $Ca_{2.45}Fe^{3+}_{9.04}Al_{1.74}Fe^{2+}_{0.16}Si_{0.6}O_{20}$. *Neues Jahrbuch Miner. Abh*, vol. 173, no.1, p. 93-117.

Mumme, W.G. 2003. The crystal structure of SFCA-II, $Ca_{5.1}Al_{9.3}Fe^{3+}_{18.7}Fe^{2+}_{0.9}O_{48}$ a new homologue of the aenigmatic structure-type, and structure refinement of SFCA-type, $Ca_2Al_5Fe_7O_{20}$. Implications for the nature of the "ternary-phase solid-solution" previously reported in the CaO-Al_2O_3-iron oxide system. *Neues Jahrbuch Miner. Abh*, vol. 178, no.3, p. 307-335.

Patrick, R.C. & Lovel, R.R. 2001. Leaching dicalcium silicates from iron ore sinter to remove phosphorus and other contaminants. *ISIJ*. vol. 41. no. 2. p. 128-135.

Patrick, T.R.C. & Pownceby M.I. 2002. Stability of Silico-Ferrite of Calcium and Aluminum (SFCA) in air-solid solution limits between 1240˚C and 1390˚C and phase relationships within the Fe_2O_3-CaO-Al_2O_3-SiO_2 (FCAS) system. *Metallurgical and Materials Transactions B*, vol. 33B, p. 79-89.

Pimenta, H. P. & Seshadri, V. 2002. Characterisation of structure of iron ore sinter and its behaviour during reduction at low temperatures. *Ironmaking and Steelmaking* vol. 29 no. 3. p. 169-174.

Ponghis, N. & Leroy, V. 1971. Study on the structure of iron-ore sinters: Sintering reactions. *C.R.M*. no. 28. p. 17-23.

Pownceby, M.I., Clout, J.M.F. & Fisher-White, M.J. 1998. Phase equilibria for the Fe_2O_3-rich part of the system Fe_2O_3-CaO-SiO_2 in air at 1240-1300˚C. *Trans. Instn Min. Metall*., vol. 107, p. 1-9.

Pownceby, M.I. & Patrick, T.R.C. 2000. Stability of SFC (silico-ferrite of calcium): solid solution limits, thermal stability and selected phase relationships within the Fe_2O_3-CaO-SiO_2 (FCS) system. *European Journal of Mineralogy*. vol. 12. p. 455-468.

Pownceby M.I. & and Clout, J.M.F. 2000. Phase relations in the Fe-rich part of the system Fe_2O_3(-Fe_3O_4)-CaO-SiO_2 at 1240-1300°C and oxygen partial pressures of 5×10^{-3} atm: implications for iron ore sinter. *Trans. Instn. Min. Metall*. vol. 109. p. 36-48.

Pownceby, M.I. & Clout, J.M.F. 2003. Importance of fine ore chemical composition and high temperature phase relations: applications to iron ore sintering and pelletising. *Mineral Processing and Extractive Metallurgy*, vol. 112, p. 44-51.

Scarlett, N.V.Y., Pownceby, M.I., Madsen, I.C. & Christensen, A.N. 2004. Reaction sequences in the formation of silico-ferrites of calcium and aluminum in iron ore sinter. *Metallurgical and materials transactions B*. vol. 35B. p. 929-936.

Scarlett, N.V.Y., Madsen, I.C., Pownceby, M.I. & Christensen, A.N. 2004. *In situ* X-ray diffraction analysis of iron ore sinter phases. *Journal of Applied Crystallography*, vol. 37. p. 262-268.

Steel Statistical Yearbook. 2006. International Iron and Steel Institute. Also available at: http://www.worldsteel.org (accessed 25 May 2007).

The Steel Authority of India. 2005. Coke Ovens-Sinter-BF-BOF Route. Also available at: http://www.sail.co.in/learning_coke.asp (8 March 2006).

Verein Deutscher Eisenhuttenleute. 1995. Slag Atlas. 2nd Edition. Verlag Stahleisen GmbH, D-Dusseldorf. Germany.

Watson, J. S. 1996. Fast, Simple Method of Powder Pellet Preparation for X-Ray Fluorescence Analysis. *X-Ray Spectrometry*. vol. 25. p. 173-174.

Woollacott, L.C. & Eric, R.H. 1994. *Mineral and metal extraction an overview*. Cape: The South African Institute of Mining and Metallurgy.

10. Acknowledgements

Firstly I would like to give special thanks to my supervisor Prof JPR de Villiers for giving me this opportunity to continue my studies. Without his guidance, expertise and of course patience this project would never have succeeded.

To my co-supervisor Prof AM Garbers-Craig for her advice and direction.

I'd like to thank my parents for their contribution to everything I have ever attempted. Their financial support during my undergrad studies and all the second chances I received. Especially to my dad who always believes in me.

Thank you to Peter Nel my fiancé for suggesting the career change from biochemistry to geology, it was one of the best choices I ever made. Thanks also for the moral support and love. I realize you worked very hard to give me a chance to fulfill my dreams.

Special thanks to Ms M Loubser and Dr S Verryn for the lovely office space, it was great to be part of the laboratory. Dr S Verryn for teaching me how to complete XRD analyses and technical support. Ms M Loubser for all XRF analyses and special help with the analyses of the sol gels.

Thank you to Mr P Graeser for the microprobe analyses and guidance toward understanding the operation of the process.

To Mr C Coetzee for all SEM analyses.

To Mr M Claassen for all polished sections used during the project.

To Mr K Ramela for teaching me the sample preparation procedures.

To Mr Martiens Schoeman, Mr L Labuscagne and the late Mr K van Baalen at the Vanderbijl Park sinter plant for assistance in sampling, plant operation and contributing ideas.

To Ms M van der Vyver, Mr A Dippenaar and Ms M Mashao at Kumba Iron Ore for their assistance with pot tests and point counting.

A special thanks to Kumba Iron Ore for the bursary and financial support.

11. Appendix

Appendix 1

Plant descriptions for samples taken in 2005

Sample 1 – Accretion material (sticker)
Sample 2 – External return
Sample 3 – Internal return
Sample 4 – Normal sinter

Plant descriptions for samples taken in 2006

Daily reports on plant operation. The problems that occurred are indicated together with the time the delay associated with it. Instances when samples were taken are indicated in red. A brief description of the various problems will follow.

Bins full: Bins into which newly formed sinter is transported are full
Fire bars: Grid underneath pallet car
Fire bar on belt: Piece of grid fell onto conveyor belt
Fix plate inside screen: Fix the plate inside the screening device
No gas pressure: No gas pressure for ignition flame
Replace fire bar on car: Replace grid underneath pallet car
Replace pallet car: Replace the entire pallet car
Shute block with fire bars: Shute is blocked by grid from pallet car
Sinter burn through: The specific bed which has been used for production is finished
Sticker: Large piece of agglomerated sinter material that has to be broken down physically before production can continue
Surge hopper empty: New sinter material has to be added to the charge that feeds the conveyor belt
Overload: Conveyor belt overloaded

Table 17: Daily plant operation and sampling times for Plant A and B for 14/04/2006

14/04/2006	**Plant A**	
Start	End	Reason
23:34	23:37	Fire bars
00:31	00:36	Sticker
04:49	04:52	Sticker
05:25	08:01	Bins full
08:10	08:14	Fire bar on belt
08:42	08:51	Sinter burn through
09:34	09:38	Fire bar on belt
10:02	10:06	Fire bar on belt
10:22	10:27	Replace firebars
11:00		Samples taken
11:00	11:06	Fire bars
11:19	11:22	Replace fire bars
11:36	11:45	Replace pallet car
13:18	13:21	Fire bar on belt
14:45	14:48	Fire bar on belt
15:00		Samples taken
16:00	18:11	Bins full
18:19	18:22	No gas pressure
19:00		Samples taken
19:44	20:00	No gas pressure
23:00		Samples taken

14/04/2006	**Plant B**	
Start	End	Reason
23:16	23:24	Replace fire bars
23:35	23:38	Fire bars
05:25	08:02	Bins full
08:06	08:12	Surge hopper empty
08:44	08:52	Sinter burn through
09:54	10:04	Shute block fire bars
10:47	10:59	Shute block fire bars and side walls
11:00		Samples taken
11:47	11:51	Fire bars
13:31	13:34	Fire bar on belt
14:24	14:28	Shute block fir bars
15:00		Samples taken
16:00	18:12	Bins full
18:19	18:23	No gas pressure
19:00		Samples taken
19:43	20:00	No gas pressure
23:00		Samples taken

Table 18: Daily plant operation and sampling times for Plant A and B for 15/04/2006

15/04/2006	**Plant A**	
Start	End	Reason
22:53	22:56	No gas pressure
00:14	00:22	Replace fire bars
00:24	00:38	Replace fire bars
04:43	06:23	Bins full
07:00	Samples taken	
07:00	07:07	Sinter burn through
08:17	08:26	Replace fire bars
11:00	Samples taken	
11:45	11:48	Fire bar on belt
15:00	Samples taken	
19:00	Samples taken	
23:00	Samples taken	
15/04/2006	**Plant B**	
Start	End	Reason
22:08	22:14	No gas pressure
22:22	22:28	No gas pressure
22:32	22:37	No gas pressure
02:36	02:46	No gas pressure
04:17	06:22	Bins full
06:25	06:31	Surge hopper empty
07:00	Samples taken	
07:02	07:12	Sinter burn through
07:59	13:57	Fix plate inside screen
11:00	Samples taken	
14:36	14:41	Sinter burn through
15:00	Samples taken	
17:29	17:32	Sticker
18:45	18:48	Fire bars
19:00	Samples taken	
20:05	20:14	Replace fire bars
23:00	Samples taken	

Table 19: Daily plant operation and sampling times for Plant A and B for 16/04/2006

16/04/2006	**Plant A**	
Start	End	Reason
22:15	22:27	Replace fire bars
03:00	Samples taken	
03:02	03:07	Fire bars
04:43	05:55	Bins full
06:34	06:37	Sticker
07:00	Samples taken	
10:05	10:10	Sticker
15:32	15:44	Replace fire bars
15:55	15:59	Fire bars
19:19	19:22	Sticker
19:37	19:40	Sticker
21:26	21:33	Replace fire bars
16/04/2006	**Plant B**	
Start	End	Reason
22:08	22:20	Sticker
22:20	22:24	Sticker
22:47	23:07	Replace pallet car
01:13	01:26	Replace pallet car
03:00	Samples taken	
03:19	03:49	Overload
04:43	05:53	Bins full
06:30	06:38	Sinter burn through
07:00	Samples taken	
09:19	09:25	Replace fire bars
09:31	09:49	Sticker
09:54	09:58	Fire bars
11:21	11:35	Sticker
18:43	18:50	Sticker
21:34	21:37	Sticker

Personal sample descriptions

Table 20: Sample numbers assigned to the different samples listed in Tables 17-19

14/11:00	**Sample No**	**14/15:00**	**Sample No**	**14/23:00**	**Sample No**
Normal B-Plant	1	Fines A-Plant	21	Normal A-Plant	8
Fines B-Plant	2	Fines B-Plant	46	Normal B-Plant	10
Normal A-Plant	3	Normal A-Plant	47	Fines A-Plant	30
Fines A-Plant	4	Normal B-Plant	48	Fines B-Palnt	31

Table 21: Sample numbers assigned to the different samples Tables 17-19 (continued)

15/07:00	**Sample No**	**15/23:00**	**Sample No**	**16/03:00**	**Sample No**	**16/07:00**	**Sample No**
Fines B-Plant	17	Normal A-Plant	6	Fines A-Plant	18	Fines A-Plant	19
Fines A-Plant	25	Fines A-Plant	9	Normal A-Plant	22	Fines B-Plant	20
Normal A-Plant	49	Normal B-Plant	32	Fines B-Plant	26	Normal A-Plant	24
Normal B-Plant	50	Fines B-Plant	33	Normal B-Plant	28	Normal B-Plant	27

Appendix 2

The mineral analyzer

The mineral analyzer uses electron back scatter (EBS) intensity together with the combined distribution of Ca, Fe and Si to define the phases present.

MLA results for the samples taken in 2005

Table 22: MLA results for samples taken in 2005

Mineral	Al (%)	Ca (%)	Cr (%)	Fe (%)	K (%)	Mg (%)	Mn (%)	O (%)	Si (%)	Ti (%)	V (%)
Silicate	2.74	29.87	0.22	14.00	0.92	0.00	0.17	29.53	19.01	3.25	0.20
SFCA-A	3.17	12.67	0.00	48.94	0.00	0.85	0.47	26.77	6.05	1.08	0.00
SFCA-B	1.73	7.84	0.00	60.26	0.00	2.02	1.18	25.53	1.44	0.00	0.00
Iron Oxide	0.00	2.21	0.00	67.16	0.00	3.95	2.10	24.60	0.00	0.00	0.00

Note that this analysis was conducted in order to determine the heterogeneity of the sinter material, therefore no standards and counting times are available.

Appendix 3

XRD results for the samples taken in 2005, 2006, sol gels and standard deviation values

Table 23: XRD results for samples taken in 2005 shown in wt%

Sample 1	C_2S	8.66	**Sample 2**	C_2S	8.22
	Hematite	8.27		Hematite	15.51
	Magnetite	27.6		Magnetite	25.03
	SFCA	16.22		SFCA(t)	15.36
	SFCAII	22.25		SFCAII	17.93
	Silicon	17		Silicon_	17.94
Sample 3	C_2S	7.2	**Sample 4**	C_2S	8.28
	Hematite	22.15		Hematite	13.45
	Magnetite	22.63		Magnetite	23.57
	SFCA(t)	11.72		SFCA(t)	17.71
	SFCAII	18.29		SFCAII	20.77
	Silicon_	18.01		Silicon_	16.22

Table 24: XRD results for the homogeneity tests conducted on the samples taken in 2005 shown in wt%

Remounts											Tot	Avg
C2S	8.810	9.080	9.130	8.860	8.250	8.720	9.000	9.310	8.530	9.290	88.980	8.898
Hematite	8.230	8.470	8.310	8.600	8.400	8.310	8.220	8.190	8.440	8.380	83.550	8.355
Magnetite	27.660	27.280	26.960	27.370	28.110	27.650	27.450	27.290	27.420	27.090	274.280	27.428
SFCA	16.380	16.330	16.500	16.210	16.020	16.090	16.700	16.610	16.340	16.390	163.570	16.357
SFCAII	22.060	22.060	22.000	22.140	22.340	22.130	21.800	21.770	22.350	21.820	220.470	22.047
Silicon	16.850	16.780	17.100	16.830	16.890	17.090	16.820	16.820	16.930	17.020	169.130	16.913
Sub samples												
C2S	8.810	8.790	8.860	9.110	9.150	8.930	9.150	8.860	9.450	8.980	90.090	9.009
Hematite	8.230	8.620	8.570	8.690	8.400	8.430	8.490	8.580	8.580	8.240	84.830	8.483
Magnetite	27.660	27.210	27.090	26.970	27.110	27.610	27.230	26.480	27.430	27.080	271.870	27.187
SFCA	16.380	16.520	15.780	16.290	16.780	15.830	16.540	15.420	16.090	16.580	162.210	16.221
SFCAII	22.060	22.280	22.660	21.780	21.930	22.580	21.630	23.580	21.410	21.810	221.720	22.172
Silicon	16.850	16.590	17.040	17.160	16.640	16.620	16.960	17.090	17.040	17.300	169.290	16.929
Repeats												
C2S	9.150	9.240	8.880	8.760	8.980	8.800	9.330	9.050	8.660	9.190	90.040	9.004
Hematite	8.290	8.250	8.380	8.290	8.250	8.240	8.290	8.300	8.350	8.260	82.900	8.29
Magnetite	27.000	27.580	27.430	27.290	27.180	27.310	27.340	27.100	27.210	27.470	272.910	27.291
SFCA	16.320	15.130	16.020	16.390	16.300	16.310	15.780	16.120	16.280	15.950	160.600	16.06
SFCAII	22.280	22.730	22.190	22.230	22.210	22.290	22.210	22.430	22.340	22.270	223.180	22.318
Silicon	16.950	17.070	17.100	17.030	17.080	17.040	17.060	17.010	17.160	16.860	170.360	17.036

Table 25: Standard deviation values for the XRD analyses of the homogeneity tests conducted on the samples taken in 2005

	Remounts	**Sub Samples**	**Repeats**		**Remounts**	**Sub Samples**	**Repeats**
C2S	8.810	8.810	9.150	Hematite	8.230	8.230	8.290
	9.080	8.790	9.240		8.470	8.620	8.250
	9.130	8.860	8.880		8.310	8.570	8.380
	8.860	9.110	8.760		8.600	8.690	8.290
	8.250	9.150	8.980		8.400	8.400	8.250
	8.720	8.930	8.800		8.310	8.430	8.240
	9.000	9.150	9.330		8.220	8.490	8.290
	9.310	8.860	9.050		8.190	8.580	8.300
	8.530	9.450	8.660		8.440	8.580	8.350
	9.290	8.980	9.190		8.380	8.240	8.260
Average	8.898	9.009	9.004	**Average**	8.355	8.483	8.290
Std Deviation	0.336	0.206	0.225	**Std Deviation**	0.128	0.157	0.045

Table 26: Standard deviation values for the XRD analyses of the homogeneity tests conducted on the samples taken in 2005 (continued)

	Remounts	**Sub Samples**	**Repeats**		**Remounts**	**Sub Samples**	**Repeats**
Magnetite	27.660	27.660	27.000	SFCA(t)	16.380	16.380	16.320
	27.280	27.210	27.580		16.330	16.520	15.130
	26.960	27.090	27.430		16.500	15.780	16.020
	27.370	26.970	27.290		16.210	16.290	16.390
	28.110	27.110	27.180		16.020	16.780	16.300
	27.650	27.610	27.310		16.090	15.830	16.310
	27.450	27.230	27.340		16.700	16.540	15.780
	27.290	26.480	27.100		16.610	15.420	16.120
	27.420	27.430	27.210		16.340	16.090	16.280
	27.090	27.080	27.470		16.390	16.580	15.950
Average	27.428	27.187	27.291	**Average**	16.357	16.221	16.060
Std Deviation	0.324	0.340	0.176	**Std Deviation**	0.214	0.431	0.381

Table 27: Standard deviation values for the XRD analyses of the homogeneity tests conducted on the samples taken in 2005 (continued)

	Remounts	**Sub Samples**	**Repeats**		**Remounts**	**Sub Samples**	**Repeats**
SFCAII	22.060	22.060	22.280	Silicon	16.850	16.850	16.950
	22.060	22.280	22.730		16.780	16.590	17.070
	22.000	22.660	22.190		17.100	17.040	17.100
	22.140	21.780	22.230		16.830	17.160	17.030
	22.340	21.930	22.210		16.890	16.640	17.080
	22.130	22.580	22.290		17.090	16.620	17.040
	21.800	21.630	22.210		16.820	16.960	17.060
	21.770	23.580	22.430		16.820	17.090	17.010
	22.350	21.410	22.340		16.930	17.040	17.160
	21.820	21.810	22.270		17.020	17.300	16.860
Average	22.047	22.172	22.318	**Average**	16.913	16.929	17.036
Std Deviation	0.207	0.635	0.162	**Std Deviation**	0.118	0.246	0.083

Table 28: XRD results for samples taken in 2006 shown in wt%

Normal B-Plant	T1	T48	T10	T50	T32	T28	T27	**Total**	**Avg**
C2S	7.47	7.1	7.97	7.81	8.24	7.35	7.45	53.39	7.6271
Hematite	11.02	11.36	12.06	12.01	11.94	13.6	9.89	81.88	11.697
Magnetite	34.1	32.01	32.5	32.74	32.8	33.65	36.01	233.81	33.401
SFCA	13.17	14.23	13.44	12.88	13.33	12.63	13	92.68	13.24
SFCA II	13.67	14.35	14.12	14.42	13.6	12.46	13.4	96.02	13.717
Silicon	20.56	20.96	19.91	20.14	20.09	20.3	20.25	142.21	20.316
Fines B-Plant	T2	T46	T31	T17	T33	T26	T20		
C2S	5.66	5.55	6.36	6.94	5.44	6.98	6.58	43.51	6.2157
Hematite	21.93	23.5	23.65	19.36	22.21	19.64	18.33	148.62	21.231
Magnetite	29.39	26.46	29.01	29.95	28.56	30.2	32.18	205.75	29.393
SFCA(t)	12.69	11.39	9.29	10.87	10.15	10.41	9.25	74.05	10.579
SFCAII	8.75	11.98	10.36	11.37	11.37	11.59	12.31	77.73	11.104
Silicon_	21.58	21.13	21.33	21.5	22.26	21.18	21.36	150.34	21.477
Normal A-Plant	T3	T47	T8	T49	T6	T22	T24		
C2S	6.08	6.7	6.81	7.5	6.77	6.78	6.79	47.43	6.7757
Hematite	12.17	12.57	12.12	11.48	11.79	11.6	11.69	83.42	11.917
Magnetite	33.24	32.73	34.49	31.71	33.83	34.08	35.02	235.1	33.586
SFCA(t)	14.37	13.45	12.4	13.3	13.41	13.41	12.24	92.58	13.226
SFCAII	13.32	14.11	13.58	15.6	13.97	13.8	13.72	98.1	14.014
Silicon_	20.83	20.43	20.61	20.42	20.24	20.33	20.55	143.41	20.487
Fines A-Plant	T4	T21	T30	T25	T9	T18	T19		
C2S	6.02	6.48	7.16	7.14	6.89	6.5	6.11	46.3	6.6143
Hematite	19.82	19.17	21.73	15.81	20.49	20.43	21.89	139.34	19.906
Magnetite	32.26	30.98	29.13	31.65	31.51	31.58	30.67	217.78	31.111

SFCA(t)	10.63	10.34	10.16	11.55	10.53	9.55	8.78	71.54	10.22
SFCAII	9.82	12.27	11.16	13.12	9.94	11.04	11	78.35	11.193
Silicon_	21.45	20.75	20.66	20.73	20.63	20.9	21.56	146.68	20.954

Table 29: XRD results for the sol gels - CF and C_2S shown in wt%

CF results	**Wt%**
C_2F	1.09
CF	98.91
CaO (Lime)	0.00
C_2S results	**Wt%**
C_2S	1.74
C_3S	48.14
CaO (Lime)	50.13

Table 30: XRD results for the sol gel – CF shown in wt%

C_2F	93.88
CF	6.12

Table 31: XRD results for the pot tests shown in wt%

(-5mm)	**%**
C2S beta Mumme	8.7
Hematite	22.51
Magnetite	33.92
SFCA(t)_Fixed	10.92
SFCAII_Fixed	23.95
(+5mm)	**%**
C2S	7.44
Hematite	16.81
Magnetite	27.05
SFCA	18.72
SFCA II	29.97

Appendix 4

XRF results for samples taken in 2005, 2006, sol gels with their respective standard deviation and limit of detection values

Table 32: XRF results for samples taken in 2005

Sample Compositions				
	Sample 1	Sample 2	Sample 3	Sample 4
SiO_2	7.413	7.089	7.130	6.744
TiO_2	0.201	0.134	0.124	0.117
Al_2O_3	1.119	1.219	1.328	1.013
Fe_2O_3	66.701	61.707	63.626	66.884
MnO	1.098	1.179	1.245	1.117
MgO	2.845	3.777	4.326	2.982
CaO	13.596	12.558	12.368	11.672
Na_2O	0.332	0.277	0.268	0.275
K_2O	0.163	0.137	0.132	0.082
P_2O_5	0.134	0.128	0.130	0.136
Cr_2O_3	0.030	0.019	0.020	0.021
NiO	0.007	0.002	0.003	0.004
V_2O_5	0.010	0.007	0.007	0.007
ZrO_2	0.000	0.003	0.003	0.003
SO3	0.385	0.449	0.955	0.571

Table 33: Standard deviation and limit of detection for XRF results for samples taken in 2005

STANDARD DEVIATION AND LIMIT OF DETECTION:			
	Instrumental	Experimental	
	std dev.(%)		LOD
SiO2	0.4	1.039661678	0.02
TiO2	0.03	1.278850627	0.0032
Al2O3	0.3	1.685553911	0.01
Fe2O3	0.3	0.215441594	0.0097
MnO	0.0065	1.527965659	0.0013
MgO	0.1	1.411755556	0.0118
CaO	0.07	0.333582662	0.01
Na2O	0.11	1.867310893	0.0265
K2O	0.06	5.049338604	0.005
P2O5	0.08	1.371184676	0.01
Cr2O3	0.0053	3.013237447	0.0006
NiO	0.01	3.757277637	0.0013
V2O5	0.0018	1.397397092	0.0008
ZrO2	0.005	0	0.0009
CuO	0.0037	17.70199117	0.0003

Table 34: XRF results for samples taken in 2006

	S 1_N-B	S 10_N-B	S 27_N-B	S 28_N-B	S 32_N-B	S 48_N-B	S 50_N-B
SiO_2	4.21	4.38	4.41	4.21	4.22	4.23	4.02
TiO_2	0.09	0.10	0.09	0.09	0.09	0.09	0.09
Al_2O_3	1.24	1.30	1.29	1.20	1.26	1.24	1.19
Fe_2O_3	61.30	64.39	63.96	61.70	60.77	61.90	58.90
MnO	0.86	0.98	0.92	0.87	0.92	0.91	0.90
MgO	2.70	2.94	2.88	2.72	2.73	2.74	2.70
CaO	9.07	9.65	9.52	9.05	9.31	9.22	8.90
Na_2O	0.00	0.01	0.01	0.00	0.00	0.00	0.00
K_2O	0.13	0.13	0.12	0.13	0.13	0.13	0.12
P_2O_5	0.10	0.11	0.11	0.10	0.10	0.10	0.10
Cr_2O_3	0.02	0.02	0.03	0.02	0.02	0.02	0.02
NiO	0.00	0.00	0.00	0.00	0.00	0.00	0.00
V_2O_5	0.01	0.01	0.01	0.01	0.01	0.01	0.01
ZrO_2	0.00	0.00	0.00	0.00	0.00	0.00	0.00

Table 35: XRF results for samples taken in 2006 (continued)

	S 2_F-B	S 17_F-B	S 20_F-B	S 26_F-B	S 31_F-B	S 33_F-B	S 46_F-B
SiO_2	4.51	4.56	4.64	4.23	4.49	4.44	4.62
TiO_2	0.09	0.09	0.09	0.09	0.09	0.09	0.09
Al_2O_3	1.27	1.31	1.27	1.25	1.24	1.25	1.27
Fe_2O_3	57.28	57.14	58.40	61.18	58.71	55.96	56.47
MnO	0.96	1.07	0.94	0.90	0.98	0.95	0.91
MgO	2.84	2.97	2.90	2.66	2.91	2.80	2.85
CaO	9.07	9.32	9.22	8.84	9.06	9.42	9.04
Na_2O	0.00	0.00	0.00	0.00	0.00	0.00	0.00
K_2O	0.14	0.15	0.14	0.13	0.14	0.13	0.14
P_2O_5	0.10	0.10	0.10	0.10	0.10	0.10	0.10
Cr_2O_3	0.02	0.03	0.03	0.02	0.02	0.03	0.02
NiO	0.00	0.00	0.00	0.00	0.00	0.00	0.00
V_2O_5	0.01	0.01	0.01	0.01	0.01	0.01	0.01
ZrO_2	0.00	0.00	0.00	0.00	0.00	0.00	0.00

Table 36: XRF results for samples taken in 2006 (continued)

	S 3_N-A	S 6_N-A	S 8_N-A	S 22_N-A	S 24_N-A	S 47_N-A	S 49_N-A
SiO_2	4.63	4.91	4.20	4.02	4.12	4.00	4.00
TiO_2	0.08	0.10	0.09	0.09	0.09	0.08	0.09
Al_2O_3	1.32	1.37	1.25	1.19	1.24	1.18	1.19
Fe_2O_3	57.68	61.16	63.97	60.85	63.85	59.33	59.89
MnO	0.78	1.03	0.93	0.84	0.94	0.83	0.92
MgO	2.90	3.09	2.78	2.56	2.66	2.52	2.71
CaO	10.51	9.73	9.20	8.66	8.85	8.54	8.89
Na_2O	0.00	0.00	0.01	0.00	0.00	0.00	0.00
K_2O	0.13	0.16	0.13	0.12	0.12	0.12	0.12
P_2O_5	0.12	0.11	0.11	0.10	0.10	0.10	0.10
Cr_2O_3	0.02	0.02	0.02	0.02	0.02	0.02	0.03
NiO	0.00	0.00	0.00	0.00	0.00	0.00	0.00
V_2O_5	0.01	0.01	0.01	0.01	0.01	0.01	0.01
ZrO_2	0.00	0.00	0.00	0.00	0.00	0.00	0.00

Table 37: XRF results for samples taken in 2006 (continued)

	S 4_F-A	S 9_F-A	S 18_F-A	S 19_F-A	S 21_F-A	S 25_F-A	S 30_F-A
SiO_2	4.20	4.44	4.30	4.26	4.25	4.61	4.36
TiO_2	0.09	0.09	0.09	0.09	0.09	0.09	0.09
Al_2O_3	1.23	1.22	1.23	1.27	1.23	1.32	1.27
Fe_2O_3	60.90	60.98	61.96	62.31	63.07	60.61	63.62
MnO	0.91	0.97	0.86	0.86	0.92	1.04	1.02
MgO	2.68	2.65	2.69	2.66	2.62	2.93	2.74
CaO	8.64	8.56	8.65	8.61	8.63	9.37	9.09
Na_2O	0.00	0.00	0.00	0.00	0.00	0.00	0.01
K_2O	0.13	0.13	0.14	0.14	0.13	0.13	0.14
P_2O_5	0.10	0.10	0.10	0.10	0.10	0.11	0.11
Cr_2O_3	0.02	0.02	0.02	0.02	0.02	0.03	0.02
NiO	0.00	0.00	0.00	0.00	0.00	0.00	0.00
V_2O_5	0.01	0.01	0.01	0.01	0.01	0.01	0.01
ZrO_2	0.00	0.00	0.00	0.00	0.00	0.00	0.00

Table 38: Standard deviation and limit of detection for XRF results for samples taken in 2006

STANDARD DEVIATION AND LIMIT OF DETECTION:		
	std dev.(%)	LOD
SiO2	0.4	0.02
TiO2	0.03	0.0032
Al2O3	0.3	0.01
Fe2O3	0.3	0.0097
MnO	0.0065	0.0013
MgO	0.1	0.0118
CaO	0.07	0.01
Na2O	0.11	0.0265
K2O	0.06	0.005
P2O5	0.08	0.01
Cr2O3	0.0053	0.0006
NiO	0.01	0.0013
V2O5	0.0018	0.0008
ZrO2	0.005	0.0009
CuO	0.0037	0.0003

XRF results for synthetic SFCA

Table 39: XRF results for sol gel 1 method for SFCA

%	**SG2-2fb**	**SG2-2filter**
SiO_2	3.34	2.99
TiO_2	0.01	
Al_2O_3	3.04	3.65
Fe_2O_3	76.60	76.47
MnO	0.01	
MgO	1.05	0.92
CaO	15.90	15.46
Na_2O	0.01	
K_2O	0.01	
P_2O_5	0.01	
Cr_2O_3	0.03	0.04
NiO	0.01	
CuO	0.05	
LOI	0.00	
TOTAL	100.05	99.53

Table 40: XRF results for sol gel 1 method for SFCA and C_2S

%	**GSNcert**	**GSN**	**SFCA**	**C2S**
SiO_2	**65.80**	66.00	4.68	33.25
TiO_2	**0.68**	0.65	0.01	0.00
Al_2O_3	**14.67**	14.84	2.97	0.01
Fe_2O_3	**3.75**	3.67	75.16	0.00
MnO	**0.06**	0.05	0.02	0.00
MgO	**2.30**	2.13	0.71	0.00
CaO	**2.50**	2.43	15.59	67.25
Na_2O	**3.77**	3.64	0.01	0.07
K_2O	**4.63**	4.63	0.01	0.00
P_2O_5	**0.28**	0.28	0.00	0.00
Cr_2O_3	**0.008**	0.01	0.03	0.00
NiO	**0.0043**	0.01	0.00	0.00
V_2O_5	**0.01**	0.01	0.01	0.00
ZrO_2	**0.03**	0.02	0.00	0.00
LOI	**1.32**	1.29	-0.09	0.72
TOTAL	**99.82**	99.66	99.10	101.31

Table 41: Standard deviation and limit of detection for XRF results for sol gel 1 method for SFCA and C_2S

STANDARD DEVIATION AND LIMIT OF DETECTION:		
	std dev.(%)	LOD
SiO2	0.4	0.02
TiO2	0.03	0.0032
Al2O3	0.3	0.01
Fe2O3	0.3	0.0097
MnO	0.0065	0.0013
MgO	0.1	0.0118
CaO	0.07	0.01
Na2O	0.11	0.0265
K2O	0.06	0.005
P2O5	0.08	0.01
Cr2O3	0.0053	0.0006
NiO	0.01	0.0013
V2O5	0.0018	0.0008
ZrO2	0.005	0.0009
CuO	0.0037	0.0003

Appendix 5

Microprobe results for samples taken in 2005, 2006, sol gels and their cluster analyses values

Table 42: Microprobe data for samples taken in 2005 (Sample 2)

DataSet/Point	O	Mg	Al	Si	Ca	Mn	Fe	Total
31 / 1 .	28.46	2.97	1.2	0.47	4.98	1.45	58.82	98.35
32 / 1 .	28.39	3.59	1.04	0.43	4.65	1.72	59.07	98.89
33 / 1 .	28.24	2.26	1.27	0.99	7.31	1.32	56.93	98.33
34 / 1 .	28.83	2.29	1.24	0.93	7.13	1.36	56.96	98.75
47 / 1 .	27.73	1.72	1.02	0.72	7.35	1.24	58.86	98.65
48 / 1 .	27.63	1.71	1	0.74	7.37	1.19	58.68	98.32
49 / 1 .	26.48	2.22	0.75	0.01	2.21	1.1	65	97.76
50 / 1 .	26.67	2.26	0.73	0.01	2.04	1.08	64.94	97.71
51 / 1 .	26.56	1.99	0.73	0	2.09	1.04	65.68	98.08
52 / 1 .	26.25	1.96	0.71	0.03	2.13	0.98	65.53	97.58
53 / 1 .	29.3	0.91	1.75	0.72	7.74	0.63	58.65	99.7
54 / 1 .	29.13	0.84	1.83	0.76	7.42	0.59	58.75	99.31
39 / 1 .	28.5	1.74	1.11	0.69	7.19	1.25	58.29	98.77
40 / 1 .	28.11	1.74	1.08	0.7	7.26	1.17	57.95	98.01
41 / 1 .	27.51	3.18	0.46	0.05	3.03	1.91	62.05	98.18
42 / 1 .	27.79	2.4	0.8	0.33	4.9	1.56	60.3	98.09
59 / 1 .	26.69	4.92	0.82	0.01	2.37	1.7	61.56	98.07
60 / 1 .	27.13	4.97	0.83	0.03	2.42	1.72	61.26	98.36
61 / 1 .	26.97	4.99	0.78	0.01	2.46	1.66	61.64	98.53
62 / 1 .	26.51	5.1	0.78	0.05	2.38	1.7	61.35	97.88
23 / 1 .	28.98	4.33	0.55	0.39	3.24	1.3	60.45	99.23
24 / 1 .	30.56	2.55	0.87	3.01	8.39	0.9	53.33	99.62
25 / 1 .	27.72	4.01	0.61	0.01	2.07	1.19	62.35	97.96
26 / 1 .	27.5	4.06	0.55	0.06	2.13	1.27	62.22	97.8
9 / 1 .	26.84	3.68	0.78	0.01	1.54	1.56	63.34	97.75
10 / 1 .	26.77	3.64	0.8	0.03	1.47	1.57	63.27	97.55
11 / 1 .	26.82	3.59	0.84	0	1.58	1.61	63.52	97.97
12 / 1 .	27.01	3.64	0.85	0.01	1.62	1.58	63.25	97.96
13 / 1 .	27.33	1.53	1.37	1.13	7.19	0.94	58.02	97.5
14 / 1 .	27.21	1.54	1.36	1.16	7.34	0.95	57.84	97.39
15 / 1 .	27.85	5.13	1.04	0.15	3.21	1.59	59.63	98.59
16 / 1 .	27.79	4.89	1.16	0.14	3.27	1.45	59.94	98.65
17 / 1 .	27.95	5.11	1.05	0.01	2.49	1.64	60.46	98.71
18 / 1 .	27.93	5.03	1.04	0.03	2.49	1.64	60.37	98.52
1 / 1 .	26.79	0	0.04	0.4	-0.02	0	69.55	96.79
2 / 1 .	26.19	0	0.11	0.45	0	0.01	68.99	95.74
3 / 1 .	26.55	0.01	0	0.35	0	0	69.6	96.52
4 / 1 .	26.47	0.02	0	0.3	-0.01	0.01	69.42	96.23
5 / 1 .	27.45	4.35	0.79	0	2.22	1.45	61.53	97.78
6 / 1 .	27.3	4.31	0.79	0.03	2.23	1.59	61.67	97.91

DataSet/Point	O	Mg	Al	Si	Ca	Mn	Fe	Total
7 / 1 .	27.77	4.19	0.8	0	2.22	1.59	61.58	98.15
27 / 1 .	26.41	0.01	0.42	0.44	0.23	0.02	68.67	96.2
28 / 1 .	26.35	0.01	0.41	0.59	0.29	0.02	68.26	95.92
29 / 1 .	26.42	0.01	0.43	0.52	0.13	0.02	68.16	95.69
30 / 1 .	26.33	0	0.44	0.6	0.14	0.05	67.85	95.41
43 / 1 .	26.72	0.03	0.06	0.39	0.02	0.04	69.55	96.8
44 / 1 .	26.38	0.01	0.05	0.26	0.01	0.04	69.85	96.61
45 / 1 .	26.77	0.01	0.04	0.17	0	0.05	70.61	97.64
46 / 1 .	26.34	0.02	0.05	0.13	0.03	0.04	70.16	96.75
35 / 1 .	28.27	0	2.28	2.26	-0.01	0.02	65.01	97.83
36 / 1 .	27.48	0	1.48	1.58	0.01	-0.02	66.5	97.05
37 / 1 .	27.37	0.01	0.97	1.06	0.01	0.02	67.53	96.97
38 / 1 .	27.39	0	1.12	1.4	0.03	0.02	66.57	96.53
63 / 1 .	30.2	0.11	0.5	4.29	29.92	3.13	30.2	98.34
64 / 1 .	30.32	0.11	0.48	4.3	30.02	3.11	30.46	98.8
65 / 1 .	30.39	0.13	0.47	3.99	30.03	3.15	30.5	98.66
66 / 1 .	30.57	0.11	0.48	4.08	30.02	3.01	30.6	98.88
67 / 1 .	29.17	0.2	0.72	1.69	28.27	1.73	36.75	98.54
68 / 1 .	29.11	0.2	0.73	1.54	29.28	1.71	36.1	98.67
69 / 1 .	29.14	6.28	0.92	0.03	4.69	5.95	53.75	100.76
70 / 1 .	28.87	6.3	0.94	0.07	4.45	5.87	53.2	99.7
55 / 1 .	29.5	0.38	0.53	1.62	28.31	0.7	38.05	99.1
56 / 1 .	29.3	0.14	0.54	1.69	27.88	0.76	37.99	98.31
57 / 1 .	31.93	4.69	0.48	1.23	12.97	0.98	49.76	102.05
58 / 1 .	30.89	6.77	0.57	0.43	7.5	1.08	53.45	100.69
19 / 1 .	26.72	-0.01	0.87	0.06	0.01	-0.01	68.57	96.23
20 / 1 .	26.84	-0.01	0.95	0.12	-0.01	0	68.39	96.29
21 / 1 .	26.76	0.01	0.79	0.13	-0.01	-0.02	68.24	95.93
22 / 1 .	26.69	0	0.82	0.13	-0.01	0.01	68.82	96.47

Table 43: Microprobe data for samples taken in 2005 (Sample 3)

DataSet/Point	O	Mg	Al	Si	Ca	Mn	Fe	Total
33 / 1 .	27.19	2.38	0.56	0.01	3.06	2.41	62.95	98.55
34 / 1 .	26.95	2.37	0.51	0.07	2.94	2.45	63.02	98.31
35 / 1 .	27.86	1.03	1.18	0.7	7.26	1.67	58.63	98.34
36 / 1 .	27.61	1.06	1.18	0.7	7.21	1.71	58.65	98.11
37 / 1 .	27.8	0	0.2	0.35	0.36	0.04	69.19	97.96
38 / 1 .	28.11	0	0.19	0.37	0.35	0.03	69.19	98.25
83 / 1 .	30.1	1.71	2.38	1.6	7.95	0.75	55.23	99.72
84 / 1 .	29.39	2.04	2.25	1.3	7.05	0.85	56.28	99.16
85 / 1 .	29.72	1.82	2.79	1.13	6.97	0.84	56.18	99.44
86 / 1 .	29.14	1.7	2.75	1.31	7.16	0.83	56.13	99.01
51 / 1 .	28.2	4.26	0.45	0.02	2.8	0.79	62.49	99.01
52 / 1 .	28.27	4.22	0.49	0.16	3	0.77	62.16	99.07
53 / 1 .	28.34	3.67	0.49	0.3	4.7	1.01	60.89	99.41
54 / 1 .	28.16	3.29	0.58	0.56	5.03	0.83	60.66	99.1
25 / 1 .	29.37	0.43	2.08	2.55	9.49	0.43	54.38	98.73
26 / 1 .	29.11	0.42	2.09	2.45	9.25	0.45	54.58	98.34
27 / 1 .	25.79	1.41	0.37	0.04	0.73	1.16	68.62	98.12
28 / 1 .	25.71	1.38	0.37	0.04	0.75	1.12	68.41	97.78
55 / 1 .	25.96	1.4	0.43	0	1.1	1.35	67.56	97.79
56 / 1 .	25.71	1.4	0.49	0.06	1.18	1.37	67.45	97.65
57 / 1 .	25.93	1.8	0.7	0.01	1.52	1.45	66.39	97.8
58 / 1 .	25.78	1.79	0.66	0.02	1.58	1.37	66.29	97.5
59 / 1 .	29.7	0.39	1.72	1.76	9.18	0.61	56.15	99.51
60 / 1 .	29.8	0.38	1.74	1.76	9.14	0.57	56.19	99.58
7 / 1 .	26.58	0.01	0.03	0.07	0.02	0.12	70.11	96.95
8 / 1 .	26.53	0.01	0.05	0.08	0.04	0.14	69.79	96.64
9 / 1 .	27.12	0	0.02	0.33	0.01	0.16	70	97.64
10 / 1 .	26.67	0	0.01	0.17	0.01	0.2	69.84	96.9
61 / 1 .	27.3	1.71	0.54	0	2.59	1.05	65.39	98.59
62 / 1 .	27.42	1.7	0.57	0	3.02	1.07	65.4	99.19
63 / 1 .	26.84	1.73	0.47	0.03	2.87	1.17	65.08	98.18
64 / 1 .	27.14	1.81	0.45	0.18	2.99	1.15	63.9	97.61
65 / 1 .	27.98	0.96	1.17	0.6	6.79	0.79	60.71	99
66 / 1 .	28.12	0.86	1.21	0.71	7.04	0.76	60.44	99.14
21 / 1 .	29.72	2.04	1.68	1.28	8.1	0.86	56.07	99.75
22 / 1 .	29.41	1.97	1.7	1.1	7.66	0.92	56.28	99.03
23 / 1 .	29.91	2.31	1.5	1.16	7.86	0.96	56.05	99.76
24 / 1 .	30.18	1.89	1.54	1.49	8.5	0.86	55.27	99.74
15 / 1 .	27.19	0	0	0.57	0	-0.01	69.73	97.49
16 / 1 .	27.36	0.02	0	0.4	-0.01	0.01	69.74	97.53
17 / 1 .	26.52	0	0.01	0.37	0	-0.01	70.07	96.97
18 / 1 .	26.79	0.01	0.01	0.63	0.04	0.01	69.66	97.15
19 / 1 .	26.67	0.01	0.01	0.62	0.02	0	69.67	97.01
20 / 1 .	26.58	0.01	0.01	0.65	0.02	0	69.69	96.95

DataSet/Point	**O**	**Mg**	**Al**	**Si**	**Ca**	**Mn**	**Fe**	**Total**
43 / 1 .	27.57	0.01	0.19	0.12	0.06	0.01	69.93	97.88
44 / 1 .	27.51	0.02	0.11	0.13	0.04	0.02	70.13	97.96
45 / 1 .	27.41	0.02	0.01	0.32	0.03	0	69.91	97.69
46 / 1 .	27.22	0.01	0.03	0.34	0.03	0.01	70.59	98.23
39 / 1 .	28.13	4.57	0.53	0	1.73	0.99	63.07	99.02
40 / 1 .	27.67	4.56	0.57	0.06	1.76	0.94	62.94	98.5
41 / 1 .	27.56	5.51	0.75	0.02	1.48	0.9	62.54	98.76
42 / 1 .	27.24	5.44	0.73	0.04	1.6	0.9	62.25	98.2
91 / 1 .	27.72	0.02	0.02	0.49	0.04	0.02	69.72	98.03
92 / 1 .	27.63	0	0.02	0.57	0.03	0	69.55	97.78
93 / 1 .	26.87	0	0.02	0.17	0.04	0.01	70.02	97.14
94 / 1 .	26.82	0	0.03	0.18	0.05	0.02	69.81	96.91
87 / 1 .	27.41	1.8	1.32	1.4	7.09	1.09	57.32	97.42
88 / 1 .	27.6	3.48	0.61	0.02	2.19	1.73	63.25	98.88
89 / 1 .	28.07	3.49	0.61	0	2.26	1.77	63.27	99.48
90 / 1 .	27.98	3.45	0.6	0.02	2.27	1.77	63.34	99.43
47 / 1 .	27.58	0	0.03	0.02	0	0	70.88	98.51
48 / 1 .	27.68	0.01	0.02	0.05	0.02	0.07	70.79	98.64
49 / 1 .	27.31	-0.01	0.01	0.03	-0.01	0	70.65	98
50 / 1 .	27.27	-0.01	0.01	0.07	0	0.01	70.53	97.89
29 / 1 .	27.1	3.72	0.76	0	1.79	4.38	60.54	98.29
30 / 1 .	27.15	3.73	0.77	0.04	1.8	4.34	60.86	98.68
31 / 1 .	28.5	1.95	1.4	1.03	6.51	2.64	57.07	99.1
32 / 1 .	28.51	1.87	1.37	1.06	6.71	2.62	56.6	98.74
1 / 1 .	30.28	0.4	2.11	2.77	10.8	0.47	52.11	98.93
2 / 1 .	30.36	0.46	2.25	2.71	10.66	0.5	51.97	98.92
3 / 1 .	30.72	0.63	2.39	2.64	10.28	0.52	52.19	99.37
4 / 1 .	30.1	0.59	2.39	2.65	10.41	0.5	51.99	98.61
5 / 1 .	30.95	0.64	2.37	2.74	10.9	0.48	51.5	99.58
6 / 1 .	31.44	0.52	2.34	2.91	11.2	0.45	51.32	100.16
11 / 1 .	27.58	0.04	0.28	0.01	0.05	0.17	69.71	97.84
12 / 1 .	27.46	0.05	0.3	0.04	0.05	0.17	69.38	97.45
13 / 1 .	26.22	0.03	0.23	0.09	0.17	0.08	69.96	96.77
14 / 1 .	26.26	0.03	0.21	0.16	0.19	0.11	69.45	96.41
67 / 1 .	27.46	0	0.09	0.17	0.01	-0.01	70.13	97.86
68 / 1 .	27.6	-0.01	0.08	0.13	0	0	70.28	98.09
69 / 1 .	27.38	0	0.1	0.14	0.02	-0.02	70.24	97.89
70 / 1 .	27.24	0.02	0.1	0.14	0	-0.01	69.98	97.48
75 / 1 .	27.13	0.03	-0.01	0.18	-0.01	-0.02	69.99	97.34
76 / 1 .	27.09	0.03	0	0.31	0.02	0.01	69.5	96.98
77 / 1 .	27.28	0.01	0.07	0.17	0.02	0.09	69.98	97.62
78 / 1 .	27.13	0	0.03	0.14	0.01	0.02	69.89	97.21
71 / 1 .	29.26	1.24	1.18	1.16	7.73	1.82	57.31	99.7
72 / 1 .	29.2	1.22	1.19	1.21	7.57	1.8	57.65	99.83
73 / 1 .	28.73	1.22	1.11	0.89	7.1	1.81	58.32	99.17
74 / 1 .	28.72	1.22	1.12	0.95	7.32	1.82	58.14	99.29
79 / 1 .	27.42	0.01	0.15	0.15	0.04	0.09	70.01	97.85

DataSet/Point	O	Mg	Al	Si	Ca	Mn	Fe	Total
80 / 1 .	27.65	0.02	0.14	0.17	0.08	0.1	70.38	98.54
81 / 1 .	27.39	0.02	0.16	0.14	0.1	0.06	70.1	97.97
82 / 1 .	27.58	0.02	0.17	0.1	0.09	0.13	70.33	98.42

Table 44: Microprobe data for samples taken in 2005 (Sample 4)

DataSet/Point	O	Mg	Al	Si	Ca	Mn	Fe	Total
1 / 1 .	29.79	0.69	1.56	1.89	10.09	0.62	54.24	98.87
2 / 1 .	29.37	0.67	1.61	1.77	9.74	0.61	54.85	98.62
3 / 1 .	28.13	1.29	1.41	1.12	7.73	0.87	57.44	98
4 / 1 .	28.35	0.96	1.41	1.3	8.45	0.76	56.53	97.76
5 / 1 .	28.98	0.6	1.53	2.32	10.54	0.57	53.14	97.67
6 / 1 .	28.85	0.56	1.54	2.26	10.53	0.55	53.79	98.09
7 / 1 .	28.74	0.93	1.45	1.29	8.7	0.75	56.62	98.48
8 / 1 .	28.45	1.09	1.39	1.14	8.09	0.84	57.23	98.22
9 / 1 .	27.51	0.01	0.85	0.02	0.22	0.18	69.61	98.4
10 / 1 .	27.43	0.01	0.82	0.03	0.19	0.2	69.17	97.85
11 / 1 .	28.76	0.59	2.33	1.26	7.54	1.24	57.42	99.14
12 / 1 .	28.84	0.59	2.31	1.38	7.66	1.24	57.04	99.06
13 / 1 .	29.52	0.38	2.78	1.51	8.6	0.87	55.68	99.34
14 / 1 .	29.07	0.39	2.74	1.34	8.09	0.95	56.43	99.01
15 / 1 .	29.04	3.67	0.93	0.5	7.47	1.16	56.01	98.77
16 / 1 .	28.4	5.24	0.76	0.23	5.57	1.37	57.13	98.7
17 / 1 .	28.55	5.44	0.68	0.03	3.76	1.63	59.32	99.4
18 / 1 .	28.28	5.63	0.65	0.06	3.59	1.55	59.16	98.92
19 / 1 .	28.47	1.39	1.44	1	6.27	0.77	59.93	99.28
20 / 1 .	28.29	1.31	1.45	1.08	6.62	0.74	59.37	98.86
21 / 1 .	26.78	2.41	0.42	0.04	1.11	1.2	66.41	98.38
22 / 1 .	26.95	2.39	0.42	0.07	1.15	1.19	66.38	98.55
23 / 1 .	26.66	2.42	0.4	0.05	1.35	1.23	66.2	98.31
24 / 1 .	26.77	2.42	0.43	0.04	1.38	1.16	66.49	98.69
25 / 1 .	26.89	2.28	0.54	0.02	1.48	1.13	65.91	98.26
26 / 1 .	26.45	2.26	0.53	0.03	1.37	1.17	66.22	98.03
27 / 1 .	28.14	1.15	1.45	1.02	6.91	0.68	59.04	98.39
28 / 1 .	28.17	1.12	1.45	1.06	7.06	0.7	58.91	98.48
29 / 1 .	29.93	0.7	1.65	2.42	9.9	0.42	54.1	99.11
30 / 1 .	29.84	0.65	1.68	2.6	10.04	0.45	53.47	98.74
31 / 1 .	30.33	0.44	1.68	2.58	11.02	0.39	52.6	99.03
32 / 1 .	30.84	0.45	1.54	2.94	11.28	0.41	51.73	99.2
33 / 1 .	30.14	0.4	1.6	2.53	10.47	0.41	53.16	98.71
34 / 1 .	30.61	0.37	1.78	2.14	10.74	0.34	53.83	99.81
35 / 1 .	30.94	0.4	1.71	2.31	11.1	0.32	53.23	100.01
36 / 1 .	30	0.52	1.62	1.83	10.18	0.44	54.35	98.94
37 / 1 .	29.4	0.57	1.53	1.87	10.01	0.49	54.64	98.52
38 / 1 .	27.86	4.81	0.56	0.11	3.47	1.49	60.52	98.83
39 / 1 .	27.84	4.49	0.61	0.27	3.94	1.53	59.87	98.54
40 / 1 .	28.5	2.02	1.12	0.73	7.87	0.9	57.46	98.6

DataSet/Point	O	Mg	Al	Si	Ca	Mn	Fe	Total
41 / 1 .	28	2.03	1.14	0.75	7.86	0.88	57.15	97.81
42 / 1 .	28.39	2.31	1.22	0.69	7.68	0.98	57.22	98.49
43 / 1 .	28.56	2.35	1.28	0.71	7.66	1.02	57.25	98.83
44 / 1 .	28.04	5.39	0.85	0.01	2.49	2.81	58.8	98.39
45 / 1 .	28.15	5.31	0.89	0.04	2.53	2.78	58.63	98.34
46 / 1 .	28.08	5.42	0.89	0.03	2.51	2.8	58.57	98.3
47 / 1 .	29.17	4.93	0.94	0.21	3.43	2.61	57.81	99.1
48 / 1 .	28.92	5.02	0.92	0.19	3.46	2.58	57.9	98.98
49 / 1 .	27.39	3.11	0.76	0.03	1.99	1.03	64.2	98.52
50 / 1 .	27.7	3.09	0.75	0	1.97	1.07	63.97	98.55
51 / 1 .	27.21	3.27	0.76	0.03	1.9	1.08	64.11	98.35
52 / 1 .	26.87	3.24	0.8	0.05	1.83	0.96	64.11	97.86
53 / 1 .	27.1	2.96	0.74	0.01	1.67	1.03	64.8	98.31
54 / 1 .	27.1	3.01	0.7	0.03	1.62	1.07	64.83	98.35
55 / 1 .	27.21	0.01	0.05	0.13	0.02	0.09	69.75	97.26
56 / 1 .	27.3	0	0.08	0.15	0.02	0.06	69.84	97.45
57 / 1 .	26.9	0	0.07	0.16	0.01	0.06	70.06	97.26
58 / 1 .	27.24	0	0.06	0.11	0.03	0.04	70.14	97.62
59 / 1 .	27.13	0.01	0.07	0.16	0.01	0.05	69.78	97.21
60 / 1 .	28.1	4.57	0.68	0.01	2.65	1.58	61.62	99.21
61 / 1 .	27.72	4.65	0.65	0.04	2.59	1.58	61.25	98.47
62 / 1 .	28.76	1.93	1.34	0.81	7.82	0.92	57.51	99.09
63 / 1 .	28.73	1.88	1.34	0.84	7.89	0.91	57.32	98.91

Table 45: Microprobe data for samples taken in 2006 (Sample 30)

Comment	O	Mg	Al	Si	Ca	Mn	Fe
3o_5a	29.31	1.18	1.02	0.72	5.77	1.33	59.72
3o_5b	28.79	2.05	0.52	0.04	1.82	1.8	65.16
3o_5c	30.68	8.53	0.26	0.08	0.98	1.69	58.03
30_6a	30.34	2.97	0.85	0.35	2.7	18.19	45.36
30_6b	30.12	6.8	0.61	0.04	1.03	15.76	46.01
30_6c	28.66	2.62	0.72	0.01	1.65	21.63	44.15
30_2a	29.66	3.58	0.89	0.2	1.78	1.08	62.71
30_2b	36.05	0.15	1.41	7.1	21.29	0.26	33.64
30_2c	30.07	3.76	0.85	0.01	1.46	1.11	62.97
30_1a	28.94	3.24	0.66	0.01	1.47	0.96	64.6
30_1b	28.99	3.35	0.7	0.01	1.29	0.91	64.6
30_1c(brown)	37.38	0.27	1.71	13.25	26.58	0.13	20.46
30_3a	29.09	3.77	0.78	0.22	1.47	1.17	63.98
30_3b	28.35	3.99	0.78	0.03	0.96	1.22	63.63
30_3c	37.06	0.31	1.81	13.51	26.53	0.17	20.36
30_3d	37.4	0.3	1.84	13.7	27.52	0.15	19.18
30_11a	53.37	0.12	0.01	45.88	0	0	0.2
30_11b	53.23	0.12	0	45.93	0	0.02	0.18
30_11c	53.44	0.01	0.01	45.97	0	0	0.04
30_10a	52.51	0	0	45.93	0	0	0.11

Comment	O	Mg	Al	Si	Ca	Mn	Fe
30_10b	52.98	0.01	0	45.8	0	0.01	0.26
30_10c	52.75	0	0.03	45.44	0	0.01	0.96
30_12b	32.39	1.29	2.68	2.69	8.83	0.33	52.26
30_12c	29.07	0.1	0.83	0	0.13	0.1	67.66
30_8a	27.28	0.01	0.41	0.19	0.06	0	69.09
30_8b	29.12	0.01	0.15	0.17	0	0.01	69.21
30_8c	30.49	0.01	0.12	0.05	0	0	69.92
30_9a	53.07	0	0	45.78	0	0	0.73
30_9b	53.67	0	0	46.07	0.01	0	0.37
30_9c	53.37	0	0	45.98	0	0	0.42
30_9d	53.65	0.01	0.08	45.35	0.02	0	0.94
30_4c(brown)	29.37	0.01	0.05	0.22	0.01	0.01	69.43
30_4dbrown)	22.68	0.01	0.39	0.05	0.01	0	69.08
30_7a	30.24	0.01	1.15	1.37	0.07	0.04	66.83
30_7b	29.65	0.01	0.4	0.69	0.03	0.01	68.4
30_7c	29.44	0.02	0.21	0.45	0.01	0.05	68.94

Table 46: Microprobe data for samples taken in 2006 (Sample 21)

Comment	O	Mg	Al	Si	Ca	Mn	Fe
21_7a	29.9	0.02	0.02	0.23	0	0	64.11
21_7b	29.51	0.01	2.42	0.48	0.02	0.02	49.92
21_7c	30.39	0.04	0.02	0.31	0.02	0.01	69.83
21_1a	53.84	0.02	0.04	45.69	0.03	0	0.25
21_1b	53.42	0.03	0.14	45.55	0.02	0.01	0.3
21_1c	53.79	0	0.03	45.65	0	0	0.07
21_9a	29.4	2.99	0.68	0.11	1.18	1.38	64.56
21_9b	29.89	2.69	0.69	0.14	1.77	1.45	64.39
21_9c	29.57	2.99	0.62	0.01	1.19	1.43	64.89
21_2a	32.05	5.86	0.72	0.1	4.18	0.76	55.15
21_2b(brown)	32.35	0.29	1.07	2.05	18.4	0.21	46.6
21_2c	30.81	3	0.79	0.28	6.16	0.56	59.03
21_5a	29.88	3.09	0.48	0.03	1.77	1.21	64.27
21_5b	32.8	2	0.85	1.33	6.31	0.8	55.1
21_5c(brown)	35.69	0.17	1.26	7.41	20.28	0.21	36.04
21_5d(brown)	34.85	0.24	1.34	7.04	20.86	0.26	35.42
21_10a	31.19	3.74	1.18	0.86	5.23	2.15	56.41
21_10b	30.5	4.44	1.32	0.23	2.87	3.19	57.82
21_10c(needle)	38.29	0.5	1.02	5.99	21.13	1.35	35.79
21_10d	31.71	3.04	0.44	1.54	7.5	3.05	52.69
21_8a	29.36	2.46	0.76	0.01	0.91	0.8	65.92
21_8b	29.44	2.26	0.74	0	1.06	0.76	66.2
21_8c(brown)	37.06	0.1	1.92	10.84	24.39	0.1	26.08
21_8d	37.65	0.1	2.34	11.91	24.57	0.08	23.82
21_3a	31.27	6.89	0.81	0.02	2.6	0.8	58.91
21_3b	30.97	5.57	0.59	0.05	3.74	0.76	59.63
21_3c(brown)	33.22	0.24	0.75	4.51	22.8	0.18	39.22

Comment	O	Mg	Al	Si	Ca	Mn	Fe
21_4a	30.24	3.17	3.47	0.22	2.46	1.09	60.27
21_4b	32.22	2.48	0.87	0.82	5.39	0.9	56.08
21_4d(brown)	37.31	0.22	1.29	6.63	19.51	0.2	36.97

Table 47: Microprobe data for samples taken in 2006 (Sample 23)

Comment	O	Mg	Al	Si	Ca	Mn	Fe
23_1a	29.23	1.66	0.8	0.02	2.3	2.95	62.82
23_1b	30.12	1.12	0.66	0.48	4.01	3.07	61.37
23_1c	28.19	0.32	0.45	0.02	1.92	1.64	66.9
23_1d	37.16	0.29	1.07	5.82	20.32	0.99	35.9
23_1e	29.02	1.62	0.56	0.07	1.91	2.92	63.67
23_1f	29.51	0.01	0.73	0.27	0	0	68.3
23_1g	28.39	0.01	0.11	0.81	0.01	0	68.58
23_1h	29.49	0.01	0.16	0.16	0.08	0	69.17
23_7a	30.97	5.71	1.15	0.1	1.5	0.87	60.36
23_7b	32.21	6.09	0.88	0.75	2.79	0.76	57.27
23_7c	30.38	5.51	0.86	0.03	1.22	0.81	61.28
23_7d	30.62	5.5	0.94	0.01	1.49	0.84	61
23_7e	30.23	4.73	0.79	0.02	1.75	0.82	62.43
23_7f(brown)	38.92	0.38	1.16	9.51	27.39	0.14	23.31
23_7h(brown)	36.98	0.54	1.04	8.93	25.16	0.18	27.44
23_7i(brown)	37.28	0.34	1.55	7.48	22.59	0.13	30.5
23_8a	30.3	5.42	0.75	0.02	1.9	0.88	60.68
23_8b	30.65	5.7	0.8	0.04	1.86	0.99	60.29
23_8c	30.42	5.68	0.87	0.01	1.75	1.28	60.16
23_8d	30.27	5.71	0.85	0.03	1.86	1.2	60.37
23_8e	30.68	5.98	0.98	0.01	1.85	1.33	59.87
23_8f(brown)	39.72	0.54	1.28	6.33	23.26	0.28	31.46
23_8g(brown)	35.88	0.49	1.45	5.22	17.2	0.24	39.17
23_8h(brown)	35.42	0.31	0.75	9.93	29.68	0.13	23.45
23_9a	29.12	1.65	0.33	0.02	2.09	0.73	65.79
23_9b	31.42	0.86	1.04	1.42	7.44	0.41	58.69
23_9c	29.15	1.66	0.34	0.03	1.85	0.74	66.52
23_9d	28.81	1.19	0.71	0.79	3.84	0.56	63.01
23_9e	29.17	1.65	0.34	0.01	1.89	0.76	66.24
23_9f(needle)	40.11	0.2	0.77	7.82	21.24	0.17	33.53
23_9g(needle)	31.2	1.02	1.14	1.35	7.22	0.48	58.12
23_2a	29.46	2.71	0.63	0.01	1.8	0.89	64.52
23_2b	30.64	1.51	1.03	2.03	6.49	0.59	57.49
23_2c	29.56	3.47	0.41	0.02	1.33	1.08	63.86
23_2d	37.68	1.23	1.2	8.91	13.58	0.59	36.64
23_2e	30.5	2.95	0.47	0.73	3.07	0.9	61.41
23_3a	31.16	1.08	1.51	2.55	7.93	0.44	54.58
23_3b	31.85	0.66	2.49	2.71	9.26	0.26	53.2
23_3c	40.08	0.39	1.26	17	27.57	0.11	11.17
23_3d	32.62	0.46	2.43	3.47	10.67	0.2	50.7

Comment	O	Mg	Al	Si	Ca	Mn	Fe
23_3e	32.33	0.6	2.23	3.14	10.23	0.19	51.76
23_3f	38.18	0.15	0.75	10.04	26.55	0.24	24.34
23_4b	30.28	3.61	0.83	2.05	3.84	0.76	58.24
23_4c	29.28	3.52	0.73	0.03	1.29	0.79	64.13
23_4d	34.9	0.72	1.32	6.2	13.56	0.24	43.05
23_4e	34.29	0.42	1.85	6.2	14.44	0.18	42.53
23_4f	41.95	56.3	0.03	0	0.1	0.05	0.73
23_4g	30.82	7.29	0.89	0.01	0.67	0.73	59.47
23_5a	30.07	3.63	0.64	0.17	2.3	1	62.68
23_5b(grey)	35.52	0.27	1.04	7.68	22.94	0.2	33.84
23_5c	29.79	3.55	0.63	0.01	1.94	0.96	63.28
23_5d	31.02	0.1	0.88	2.24	7.42	6.15	51.97
23_5e	31.32	0.09	1.24	2.81	8.57	5.34	50.58
23_5f	31.8	0.08	0.84	3.02	8.87	4.48	51.04
23_6a	30.45	4.77	0.73	0.01	1.7	1.09	61.8
23_6b	30.27	4.81	0.73	0	1.61	1.09	61.73
23_6c	30.08	4.91	0.71	0.01	1.61	1.11	61.61
23_6d	31.61	4.38	0.93	0.52	4.05	0.94	58.73
23_6e	31.05	2.8	1.44	1.01	5.96	0.71	57.2
23_6f(grey)	30.78	0.22	2.17	8.38	21.98	0.25	31.11
23_6g(grey)	36.79	0.28	2.08	6.48	19.39	0.32	35.33
23_6h(grey)	36.15	0.42	1.55	13.77	27.59	0.28	18.69
23_6i(grey)	36.84	0.24	1.72	8.41	24.63	0.29	27.16

Table 48: Microprobe data for samples taken in 2006 (Sample 44)

Comment	O	Mg	Al	Si	Ca	Mn	Fe
44_6a	29.69	2.03	0.88	1.05	3.8	0.89	61.5
44_6b	29.75	1.92	1.19	0.87	4.6	0.77	60.86
44_6c	32.23	0.83	1.28	3.17	10.12	0.42	52.82
44_6d	31.26	1.05	1.15	2.25	8.05	0.54	56.23
44_6e	29.58	2.84	0.42	0.01	1.28	1.11	65
44_5a	30.54	3.83	0.82	0.02	1.76	1.32	62.76
44_5b	30.27	3.95	0.81	0.02	1.58	1.33	62.71
44_5c	29.94	3.85	0.85	0	1.71	1.34	62.76
44_5d	31.24	2.17	1.42	1.63	6.2	0.83	56.99
44_5e	30.19	4.02	0.91	0.02	1.79	1.42	62.4
44_5f(brown)	36.62	0.64	1.32	4.63	16.38	0.45	40.49
44_5fgbrown)	35.67	0.41	0.88	9.86	27.56	0.27	26.31
44_5hbrown)	38.15	0.59	1.24	8.07	21.88	0.39	31.98
44_1a	30.75	0.48	0.87	2.14	8.43	0.24	57.4
44_1b	28.94	1.29	0.44	0.02	1.82	0.51	67.07
44_1c	30.33	0.77	1.07	0.84	6.37	0.34	61.13
44_1d	31.3	0.5	1.32	1.38	8.15	0.28	58.2
44_1e	30.35	0.62	0.88	0.81	6.51	0.45	60.95
44_2a	29.17	1.83	0.54	0.01	1.88	1.04	66.27
44_2b	30.38	0.94	1.11	1.08	6.78	0.62	59.46
44_2c	31.19	0.58	1.32	1.77	8.86	0.44	56.69

Comment	O	Mg	Al	Si	Ca	Mn	Fe
44_2d	29.17	1.93	0.44	0.01	1.89	1.06	65.91
44_2e	34.3	0.75	0.88	2.87	11.3	0.55	48.59
44_2hbrown)	31.6	0.09	1.41	6.91	17.97	0.18	41.75
44_4a	31.97	0.9	1.77	2.33	9.68	0.61	53.06
44_4b	33.61	1.36	1.35	2.51	9.69	0.9	49.09
44_4c	30.11	4.07	0.51	0.04	1.84	2.75	61.25
44_4d	30.14	3.98	0.79	0.02	1.82	2.51	61.4
44_4e	30	3.6	0.32	0.03	1.8	2.35	62.47
44_4f(brown)	33.99	0.48	1.27	6.71	18.2	0.53	37.67
44_4g(brown)	40.01	0.09	0.82	14.25	33.16	0.16	10.64
44_4h(brown)	36.12	0.07	0.2	14.08	39.23	0.12	8.53
44_4i(brown)	36.25	0.46	1.14	6.11	17.48	0.44	38.31
44_3a	33.21	0.6	2.08	3.39	11.21	0.23	50.21
44_3b	29.77	2.93	0.73	0.02	1.61	0.96	64.35
44_3c	29.53	2.91	0.61	0	1.59	0.87	64.94
44_3d	29.93	3.31	0.86	0.36	2.29	0.84	62.76
44_3e	31.7	1.94	1.98	1.85	7.32	0.51	55.25
44_7a	30.86	5.42	0.68	0.02	1.93	1.23	60.91
44_7b	30.73	5.6	0.72	0.01	1.59	1.28	60.88
44_7c	31.16	5.66	0.76	0.1	2.16	1.27	59.93
44_7d	30.64	5.68	0.78	0	1.75	1.4	60.27
44_7e	30.76	5.61	0.7	0.03	1.36	1.27	60.63
44_7f(brown)	39.33	0.76	0.79	7.9	25.52	0.37	26.58
44_7g(brown)	36.33	0.44	0.57	10.78	33.1	0.17	17.81
44_7h(brown)	37.63	0.62	1.16	7.15	21.83	0.33	32.33
44_8a	29.31	2.49	0.68	0.01	1.9	1.17	64.63
44_8b	28.68	2.49	0.73	0.04	1.64	1.25	64.75
44_8c	27.8	2.55	0.63	0.01	1.93	1.13	64.52

Table 49: Cluster compositions for the normal sinter sample from the samples taken in 2005. Note that cluster 5 was used for the synthesis of the sol gels.

Elements	Cluster				
	1	2	3	4	5
O	26.99	27.25	28.26	28.57	29.92
Mg	2.74	0.01	5.08	1.44	0.54
Al	0.60	0.29	0.76	1.58	1.62
Si	0.03	0.11	0.10	1.03	2.27
Ca	1.57	0.07	3.33	7.68	10.43
Mn	1.11	0.10	2.03	0.90	0.46
Fe	65.30	69.76	59.22	57.45	53.63

Table 50: Cluster compositions for the normal sinter sample from the samples taken in 2006

Elements	Clusters				
	1	2	3	4	5
O	36.13	37.84	31.93	38.07	29.87
Mg	0.39	0.44	1.01	0.08	3.24
Al	1.29	0.80	1.38	0.51	0.74
Si	6.61	9.32	2.20	14.17	0.18
Ca	19.19	28.12	8.82	36.20	2.32
Mn	0.34	0.25	0.51	0.14	1.22
Fe	36.93	23.89	54.50	9.59	62.80

Table 51: Cluster compositions for the fine sinter sample from the samples taken in 2006

Elements	Cluster				
	1	2	3	4	5
O	35.36	37.36	29.73	53.68	31.21
Mg	0.27	0.10	2.07	0.02	3.65
Al	1.15	2.13	0.50	0.07	1.22
Si	5.69	11.38	0.11	45.63	0.54
Ca	20.14	24.48	0.99	0.02	4.22
Mn	0.39	0.09	0.88	0.00	1.28
Fe	38.45	24.95	65.52	0.21	56.46

Appendix 6

Point counting results for samples taken in 2006

Table 52: Point counting results for sample 21

Sample no. 21	
Relict hematite	22.8
Rhombohedral hematite	6.7
Magnetite	13.7
Magnesioferrite	24.5
Glass	5.6
Dicalcium silicate	2.3
SFCA II	2.3
SFCA	17
SFCA I	5.1
	100

Table 53: Point counting results for sample 23

Sample no. 23	
Hematite relict	8.4
Rhombic hematite	7.9
Magnetite	22.6
Magnesioferrite	22.1
Glass	6.9
Dicalcium silicate	4.4
SFCA dendretic	1.2
SFCA columnar	22.6
SFCA acicular	3.9
	100

Table 54: Point counting results for sample 30

Sample no. 30	
Hematite relict	23.5
Rhombic hematite	4.8
Magnetite	23.8
Magnesioferrite	17.3
Glass	5.8
Dicalcium silicate	1.1
SFCA dendretic	0.6
SFCA columnar	18.3
SFCA acicular	4.8
	100

Table 55: Point counting results for sample 44

Sample no. 44	
Hematite relict	12.1
Rhombic hematite	5.1
Magnetite	23.2
Magnesioferrite	17
Glass	7.4
Dicalcium silicate	1.2
SFCA dendretic	0.5
SFCA columnar	28.6
SFCA acicular	4.9
	100

Appendix 7

P value calculations formula

Formula used:

$$t = \frac{x - \mu}{s}$$

$$s = \frac{\sqrt{\Sigma^{N}_{i=1}(x_i - \bar{x})^2}}{N-1}$$

t = Student's t

(x-µ) = deviation from the mean

x̃ = mean

N = number of measurements

s = standard deviation